NTNU – Trondheim
Norwegian University of
Science and Technology

Scaling of Calcium Carbonate on a Heated Surface in a Flow Through System with Mono Ethylene Glycol.

Ketil Hyllestad

Preface

This work has been carried out at the Department of Chemical Engineering at the Norwegian University of Science and Technology (NTNU).

First I would like to thank Associate Professor Jens-Petter Andreassen for being a fantastic supervisor with a much appreciated open-door policy. I also appreciate all the assistance provided from my co-supervisors Margrethe Nergaard and Ralf Beck.

I would like to thank Lucy van de Ruit, Fiona Rankin, Dewald Vercueil, Murray Meissner, David Vogel, Sebastian Lee Klein, Leon Xu, Leif Olav Jøsang and Nick Boonzaier for proofreading my work. Thanks guys, you are the best! Down in the basement of K5 and in the corridors of K2 there are also two guys who really deserve acknowledgements. Arne Fossum and Julian Tolchard, thanks for supporting me in every possible way when it comes to acquiring equipment to the experimental setup and assisting with SEM/XRD.

In the end I would like to thank all my friends for making it easier to focus when needed and for making the life of a master's thesis student a lot more fun. Ok, mostly the fun part.

Declaration of Compliance

I, Ketil Hyllestad, hereby declare that this is an independent work according to the exam regulations of the Norwegian University of Science and Technology (NTNU).

Ketil Hyllestad

Ketil Hyllestad, Trondheim, 07.06.2013

Abstract

Efficiency of industrial heat exchangers can be reduced due to precipitation of a solid mineral layer called scale. Reversibly soluble salts such as calcium carbonate are less soluble at elevated temperatures and therefore precipitate more easily in these units. The effect is also seen in oil wells, pipelines and desalination plants among others.

The aim of this work was to determine growth rates and polymorphic composition of the formed scale at a range of inlet supersaturations, heated medium temperatures and solvent compositions. Experimental setup was prepared to study the effect of these parameters in a continuous flow system. An internally heated U-tube was placed in a reactor with constant stirring and supersaturation. Inlet/outlet temperature of the tube was continuously logged along with pH and bulk temperature.

A reduced heat transfer from the tube to the bulk solution was observed with an increased thickness of the scaled layer. The overall growth rate of aragonite decreased by 3.8% from $5.36\pm0.18\cdot10^{-6}$ kg/m$^2\cdot$s to $5.16\pm0.12\cdot10^{-6}$ kg/m$^2\cdot$s when the experimental duration was changed from 90 to 180 minutes in a water solvent. An inlet supersaturation of 6.0 and a tube temperature of 90°C were used in these experiments. The decrease in crystal growth was caused by a reduced skin-temperature with reduced heat transfer. The growth rate was reduced to $2.6\pm0.3\cdot10^{-6}$ kg/m$^2\cdot$s when the inlet supersaturation was reduced to 4.5 at comparable conditions and a time magnitude of 180 minutes. XRD- and SEM-analyses indicated a change from almost exclusively aragonite to a mixed polymorphic composition when the tube temperature was changed from 90°C to 50°C.

Experimental results proved that there is a prolonged initiation period for scale growth in monoethylene glycol solutions compared to a pure de-ionized water solvent. To study the growth of scale in a MEG solution, the experimental procedure was changed to include a pre-scale period where a uniform layer of aragonite was formed. Subsequent growth could then continue with variable solvent composition on the outside of this layer.

Heat transfer from the heated medium into the bulk solution was observed to decrease with a higher presence of MEG in the solvent, which elevated the skin-temperature. Thickness of the scaled layer was found to have a more profound

effect on crystal growth in a combined water/MEG solvent than in a water solution.

The results showed that there was a notable decrease in mass deposit with an elevated solvent concentration of MEG. Mass deposits per area after the pre-scale period were 0.90 mg/cm^2 (50wt% MEG), 0.53 mg/cm^2 (70wt% MEG) and 0.36 mg/cm^2 (90wt% MEG) at an inlet supersaturation of 6.0 and a tube temperature of 90°C. This experimental setup allowed for a separate control of the kinetic and thermodynamic contributions to scale growth. The reduced deposition at comparable levels of supersaturation was caused by reduced growth kinetics due to the increased viscosity in a solvent with MEG.

Table of Contents

Appendices

List of Symbols

Symbol	Unit	Name
a	-	Activity
A	m^2/cm^2	Area
A^*	$kg/m^2{\cdot}s$	Pre-exponential Arrhenius constant
Alk_T	mol/ kg solvent	Total alkalinity of system
b	-	Nusselt number coefficient constant
B	-	Ion proportional coefficient
c/C	mol/L, mol/kg	Concentration
Ca_{Tot}	mol/ kg solvent	Total molality of calcium in system
C_{Tot}	mol/ kg solvent	Total molality of carbon in system
C_p	J/ K${\cdot}$mol	Heat capacity
d	-	Prandtl number constant
D	m	Diameter
e	-	Reynolds number constant
E_a	J/mol	Activation energy
f	-	Viscosity rate constant
F	kg/s	Mass flow rate
g	-	Order of crystal growth process
G	J	Gibbs energy
G_L	m/s	Linear growth rate
ΔG_{crit}	J	Overall free energy change associated with formation of critical nucleus
h_i	$W/m^2 {\cdot}K$	Heat transfer coefficient of layer i
I	mol/L	Ionic strength
J	$1/ m^3{\cdot}s$	Primary nucleation rate
k	J/K	Boltzmann constant
k_i	W/m${\cdot}$K	Thermal conductivity of layer i
K_g	m/s, $kg/m^2{\cdot}s$	Overall crystal growth coefficient
K_{sp}	-	Thermodynamic solubility product

L	m	Thickness
m	kg	Mass of solid deposited in time t
$\widetilde{M}_i$	mol/kg solvent	Molality of component i
M_m	g/mol	Molar mass
n/N	mol	Mole number
Q	J	Heat transfer
r	m	Radius
R	J/ mol·K	Gas constant
R_G	kg/m²·s	Overall mass growth rate
S	-	Fundamental supersaturation/Inlet supersaturation
S_{Actual}	-	Supersaturation on growth site
S_E	J/K	Entropy
SR	-	Supersaturation ratio
t	s	Time
T	K	Temperature
U	W/m²·K	Overall heat transfer coefficient
V	m³	Volume
V_0	m³/s	Volumetric flow rate
z	-	Charge number

Symbol	Unit	Name
γ	-	Ion activity coefficient
$\gamma_\pm$	-	Mean ion activity coefficient
γ_{ef}	mN/m	Interfacial tension
δ	m/s	Fluid velocity
η	Pa·s	Viscosity
θ	-	Contact angle/ Bragg angle
μ	J/mol	Chemical potential
μ_0	J/mol	Standard potential
v	-	Moles of ions in one mole of solute
π	Pa	Negative thermodynamic pressure
ρ	g/cm^3, kg/m^3	Density
σ	-	Standard deviation
τ	s, min	Residence time
τ_T	K	Thermodynamic temperature
υ	m^3/mol	Molecular volume
φ	-	Contact angel factor
Ω	$1/m^3 \cdot s$, $1/m^2 \cdot s$	Nucleation kinetic parameter

Glossary

Term	Explanation
Activity	Effective concentration of a specimen
Alkalinity	Sum of all titradable bases, scale parameter
Aggregation	Formation of clusters in a colloidal suspension
Crystallization	Process of solid crystal formation from a solution or melt
CSTR	Continuous-stirred tank reactor
Diffusion	Transportation of particles due to a driving force
Fouling	Deposition of solid on a heated surface
Habit	Variation in relative size of crystal faces
HEN	Heterogeneous nucleation
HON	Homogeneous nucleation
IAP	Ion Activity Product
Lateral Growth	Growth in one direction
Morphology	See definition of Habit
MEG	Mono ethylene glycol
Nucleation	Number of minute solids which acts as center of crystallization
Polymorphism	Range of different crystallographic lattices with identical chemical structure
Pre-scale period	Initial period used to form a uniform scaled layer on which additional growth can continue
Scale	Deposition of solid material on a surface
Supersolubility/Supersaturation	Solution that contains more dissolved material than at equilibrium
SEM	Scanning Electron Microscopy
Skin Temperature	Temperature at the site of crystal growth
Stunting	Prevention of growth
Vortice/Vortex	Fluid region with spinning motion around an imaginary axis
XRD	X-ray Diffraction

1   Introduction

Precipitation and deposition of inorganic minerals from brine on a surface is called scale. This occurs in a number of processes involving aqueous solutions. These include oil wells, desalination plants, heat exchangers and several others. Scale control is of economic importance in the oil and gas industry, and it also has serious safety implications. The formation of a scale layer may lead to reduced flow rate of solutions and reduced efficiency of heat exchangers and performance of safety valves.

In order for scale to form, the solution must be supersaturated, meaning that there are more dissolved ions present than at equilibrium conditions. This supersaturation can be accomplished in different ways including temperature, alkalinity, pressure and concentration change as a result of evaporation, natural fluctuations, solvent removal, mixing or changes in set-points. Reservoirs in the oil and gas industry naturally contain calcium ions. The balance of CO_2 dissolved in solution and supersaturation parameters discussed, will dictate whether calcium carbonate ($CaCO_3$) will precipitate and possibly form scaled layers. This compound is reversibly soluble making it favorable to scaling at elevated temperatures such as in heat exchangers (Sandengen, 2006, Bott, 1995, Kaasa et al., 2004).

Calcium carbonate is one of the most common scaling minerals and it crystallizes into three different polymorphs with distinct crystallographic lattices: vaterite, aragonite and calcite in order of increasing stability (Ogino et al., 1987).

Mono ethylene glycol (MEG) is injected in the oil and gas industry to prevent formation of gas hydrates in the process cycles. Studies on growth of calcium carbonate in the bulk of a batch reactor with MEG are found in literature (Flaten et al., 2010, Flaten et al., 2009). This work studies growth of calcium carbonate scale on a heated surface in a continuous flow reactor at steady-state, which is more representable for conditions in industrial processes.

The experimental setup was based on the work of Nergaard (2011). An internally water heated U-tube was placed in a reactor with continuous flow of reactants and constant supersaturation. As opposed to the work by Nergaard (2011), temperatures (bulk and inlet/outlet U-tube) and pH were continuously monitored throughout the experiments. This enabled a more detailed investigation of the isolative effect of a scaled layer and of reagent consumption.

Solutions using water as solvent were used to verify the setup and investigate the effect of temperature and supersaturation on the growth rate, morphology and polymorphism in the formed scale layer. The effect of solvent composition on these scale parameters was investigated using solutions with different weight fractions of MEG in water.

Formation and growth of scale can be described using crystallization theories and existing models were used with weight data to calculate growth rates. Analysis with SEM and XRD were used to describe morphology/polymorphism.

2 Theory

This work presents a study on the precipitation (scaling) of calcium carbonate on a heated surface in the presence of MEG. Some theory on these topics will be given along with analysis techniques. Fundamental theory on crystalline matter, polymorphism, supersaturation, nucleation and crystal growth is also included.

2.1 Definition of scale

In literature, there exists a variety of different terms and definitions related to deposition of solid material on a surface. The term "scaling" is frequently used when the precipitate comes from an aqueous solution (Cowan and Weintritt, 1976). When the surface of deposition is heated, it can be referred to as "fouling" (Bott, 1995). To distinguish between formation of crystalline matter on the surface site and the process of adhering pre-formed crystals from solution, the definitions "crystallization fouling" and "particulate fouling" are often applied (Peyghambarzadeh et al., 2011).

In this paper "scaling" will be used to describe crystalline formation directly on the surface site while "particulate deposition" will refer to adhesion of solids formed in the bulk solution and then transported to the growth site.

2.2 Crystalline state

Solid matter can be characterized as either amorphous or crystalline. As opposed to the amorphous state, the units in a crystalline state have a regular pattern. The ions, atoms or molecules arrange themselves into a lattice with a high degree of internal regularity. The smallest repeating entities in a crystal are called unit cells. According to the arrangement and configuration of the unit cells, the crystal systems can generally be split into seven groups. These groups have distinct relationships between length of axes and their corresponding angels. These include cubic, hexagonal, tetragonal, rhombohedral, orthorhombic, monoclinic and triclinic systems. The different systems have distinct symmetries, appearance and also packing capabilities.

Even though there is a repeating internal structure, there are rarely two crystals that look exactly the same. A number of factors such as components present and growth conditions are determinants for the final appearance of a crystal. The

individual crystals often grow more rapidly in one direction or they may also experience stunting in another direction. This is called crystal habit and leads to a high degree of individuality in the crystal appearances (Callister and Rethwisch, 2010, Mullin, 2001).

2.2.1 Polymorphism and morphology

When a substance can form several different crystallographic lattices with identical chemical structure it is called polymorphism. These structures have different crystal systems and thus often very different appearance. The outer shape and appearance of a crystal is termed morphology and is a result of local growth rate, polymorphism, nucleation, agglomeration, phase transformation and so on. Due to these factors the different polymorphs cannot be identified only on appearance. X-ray diffraction (XRD) patterns are normally used to distinguish between them. This technique applies crystallinity and lattice parameters in the identification process (Callister and Rethwisch, 2010, Mullin, 2001).

Another important phenomenon related to polymorphism is called Oswald's rule of stages: The rule states that the less stable phases of a crystalline system will often (there are several exceptions) deposit first. The most thermodynamically stable polymorph (lowest Gibbs energy at a given temperature) will then appear either through nucleation or transformation from the unstable forms. A proposed explanation to this procedure is that the reactions with the fastest rate will dominate in the beginning, while the system with time will move towards the most thermodynamically stable shape (Mullin, 2001).

2.2.2 Crystalline defects and dislocations

Most crystalline matter has defects on an atomic scale. These imperfections are usually separated into three groups: point, line and surface defects. The first group includes points of a crystal where an atom is missing (vacancy) and points where there are more crystals than in the regular lattice (self-interstitial). In vacant points of a crystal there is a possibility for foreign atoms to relocate into the lattice structure, therefore changing the properties of the solid.

There are also two fundamental types of dislocation line defects which a crystal can experience, namely screw and edge. The latter is formed due to a shear stress applied parallel to its motion, thus creating an extra half-plane which terminates within the crystal. A screw formation, on the other hand, is formed through shear stress working perpendicular to the direction of movement. The final result is,

however, the same (Figure 2.1). In reality, the line defects in a crystal are most likely neither pure screw nor pure edge, but will contain components of both. These are called mixed dislocation. There are also some special formations possible, but in general, the dislocations formed have created lines where crystals can grow more easily as these areas are more energetically beneficial for the solid particles (Callister and Rethwisch, 2010, Mullin, 2001).
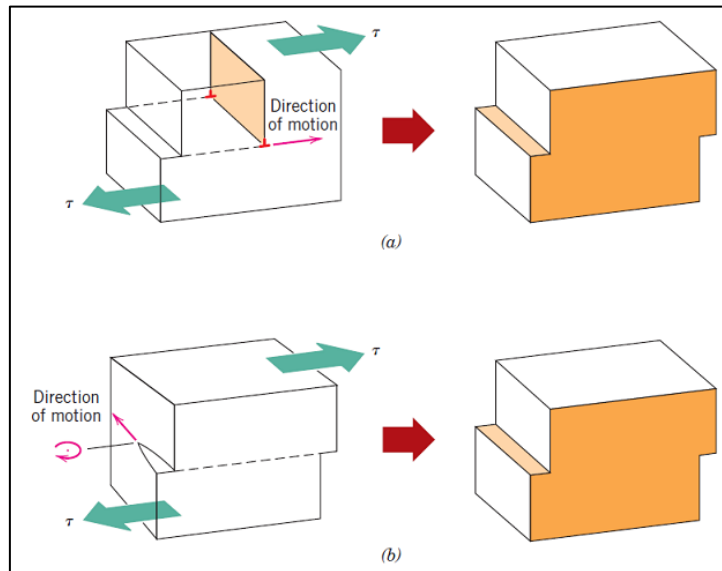

Figure 2.1: Line dislocation formation on the surface of a crystal due to (a) an edge dislocation and (b) a screw dislocation (Hayden et al., 1965).

2.3 Supersolubility and driving force

In order for a crystal to form in a liquid it is essential that the solution has reached a supersaturated state. This state can be described as a situation where there is more dissolved solid in the solution than at equilibrium conditions for a given temperature. Previous research has identified three major regions representing areas where crystal growth is impossible (stable zone), spontaneous (labile zone) and a metastable zone where crystals can grow, but normally not form spontaneously (Miers and Isaac, 1906, 1907). Figure 2.2 shows a schematic of such a solubility-supersolubility diagram.

Transfer between the different zones can be accomplished through changes in temperature or concentration. Evaporation and heating/cooling are examples of commonly used techniques to accomplish supersaturation. As shown in Figure 2.2, a decrease in temperature will make the solution more supersaturated, but for some components it is the other way around. The solubility curve is determined thermodynamically, while the supersolubility curve is related to the kinetics of the

system. The rate of cooling/heating will therefore have an influence on the width of the metastable area of the graph. These curves vary according to which components are present in the system.
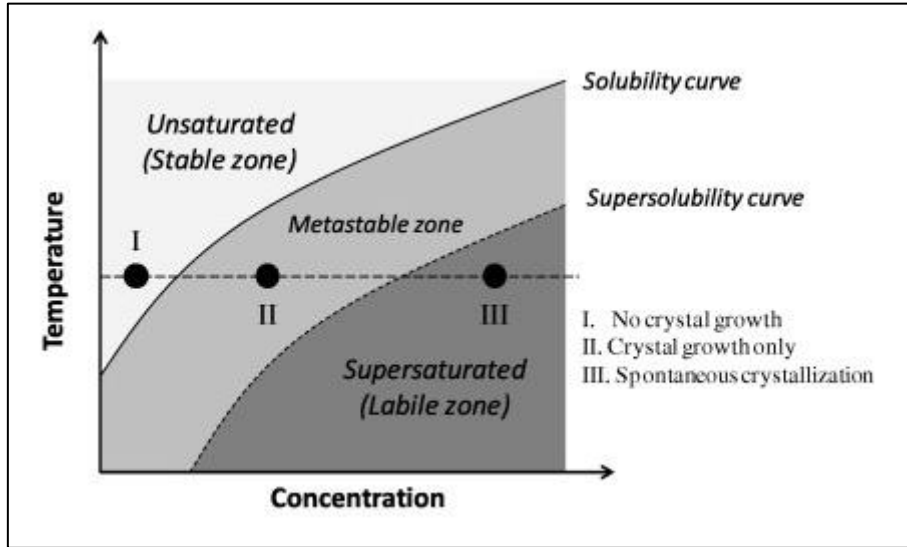

Figure 2.2: Schematic of solubility-supersolubility diagram (Liu et al., 2012).

2.3.1 Driving force

The driving force of crystallization in a solution is best explained thermodynamically in terms of difference in chemical potential ($\Delta\mu$), Equation (1). A complete derivation from thermodynamic potentials can be found in Appendix A.1.

When the chemical potential of a crystal is smaller than that of the solution ($\Delta\mu<0$) there is a driving force that ensures the possibility for nucleation and growth of crystals. The chemical potential is defined in equation (2). Standard potential is represented with μ_0 and activity with a. The activity can be seen as a product of the experimentally determined activity coefficient γ and concentration c as indicated in equation (3).

$$\Delta\mu = \mu_{Crystal} - \mu_{Solution} \tag{1}$$

$$\mu = \mu_0 + R \cdot T \cdot lna \tag{2}$$

$$a = \gamma \cdot c \tag{3}$$

The fundamental driving force behind crystallization is derived from the equations above, as shown in equations (4) and (5). SR is an expression for the supersaturation ratio in the system, while a^* represents the activity of a saturated solution (Helbæk and Kjelstrup, 2006, Mullin, 2001).

6

$$\Delta\mu = R \cdot T \cdot \ln\left(\frac{a}{a^\star}\right) = R \cdot T \cdot ln\ SR \tag{4}$$

$$SR = \exp\left(\frac{\Delta\mu}{R \cdot T}\right) = \frac{a}{a^\star} \tag{5}$$

2.3.2 Electrolyte solutions

Electrolyte solutions such as crystalline matter are better expressed using mean ionic activity ($a_\pm$) as defined in equation (6), since the interactions between ions are often significant even at low concentrations. The symbol v is here used as the total number of ion moles in one mole of solute. Introducing this into equation (4) gives a new expression containing the driving force of electrolyte solutions as shown in equation (7).

$$a = a_\pm^v \tag{6}$$

$$\frac{\Delta\mu}{R \cdot T} = v \cdot \ln SR = v \cdot \ln\frac{a_\pm}{a_\pm^\star} \tag{7}$$

Activity cannot be measured as an experimental value, but it can be calculated from concentration and the ion activity coefficient as shown in equation (3). The ion activity coefficient for very dilute electrolyte solutions is calculated using the Debye-Hückel equation as shown in equation (8), (Helbæk and Kjelstrup, 2006). B is the proportional constant; charge number is indicated with z, while I represent the ionic strength. The mean ion activity can then be calculated from equation (9) using IAP as the ion activity product.

$$\log\gamma_\pm = -|z_+| \cdot |z_-| \cdot B \cdot \sqrt{I} = -|z_+| \cdot |z_-| \cdot B \cdot \sqrt{\left(\frac{1}{2} \cdot \sum_i c_i \cdot z_i^2\right)} \tag{8}$$

$$a_\pm = (a_+^{v+} \cdot a_-^{v-})^{\frac{1}{v}} = \gamma_\pm \cdot c = IAP^{\frac{1}{v}} \tag{9}$$

Expressions for sparingly soluble electrolytes are best explained using solubility products. Equation (10) represents the supersaturation of these solutions. This expression is developed from equation (7) by inserting K_{sp} as the activity product of the salt. An increase in supersolubility implies a larger driving force and thus possibility of nucleation/growth (Nielsen, 1964, Mullin, 2001).

$$S = SR^{\frac{1}{v}} = \left(\frac{IAP}{K_{sp}}\right)^{\frac{1}{v}} \tag{10}$$

2.4 Nucleation

Supersaturated solutions are in a state where crystal formation is possible. The stage where the first particles are formed is called nucleation and can be split into two different mechanisms: Primary and secondary nucleation. Initiation of primary nucleation requires the solution to be in the labile zone of the solubility-supersolubility curve, as shown in Figure 2.2. Secondary nucleation can also be observed in the metastable zone.

The difference between the two mechanisms is that when a solid crystal of the same component is present in the solution it is defined as secondary nucleation, whereas when it is not, the formation is described as primary nucleation. The latter case can further be divided into heterogeneous and homogeneous depending on whether there are foreign particles present, or if the nucleation is completely spontaneous. Factors such as agitation, friction and mechanical shock may also influence this process (Mullin, 2001).

Supersaturation and temperature have a large effect on the rate of primary nucleation (J). Solutions of higher supersaturation level or temperature will form solid particles at a faster rate according to equation (11). The interfacial tension also affects the nucleation rate; here symbolized with γ_{ef}. Molecular volume is represented as υ. According to previous research, the kinetic parameter Ω in this equation is dependent on the same parameters as the exponential part. The rate of diffusion is also included in it, as well as the solvent viscosity (Kashchiev and van Rosmalen, 2003).

$$J = \Omega \cdot \exp\left[-\frac{16 \cdot \pi \cdot \gamma_{ef}^3 \cdot \upsilon^2}{3 \cdot k^3 \cdot T^3 \cdot (\ln S)^2}\right] \tag{11}$$

Nucleation of particles on a heated surface can be described as heterogeneous nucleation (HEN) since there normally will be some foreign particles in the solution acting as substrates for nucleation (Chen et al., 2005). This mechanism requires less energy than homogenous nucleation (HON) due to smaller contact angels between the phases of the system. Equations (12) and (13) show the relationships as a function of the angel between the crystalline deposit and the surface of the foreign particle. A contact angle (θ) between 0° and 180° represents a wetting of the surface with crystalline matter which gives a free energy of HEN lower than HON and therefore also an easier nucleation. The overall free energy change associated with the formation of critical nucleus is symbolized with ΔG_{crit} in equation (12) (Mullin, 2001).

$$\Delta G_{crit,hetr} = \varphi \cdot \Delta G_{crit,hom} \tag{12}$$

$$\varphi = \frac{1}{4}(2 + cos\theta)(1 - cos\theta)^2 \tag{13}$$

The time period from the moment that supersaturation is achieved until the appearance of crystals with detectable size is called induction time. This is mainly influenced by supersaturation, the presence of impurities, agitation and solution viscosity.

Nucleated particles can either re-dissolve in the solution or continue to grow into larger crystals. This will depend on the size of the formed particle, where solids smaller than an observed critical size will redissolve. The mechanism behind this is the tendency of solids to adjust towards a minimum surface energy. The process is called Oswald ripening and states that larger particles grow at the expense of the smaller ones (Liesegang, 1911, Mullin, 2001).

2.5 Crystal growth

Nucleated particles above the critical size will begin to grow into visible crystals. Numerous mechanisms to describe this growth have been proposed in literature. Some of these are discussed in this section along with morphology variations.

2.5.1 Crystal growth theories

Adsorption layer theories are based on the idea that units of the crystallizing substance are not integrated directly into the lattice when they arrive at the crystal face. The arrived substances will rather move on the surface creating a layer of units that are in equilibrium with the bulk solution. The units migrate until they arrive at the spot with the largest attractive forces, where they then link into the lattice. This "center of crystallization" will then continue to grow until completion. Further growth only occurs when a new center is formed, resulting in only one surface layer growing at any given time (Volmer, 1939, Mullin, 2001).

Diffusion-reaction theories propose that the adsorption of a unit into the crystalline lattice from the bulk solution can be split into two operations. First the ion/molecule is transported through a diffusion process to the solid surface before being added into the lattice through a first-order reaction (Berthoud, 1912, Valeton, 1924). An overall equation for general mass growth (R_G), according to this model is given in equation (14), where m represents mass of solid deposited in time. Growth order is displayed with the symbol g (Mullin, 2001).

$$R_G = \frac{1}{A} \cdot \frac{dm}{dt} = K_g \cdot (c - c^\star)^g \qquad (14)$$

Birth and spread models (polynuclear growth) describes nucleation of particles on the surface followed by monolayer spread. These models are based on the theory that the solids will develop several sites where growth can occur simultaneously (O'Hara and Reid, 1973). It is important to stress that the theories described above can all be applied during the growth period.

2.5.2 Growth rate mechanisms

The growth rate in crystalline matter can be expressed as a function of supersaturation. Implementing the relationship between supersaturation and concentrations ($S = c/c^*$) gives equation (15) from equation (14). Note that the growth constant (K_g) will not be the same in the two equations and that the temperature effect on growth is included in this unit. The equation expresses the overall growth rate (kg/m^2·s) of a crystal/crystal layer and can be calculated based on knowledge of mass, experimental duration and growth area.

The growth constant can be expressed according to an Arrhenius correlation as shown in equation (16). Here, A* represents a constant coefficient; E$_a$ the activity energy; R the universal gas constant; and T the temperature.

Impurities in the solution can have a large effect on the growth rate and can in some cases completely block the growth in certain regions. This is not accounted for in the mechanisms and should always be kept in mind. Equation (17) shows growth rate of a crystal or crystal layer if it is assumed that it can be characterized from only one linear dimension (for example the thickness of a scaled layer) (Mullin, 2001, Olderøy et al., 2009, Nielsen and Toft, 1983).

$$R_G = \frac{1}{A} \cdot \frac{dm}{dt} = K_g \cdot (S - 1)^g \qquad (15)$$

$$K_g = A^* \cdot \exp\left[\frac{-E_a}{R \cdot T}\right] \qquad (16)$$

$$G_L = \frac{dL}{dt} \qquad (17)$$

Crystals grow through integration of new crystal units into the surface. This integration normally occurs at active centers where there is a kink or step resulting in high attractive forces. There exist several mechanisms based on the magnitude of the solution supersaturation and whether the active points are created by defects in

10

the lattice or nucleation on the surface. Generally these mechanisms are split into regions with separate growth orders, as shown in Figure 2.3. The three major mechanisms are spiral growth (A), growth by two-dimensional nucleation (B) and rough growth (C).
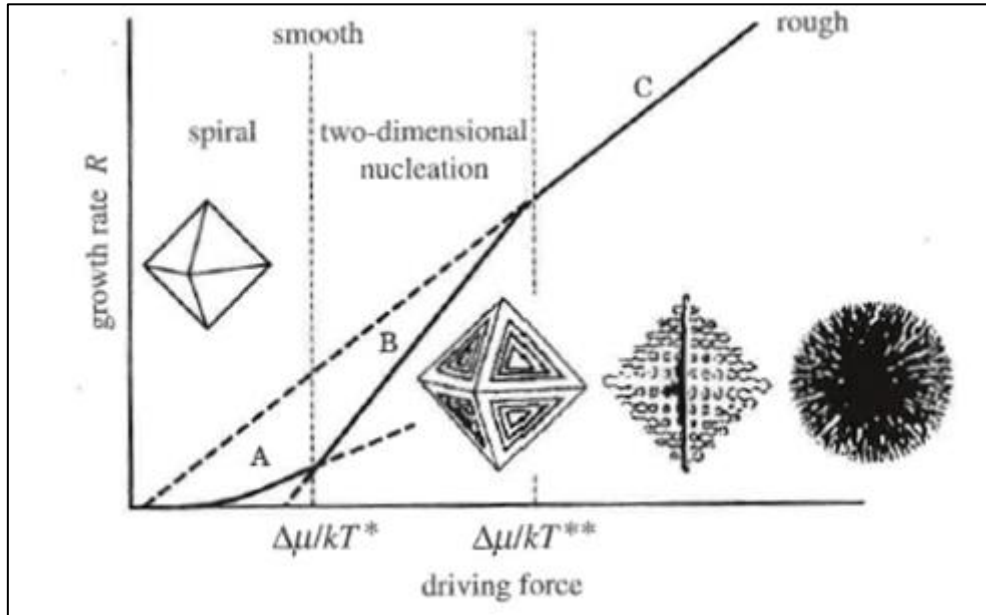

Figure 2.3: Changes in growth rate and morphology as a function of driving force (supersaturation) (Sunagwa, 2005).

At low levels of supersaturation, surface growth is favored over surface nucleation. Screw locations in the crystalline lattice have active centers along the entire dislocation. This can then result in spiral curvature growth perpendicular to the solid surface as new units integrate into the structure and push the defect forwards. The reaction is the determining step in this region resulting in a growth order of two (shown in equation (15) as g).

Higher supersaturation makes two-dimensional nucleation the determining mechanism. In this region nucleation occurs on the surface and generates kinks which further support the growth of the crystal layer. Meanwhile, other nuclei are also formed. Growth order (g) is found to be larger than two here. The roughness of the surface is determined by the rate of lateral growth compared to rate of nucleation. Low supersaturations yield a smooth surface due to the domination of lateral growth. At higher supersaturations, whereas nucleation rate is determining, the result will be a rough surface.

At even higher supersaturations, diffusion will become the rate determining step. In this region there are several places where a new unit can integrate into the crystal lattice which creates a deficit of new units. The mechanism is named rough growth

11

and in this region units will attach anywhere on the surface. Since the growth is linear, the growth order (g) in equation (15) has a magnitude of one (Olderøy et al., 2009).

When the supersaturation is in the region of rough growth and the crystallization occurs rapidly, the crystals can grow into a tree-like formation named dendrites. The parts furthest into the supersaturated medium experience the highest level of supersaturation and will therefore grow quickest resulting in the significant shape illustrated in Figure 2.4 (Mullin, 2001). Particles can also grow into a special spherical shape named spherulite with two hollow pockets on the inside (Andreassen, 2005).
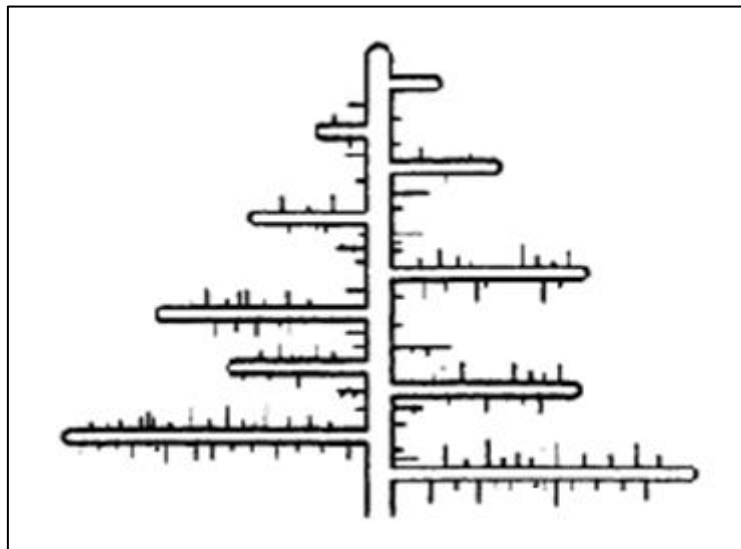
Figure 2.4: Schematic of dendritic growth (Mullin, 2001), p.25.

2.6 Calcium carbonate

This work will focus on the crystallization and growth rate of solids in a calcium carbonate system. In aqueous solutions this system reacts according to equations (18)-(21), (Olderøy et al., 2009).

$$CO_2(g) \leftrightarrow CO_2(aq) \tag{18}$$

$$CO_2(aq) + H_2O \leftrightarrow H^+ + HCO_3^- \tag{19}$$

$$HCO_3^- \leftrightarrow H^+ + CO_3^{2-} \tag{20}$$

$$Ca^{2+} + CO_3^{2-} \leftrightarrow CaCO_3(s) \tag{21}$$

The amount of each carbonate species present in the system is closely related to the pH, which is illustrated in Figure 2.5. This is also related to the supersaturation of the system, as discussed in Section 2.6.1, and therefore the growth of crystals.
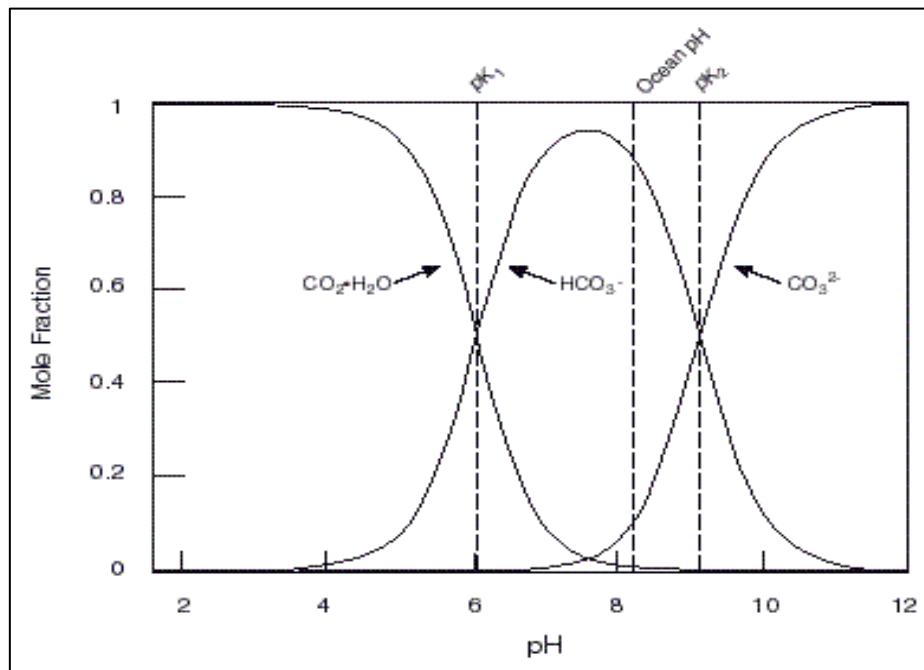
Figure 2.5: Schematic of bicarbonate - carbonate pH distribution diagram (Jacob, 1999).

2.6.1 Derivation of supersaturation expression

An expression for the supersaturation of the calcium carbonate system can be derived from equation (4) with the components shown in equation (21). The derived relationship between chemical potentials and the respective activities is given in equation (22).

$$\Delta\mu = \mu_{Ca^{2+}}^L - \mu_{Ca^{2+}}^S + \mu_{CO_3^{2-}}^L - \mu_{CO_3^{2-}}^S = R \cdot T \cdot \ln\left(\frac{a_{Ca^{2+}} \cdot a_{CO_3^{2-}}}{a_{Ca^{2+}}^\star \cdot a_{CO_3^{2-}}^\star}\right) \quad (22)$$

Combining the results obtained in equation (10) and (22) gives the supersaturation for the calcium carbonate system, shown in equation (23). This system has two moles of ions for every dissolved mole of solute ($v=2$) as shown in equation (21). The final expression for supersaturation can therefore be derived as in equation (24). The ion activity product, as mentioned previously, can be calculated using equations (8)-(9).

$$S = SR^{\frac{1}{v}} = \left(\frac{IAP_{CaCO_3}}{K_{sp_{CaCO_3}}}\right)^{\frac{1}{v}} = \left(\frac{a_{Ca^{2+}} \cdot a_{CO_3^{2-}}}{a_{Ca^{2+}}^\star \cdot a_{CO_3^{2-}}^\star}\right)^{\frac{1}{v}} \quad (23)$$

$$S = \sqrt{SR} = \sqrt{\frac{a_{Ca^{2+}} \cdot a_{CO_3^{2-}}}{a_{Ca^{2+}}^\star \cdot a_{CO_3^{2-}}^\star}} = \sqrt{\frac{IAP_{CaCO_3}}{K_{sp_{CaCO_3}}}} \quad (24)$$

From equation (24) and the relationship in equation (3) it is evident that an increased concentration of carbonate (CO_3^{2-}) will elevate the supersaturation. From Figure 2.5 it can be concluded that an increase in pH will raise the supersaturation of the system. Precipitation of calcium carbonate will, on the other hand, decrease the pH as carbonate ions are removed from the solution.

Calcium carbonate is an inorganic salt and unlike most other salts it is inversely soluble. This means that increased temperatures lead to a higher rate of precipitation, contrary to the effect shown in Figure 2.2. Heated surfaces (such as tubes in heat exchangers) will therefore have an increased probability of experiencing the formation of solid $CaCO_3$ from the passing solution (Bott, 1995).

2.6.2 Calculation of supersaturation and alkalinity

The supersaturation of a mineral system can be calculated automatically through simulation programs such as MultiScale 7.0®, which is based on the Pitzer model (Pitzer, 1973, Pitzer, 1986). The input parameters typically include temperature, pressure, total alkalinity and concentration of reactants. However, the model does not account for the kinetics of the system. It is merely a thermodynamic tool. Pressure, alkalinity and reactant concentration have been kept constant in the experiments used in this work. The effect of temperature changes on growth and polymorphism has been discussed in Section 4.

The total alkalinity of a system is defined as the sum of all titratable bases (Kaasa, 1998). It is a parameter used to describe composition, buffer capacity, pH-behavior and also carbonate scaling. Unlike pH measurements, alkalinity is not affected by pressure or temperature changes, provided that there is no solvent evaporation and precipitation of minerals which are not accounted for in the alkalinity equation.

Alkalinity can be measured through titration or calculated from a total electron neutrality balance for the system. A derivation of the equation with the reactants used in this study (Na_2CO_3 and $Ca(NO_3)_2$) has been included in Appendix A.2. The result is shown as equation (25). The total mass balance for carbon and calcium needed in the supersaturation calculations are included as equation (26) and (27).

$$Alk_T = \widetilde{M}_{CaHCO_3^+} + 2 \cdot \widetilde{M}_{CaCO_3^0(aq)} - \widetilde{M}_{H^+} + \widetilde{M}_{OH^-} + 2 \cdot \widetilde{M}_{CO_3^{2-}} \quad (25)$$
$$+ \widetilde{M}_{HCO_3^-}$$

$$C_{Tot} = \widetilde{M}_{HCO_3^-} + \widetilde{M}_{CaHCO_3^+} + \widetilde{M}_{CaCO_3^0(aq)} + \widetilde{M}_{CO_3^{2-}} + \widetilde{M}_{CO_2(aq)} \quad (26)$$

$$Ca_{Tot} = \widetilde{M}_{Ca^{2+}} + \widetilde{M}_{CaHCO_3^+} + \widetilde{M}_{CaCO_3^0(aq)} \quad (27)$$

The concentrations of reactants required to maintain a desired supersaturation in solution can be calculated through iteration in Multiscale.

2.6.3 Polymorphism of calcium carbonate

Calcium carbonate has three different anhydrous polymorphic states it can crystallize into. These are calcite (trigonal-rhombohedral), aragonite (orthorhombic) and vaterite (hexagonal). Calcite is the most stable polymorph and vaterite the least. From literature it has been found that at high levels of supersaturation vaterite is formed more often than the other polymorphs. It has also been shown that at low temperatures calcite will form most frequently, while at high temperatures aragonite formation is favored. As calcite is the most stable form, solids initially precipitated as one of the other polymorphs will transform into this state over a sufficient period of time (Ogino et al., 1987). The trends of polymorphic abundance in solutions of calcium carbonate and water are shown schematically in Figure 2.6.

The presence of co-solvents such as MEG (Methyl Ethylene Glycol) in the solution can change the quantity of the different polymorphs formed and also the size of the particles. Flaten and co-workers (2009) found that increasing concentration of MEG favors the formation of vaterite and reduces the size of precipitated particles.
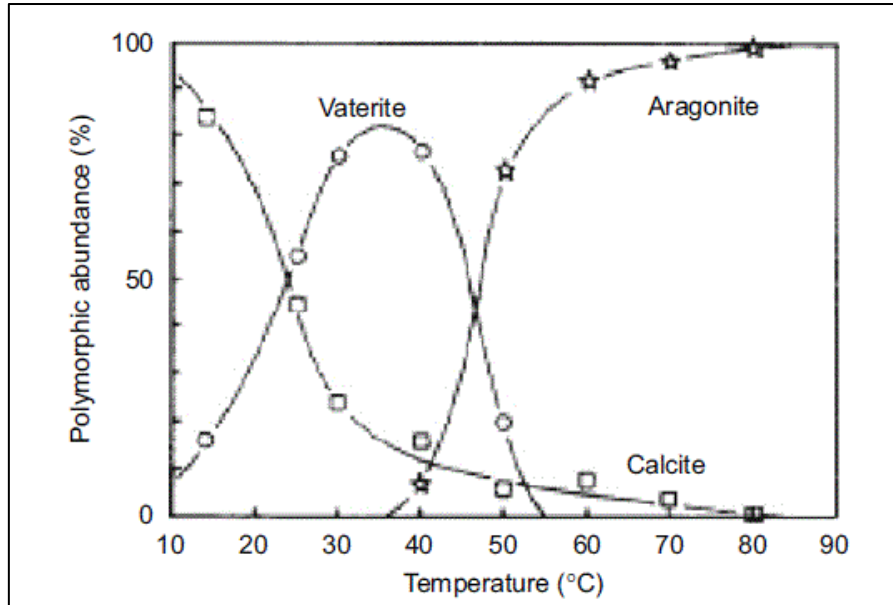
Figure 2.6: Polymorphic abundance as a function of temperature (Ogino et al., 1987).

The three polymorphs have very different appearances. Aragonite is normally found as needle shaped particles, calcite as cubes and vaterite with a plate/spherulitic shape (Flaten et al., 2009), (Andreassen and Hounslow, 2004).

The solubility products of the three polymorphs are not the same and can be found from the experimentally determined equations (28)-(30) below (Plummer and Busenberg, 1981). The temperatures are given in Kelvin.

$$\log K_{sp,Calcite} = -171.9065 - 0.077993 \cdot T + \frac{2839.319}{T} \qquad (28)$$
$$+ 71.595 \cdot \log T$$

$$\log K_{sp,Aragonite} = -171.9773 - 0.077993 \cdot T + \frac{2903.293}{T} \qquad (29)$$
$$+ 71.595 \cdot \log T$$

$$\log K_{sp,Vaterite} = -172.1295 - 0.077993 \cdot T + \frac{3074.688}{T} \qquad (30)$$
$$+ 71.595 \cdot \log T$$

The equations for solubility products of the polymorphs were used with equations for the amorphous phases (Brecevic and Nielsen, 1989, Clarkson et al., 1992) and plotted by Andreassen and co-workers (2012) shown in Figure 2.7. This figure illustrates the relationship between solubility product and temperature for different polymorphs. Equation (31) can be used in the calculations between polymorphs.

$$S_1 = S_2 \cdot \sqrt{\frac{K_{sp,2}}{K_{sp,1}}} \qquad (31)$$
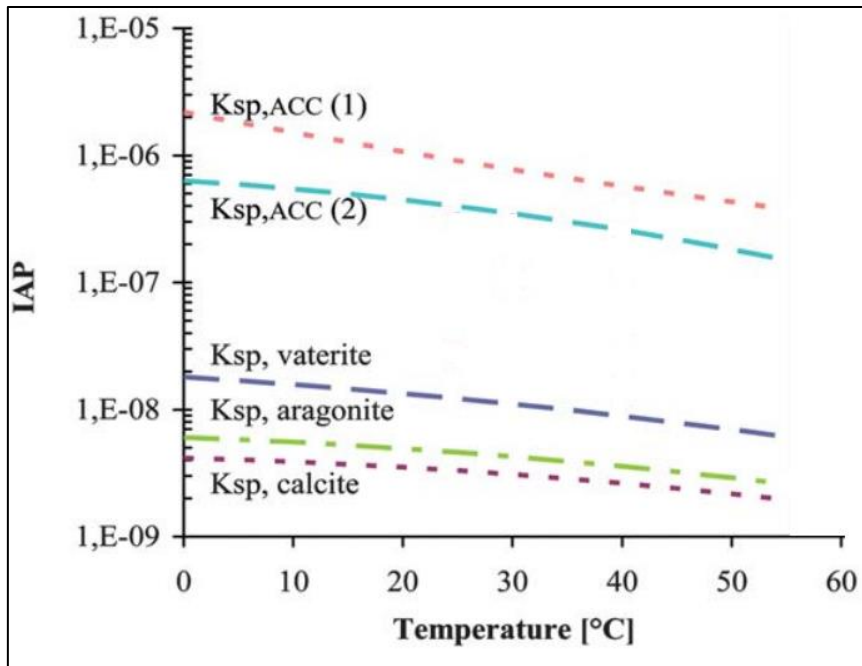
Figure 2.7: Solubility product lines for calcium carbonate polymorphs and amorphous phases (Andreassen et al., 2012).

2.7 Scaling

Scaling is the precipitation of a solid deposit on a surface. The potential formation and growth of this layer is related to its exposure to a supersaturated solution. The formed layer is often undesirably hard and can impede flow and reduce the efficiency of equipment such as safety valves and heat exchangers.

Complete prevention of scale growth is normally impossible or at least not economically feasible (Reitzer, 1964). There are, however, a range of different scale inhibitors which can reduce growth and change polymorphism. These will not be studied in this work.

The time required to form solid particles of visible size is referred to as the induction time in nucleation theory. When discussing surface scale growth, the time required to form a uniform initial layer, on which subsequent growth can continue, is often referred to as the initiation period. It is dependent on the rate of nucleation, and consequently parameters such as supersaturation, temperature, viscosity and surface tension shown in equation (11) which affect nucleation.

The deposition of scale can be separated into three regions as shown in Figure 2.8. In region A the adhesion process is initiated before the growth rate reaches a steady state in region B. At one stage the rate of deposition may gradually increase until it is on the level of adhesion. At this point the scale layer will have approximately constant thickness as shown in region C (Bott, 1995, Rankin and Adamson, 1973).
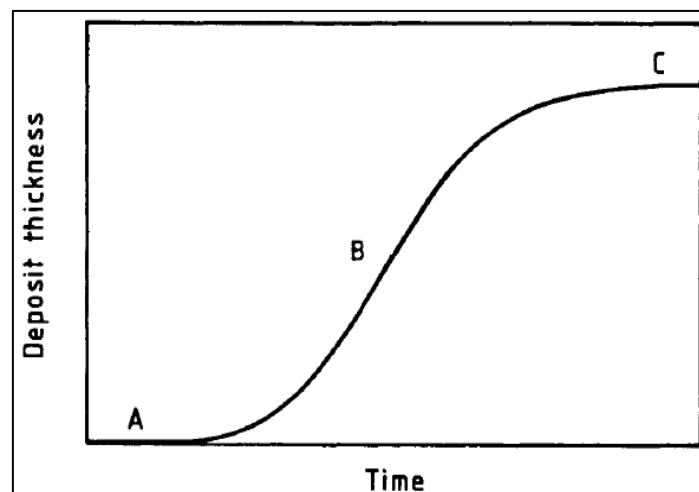
Figure 2.8: Change of deposition with time (Bott, 1995), p. 4.

In the oil and gas industry there are several different salts which can form scale layers and therefore there is a high level of complexity associated with the problem. The driving force is supersaturation, and in the industry this can frequently change

18

due to evaporation, solvent removal, pressure change, stream mixing or alkalinity fluctuations. The effect of alkalinity on supersaturation, and therefore scale formation, is illustrated in Figure 2.9. Control of this parameter is important, but can be difficult (Sandengen, 2006, Cowan and Weintritt, 1976, Kaasa, 1998).
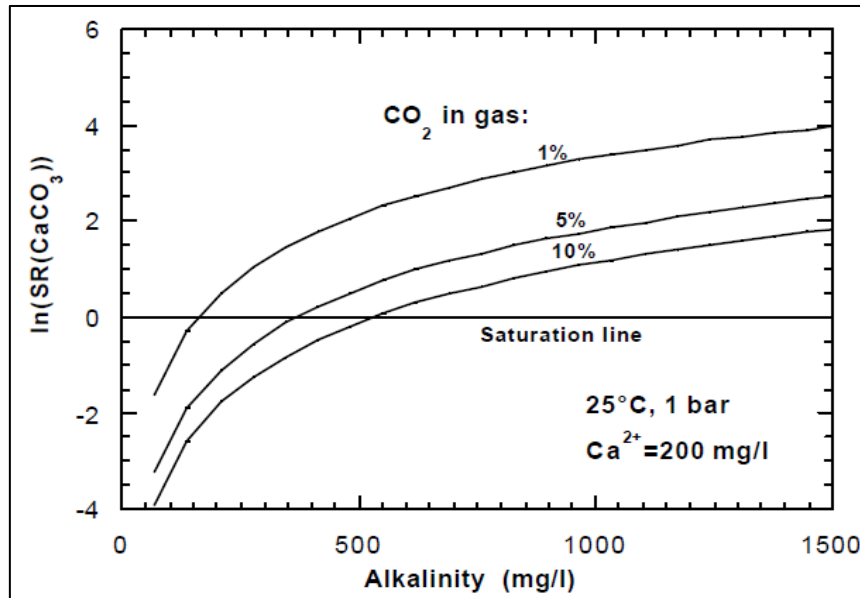

Figure 2.9: Effect of alkalinity on supersaturation of calcium carbonate with 200 mg/l Ca²⁺ at 25°C under different pressures of CO₂ (Kaasa, 1998).

Gas hydrates, like scale, pose a serious issue in the industry. This is a crystalline solid connected to a gas molecule caged in by water molecules (Kan et al., 2002). These gas hydrate units can plug wells and prevent production. Several inhibitors are therefore used to prevent the formation of such hydrates.

MEG is commonly used as a hydrate inhibitor, but this also decreases the solubility of calcium carbonate in the system. Water reduces the electric field between ions in an aqueous solution. However, addition of MEG limits this effect and therefore decreases the solubility. Combined with increased carbonate activity, as a result of higher alkalinity, MEG favors scaling of calcium carbonate layers in the system (Kaasa et al., 2004, Sandengen, 2006, Flaten et al., 2009).

The effect of increased MEG concentration is reversed when the supersaturation level is adjusted to account for the change in solubility and alkalinity (Flaten et al., 2010).

2.8 Heat transfer and experimental reactors

Precipitation of calcium carbonate is a serious problem in heat exchanger due to its inverse solubility. This often results in scaled layers on the surfaces which reduces heat transfer and therefore the efficiency of the equipment.

Experiments on precipitation of calcium carbonate can either be studied in a batch reactor or one with continuous flow through the system, typically a continuous-stirred tank reactor (CSTR). With adequate agitation these reactors are assumed to be perfectly mixed and operated at steady-state. This implies that the conditions in the tank are the same at every point and at all times. Baffles are utilized in reactors to modify the flow and inhibit the formation of vortices. When these are placed on the reactor walls they can, however, create zones where the solution is not mixed (Jakobsen, 2008).

The effect of scale deposit on the outer surface of a metallic U-tube, which is lowered in a CSTR system, will be studied in this section. Figure 2.10 shows a schematic of such a set-up, where hot fluid is running on the inside of the tube. The transferred heat (Q) through a medium can be calculated from the product of the overall heat transfer coefficient (U), area of heat transfer (A) and temperature difference (ΔT), as shown in equation (32). For an ideal countercurrent flow with constant heat capacities, the amount of heat transferred can be more adequately represented by the logarithmic mean temperature as given in equation (33), (Skogestad, 2009).

$$Q = U \cdot A \cdot \Delta T \tag{32}$$

$$\dot{Q} = \dot{m} \cdot C_p \cdot \left(T_{Tube,in} - T_{Tube,out}\right) = U \cdot A \cdot \frac{\left(T_{Tube,in} - T_{Tube,out}\right)}{\ln\left(\dfrac{T - T_{Tube,in}}{T - T_{Tube,out}}\right)} \tag{33}$$
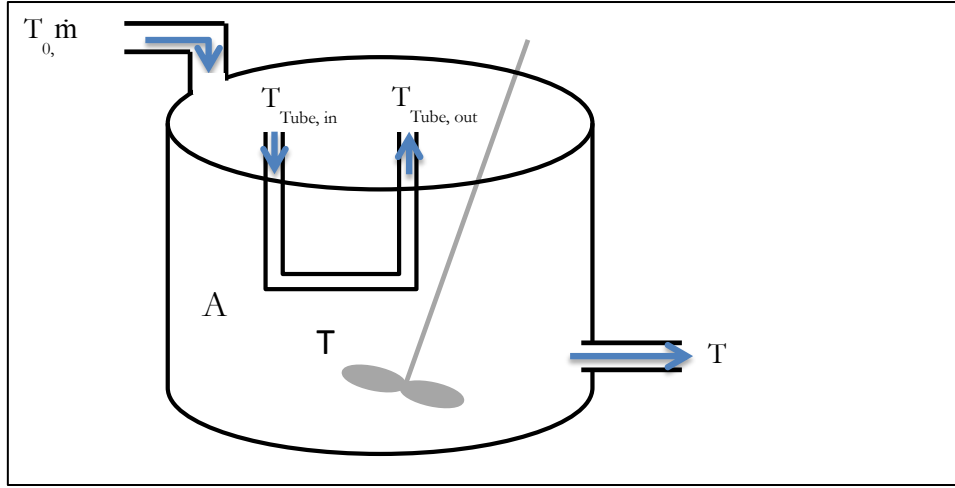
Figure 2.10: Schematic of a CSTR with a heated U-tube on the inside of the reactor (Nergaard, 2012).

Due to the isolative effect of the scaled layer, the solution temperature will decrease with increased precipitation on the heated surface. The reason for this is the reduced heat transfer from the metallic surface into the bulk solution. The return heat from liquid circulating on the inside of the tube ($T_{Tube, out}$) will also increase due to the same effect. A schematic of the heat transfer from the inside of a scaled tube and into the bulk solution is shown in Figure 2.11.

Equation (34) can be used to calculate the overall heat transfer coefficient through the tube and scaled layer. The radiuses are illustrated in Figure 2.11. The heat transfer mediums (from left to right) include: Tube liquid, tube wall, scale layer and bulk solution. Heat transfer coefficient is symbolized with h, while k_w and k_d represents the thermal conductivities of the wall and scale respectively. Equation (35) illustrates the influence of bulk viscosity (η) and heat capacity (C_p) on the heat transfer coefficient (h). The fluid velocity and density are symbolized with δ and ρ in the equation (Skogestad, 2009, Geankopolis, 2003).

Crystal units transferred from the bulk phase and into the surface growth site will experience a different temperature than the one on the inside of the tube. This temperature is called the skin-temperature as indicated in

$$U_i = \frac{1}{\dfrac{r_i}{h_{tube}} + \dfrac{\ln\left(\frac{r_0}{r_i}\right) \cdot r_i}{k_w} + \dfrac{\ln\left(\frac{r_d}{r_0}\right) \cdot r_i}{k_d} + \dfrac{1}{h_{bulk} \cdot r_d}} \tag{34}$$

$$N_{Nu} = \frac{h_{bulk} \cdot D}{k_d} = b \cdot \left(\frac{D \cdot \delta_b \cdot \rho_b}{\eta_b}\right)^d \cdot \left(\frac{C_p \cdot \eta_b}{k_d}\right)^e \cdot \left(\frac{\eta_b}{\eta_d}\right)^f \tag{35}$$
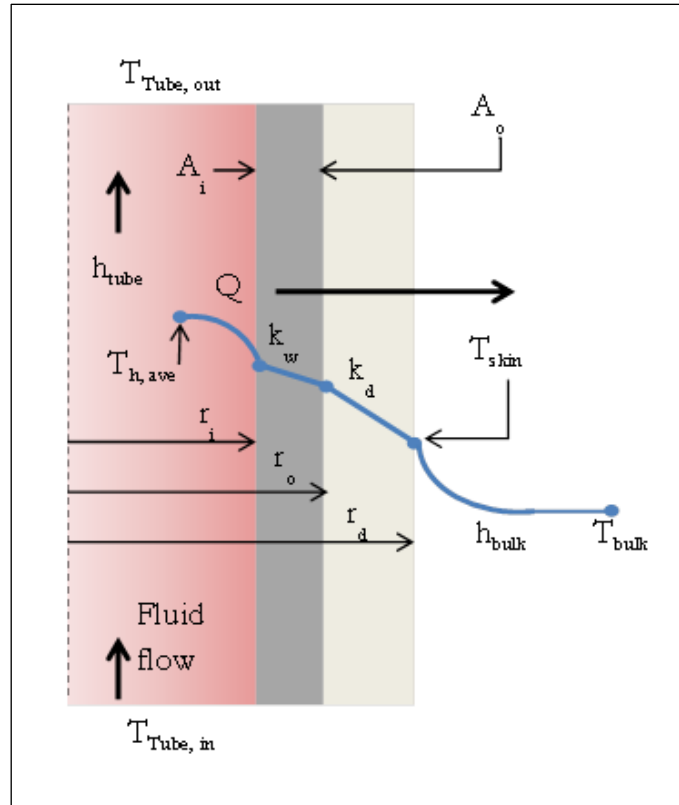
Figure 2.11: Schematic of heat transfer from the inside of a tube, through a scaled layer and into the bulk (Nergaard, 2012).

Another important parameter in such experiments is the residence time of the reactor. This can be calculated from equation (36) and indicates the time any given particle spends in the vessel. The symbol v_0 corresponds to volumetric flow rate, while F represents mass flow rate. Due to possible creation of dead zones and bypassing of inlet solution, the entire bulk solution is not changed with one residence time as indicated in Figure 2.12. This effect is referred to as residence time distribution and can be measured using a tracer, for example by injection of colored materials (Fogler, 2005).

$$\tau \equiv \frac{V}{v_0} = \frac{V \cdot C}{F} \tag{36}$$
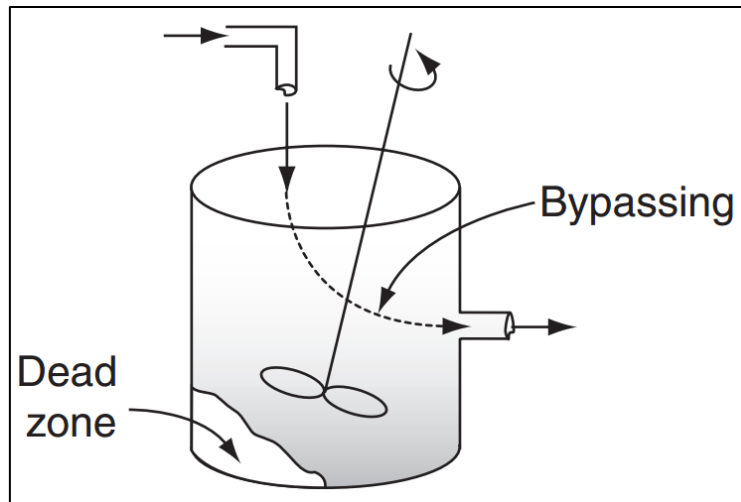
Figure 2.12: Schematic of residence time distribution effect in a CSTR (Fogler, 2005), p. 869.

2.9   Techniques for analyses

A wide range of analytical techniques can be used to determine size, morphology and polymorphism of solid particles. Sieving, microscopy, sedimentation and laser scattering are only a portion of the various methods applicable for finding the size of such units. The Scanning Electron Microscope technique has been used in this work to determine the thickness of the scaled surface and to give an indication of surface coverage/polymorphism. The identities of the different polymorphs were then, more accurately, determined with Powder X-ray diffraction (XRD).

2.9.1 Scanning electron microscope

In a scanning electron microscope (SEM), an electron beam is used to scan the sample surface. The electrons then interact with sample atoms and produce signals containing information about composition and topography. In SEM there is a possibility of electron charge build up if the surface is not conductive. This can be overcome by coating the top surface of the sample with a conductive material, but this may also hide some of the sample's topographic information. Secondary (SE) and back scattering electrons (BSE) are two different types of electrons which can be used in SEM. The former gives more information about the surface, but it is sensitive to charging. BSE is less sensitive to this charging and makes heavier elements in the sample appear brighter (Cao, 2004).

2.9.2 Powder X-ray diffraction

Powder X-ray diffraction (XRD) is a technique used to give information on a crystalline material. The x-ray beams are diffracted by the matter and generate a specific pattern. The intensity, shape and position of peaks in this pattern are then used to identify the sample (Callister and Rethwisch, 2010).

The presence of different polymorphs in calcium carbonate can be identified through XRD-analysis. However, it is much harder to quantify the amount of these polymorphs due to a large variation in crystalline lattice arrangement. Calcite has a higher degree of crystallinity than the other polymorphs and therefore often has more intensive peaks.

3   Experimental

A total of 25 experiments were done to investigate influence of supersaturation, tube temperature and weight percentage of Mono Ethylene Glycol (MEG) on growth of scale on a heated surface in a continuous flow system. A control test with only distilled water was done for comparative purposes. The same procedure and setup was applied in all experiments.

3.1   Solution preparation

Solutions in the reactant reservoirs were prepared in accordance with a desired supersaturation in the reactor. Sigma-Aldrich $Ca(NO_3)_2$ and VWR anhydrous Na_2CO_3 of analytic grade (>99 wt%) were applied to prepare the solutions. Distilled water and Univar MEG (>99 wt%) was used together with the salts to give a total weight of 25.2 kg and a desired weight percentage of MEG for each of the batch reservoirs. The containers were also adequately stirred to ensure uniform mixing. A complete list of chemicals has been listed in Appendix B. Calculations related to the preparation of reactants have been given in Appendix C, while an analysis of experimental uncertainty has been included in Appendix D.

The supersaturations in these experiments refer to the concentration of reactants in the reservoirs and the supersaturation they will give of calcite at 30°C (approximate bulk temperature). It should be noted, however, that this parameter will be lower in the reactor. Supersaturation is dependent on the number of ions in solution, polymorphism and temperature. Bulk precipitation reduces the supersaturation level. This level will also be decreased for other polymorphs than calcite according to Figure 2.7 and equation (31). The effect of temperature is complex and will be further discussed in Section 4.

3.2   Experimental setup

The experiments were performed in a 2.0 L jacketed glass reactor. An IKA stirrer with a 4-blade impeller (diameter=75 mm) and variable speed control was used to provide adequate mixing. Stirrer speed of 1000 rpm was used in all the experiments. Cooling was achieved with a Lauda RE205 thermostatic unit that circulated water continuously through the jacket of the reactor.

Solutions of sodium carbonate (Na_2CO_3) and calcium nitrate ($Ca(NO_3)_2$) were pumped separately from their reservoirs and precooled in two 2.0 L jacketed glass vessels through glass spirals submerged in pure water. Two IKA stirrers with 2-blade impellers and speeds of 1000 rpm were used to increase the cooling rate. The vessel jackets were connected in series and cooling was accomplished with a Lauda RE 205 thermostatic unit. The reactant reservoirs were placed on two Mettler Toledo scales to monitor the flow rates continuously. Reactants were then directed to the reactor from the precooling units using two Masterflex peristaltic pumps. Directly before entering the reactor, the reactants were mixed in a Y-tube and the temperature of the sodium carbonate solution was monitored with a PT-100 element logging unit.

The reactant feed tube was placed near the bottom of the reactor to reduce the possibility of bypassing or generation of dead-zones as discussed in Section 2.8. An outlet to waste ensured a measured constant volume of 2.2 L in the reactor whilst stirring, and the mean residence time was calculated as 5.2 min as shown in Appendix C.2. A simplified schematic of the experimental setup has been included as Figure 3.1, while a more complete illustration has been shown in Appendix E.
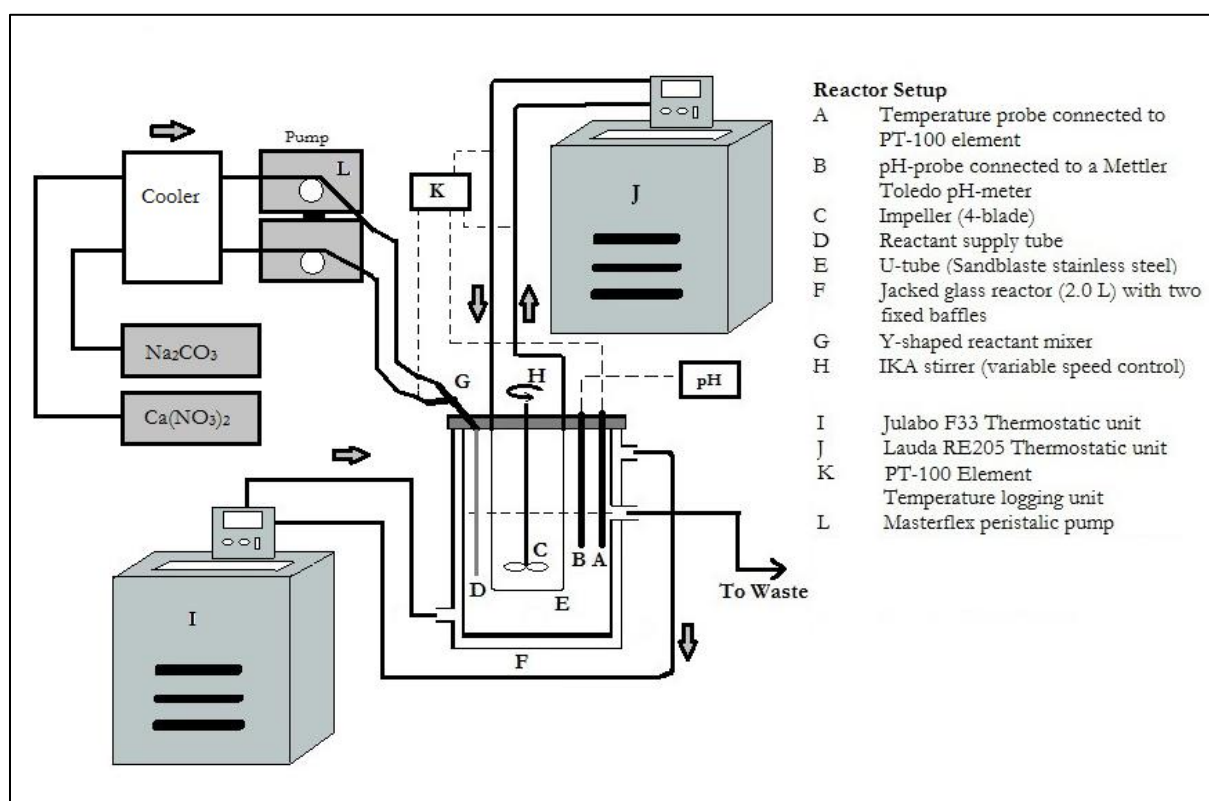
Figure 3.1: Schematic of experimental setup.

A Mettler Toledo logging device was used to measure and record pH in the reactor. Heated water was circulated on the inside of a steel U-tube (TP 316L) placed in the

26

center of the reactor. A Julabo F33 thermostatic unit provided the circulating water to the tube. Temperature of tube inlet/outlet and bulk was monitored and recorded using a PT-100 element logging unit. Relative placement of the equipment inside the reactor has been illustrated in Figure 3.2.

As shown in the figure, baffles were used to modify the flow and destroy vortices. These were placed around 0.50 cm from the reactor walls to avoid dead zones. Pictures of the U-tube and reactor have been included in Appendix E for illustrative purposes. Before any experiments were conducted, an HSE evaluation was performed as shown in Appendix F.

A	Impeller (4-blade)
B	U-tube (lowest point placed 1 cm underneath impeller)
C	Baffles (two in fixed position compared to U-tube)
D	Reactant inlet tube
E	pH/temperature -probe
F	Reactor outlet
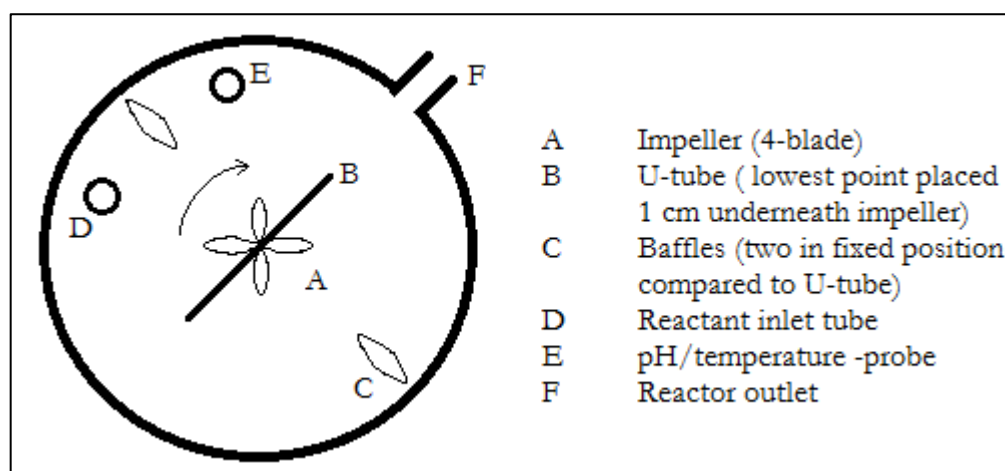
Figure 3.2: Schematic of equipment placement on the inside of the reactor.

The precooling of the reactants was done to approach the desired reactor bulk temperature of about 30°C more easily. Table 3.1 shows set-points and other constant values for the agitators, thermostatic units and the peristaltic pumps. These parameters were kept constant throughout all the experiments, although there were some fluctuations as indicated in the table.

Table 3.1: Fixed apparatus parameters

Equipment	Value[a]	Unit
Reactor agitator	1000±10	Rpm
Precooling vessel agitators	1000±50	Rpm
Julabo thermostat (heated U-tube)	Setpoint±1	°C
Lauda thermostat (reactor jacket)	20±2	°C
Lauda thermostat (precooling reactor jackets)	4.0±0.5	°C
Peristalic pumps	210±20	g/min

[a] **The fixed apparatus parameters were based on the work of Nergaard (2011). Reactor agitation level was set to ensure uniform distribution of scale.**

3.3 Experimental conditions

To examine their effect on crystal growth; tube temperature, weight percentage MEG, growth time and supersaturation level were varied in a series of experiments.

The duration of the experiment was defined from turning on to switching off the pumping of reactors from the reservoirs. Batch reservoir containers were prepared in advance and introduced successively to keep constant flow in accordance with magnitude of the time parameter. A complete summarization of performed experiments and applied parameters has been included in Table 3.2.

Table 3.2: Experiments on scale growth with variation of wt% MEG, duration after pre-scale period, temperature in tube and supersaturation of solution

Supersaturation (S)	$T_{Tube, inside}$ [°C]	MEG [weight percent]	Experimental time [min]		
4.5	90	0	-[a]	180	-
6.0	90	0	90	180	-
6.0	90	50	-	180	90+90[b]
6.0	90	70	-	180	90+90
6.0	90	90	-	-	90+90
6.0	50	0	-	180	-
6.0	50	70	-	-	90+90
6.0	90	50	90+30	90+90	90+155
12.3	90	50	30	-	-

[a] No experiments done with a given parameter is marked (-) in the table.

[b] Experiments marked with two added time intervals describes an initial period without MEG (pre-scale period) and then a continuation with the same supersaturation level and temperature for a new time interval with MEG.

3.4 Experimental procedure

Each experiment was initiated by turning on the agitators and thermostatic units at their designated set-points. A steel U-tube was weighed and placed on the inside of the empty reactor. The data logging of pH and temperatures were initiated when the pump was switched on. The system was first pumped with distilled water for approximately 30 minutes to reduce initial temperature fluctuations in U-tube and bulk. Solutions from the reactant reservoirs were then brought into the reactor at a

constant flow rate and temperature. The peristaltic pumps ensured a flow of approximately 210 g/min from each of the reservoirs.

Throughout the experiments the reactor pH was continuously monitored along with temperatures of U-tube inlet/outlet, reactant inlet and reactor bulk. The pH-probe was regularly washed in 0.50 mol/L of hydrochloric acid to remove eventual scale on the sensor. Bulk samples were extracted regularly in some of the tests with MEG to check for possible precipitation of solid particles.

At the end of each experiment the thermostatic units, agitators and pumps were shut off and the U-tube was carefully removed from the reactor as soon as possible to prevent further deposition of scale and polymorphic transformation (as discussed in Section 2.6.3). The reactor was then emptied and cleaned. Deposited scale on the inside of the reactor was removed through stirring with 0.50 mol/L hydrochloric acid. The entire inside of the vessel, as well as the Y-tube mixer, was washed with acid and then deionized water. Visual inspection and measurement of pH followed to ensure that all scale/foreign particles had been removed and the acid completely neutralized. The U-tube was washed using the same procedure after all the analyses were completed. Remaining liquid in the tubing was pumped back into the reservoirs in order to get an accurate measurement of reactants consumed.

3.5 Analysis

The scaled tube was dried for two days (selection based on a discussion in Appendix D) and weighed on a Mettler Toledo AB204-S scale accurate to four decimal places (100 µg) to determine the total mass of deposited material. It was also attempted to visually account for non-scaled regions when calculating mass deposited per area.

Deposited scale on the metal tube was then analyzed using a Hitachi S-3400 N scanning electron microscope (SEM). The U-tube was placed on a specially designed plate to keep it in a locked position without removing the scale. Some small areas were scraped off in order to measure the thickness of the layer, while the rest remained intact to inspect uniformity of the scale. No coating was applied due to possible loss of topographic information. Back scattering electrons in low-vacuum mode was normally used as method of analysis. This was done to eliminate charging of the deposited brine and produce clearer images. Voltages of 10.0-15.0 kV and a probe current of 40.0 mA were normally applied with a working distance of approximately 8.00 mm.

The SEM analysis gave an indication of polymorphs present in the scaled layer. This was then qualitatively determined through XRD analysis of the experiments where a sufficient amount of solid material could be scraped off the tube. The sample was mortared and wetted with ethanol. A few drops of this crystal slurry were then transferred to a crystal silicon sample holder. When the ethanol had vaporized, the sample was analyzed in a D8 Focus XRD unit with a LynxEye detector. Bragg Brentano mode with Cu-K radiation was used, and the sample was scanned from 18 to 75°.

The extracted bulk samples were vacuum filtrated and analyzed with SEM to check for possible precipitation of solid particles.

4   Results and Discussion

This work has focused on the growth of a scaled layer on a heated surface in a flow-through system. A set of parameters have been adjusted separately to study their effect on the morphology, polymorphism and growth rates of this layer. These parameters include: Weight percentage of Mono Ethylene Glycol (MEG); temperature of the heated surface (U-tube); and supersaturation level in the solution.

The growth of scale on a surface can be measured and labeled in numerous ways. Results presented in this work are often given as overall growth rate ($kg/m^2 \cdot s$). These rates have been calculated based on weight of scale, estimated surface area and the duration of the experiment. The experiments with a pure de-ionized water solvent at a tube temperature of 90°C have been conducted with several parallels to check reproducibility. The included double standard deviations have been calculated as shown in Appendix D. Analyses with SEM indicated that the scaled layer thickness were not uniform enough to calculate a linear growth rate (m/s).

A complete collection of SEM results have been shown in Appendix G, and the presented pictures display the scale on the tube taken from above, unless stated otherwise. Polymorphisms of calcium carbonate indicated in SEM were confirmed with XRD analysis. These results are included in Appendix H.

Temperature of tube, reactant-inlet and bulk were logged continuously throughout the experiments along with bulk pH. The collected data were edited to remove fluctuations during electrode cleaning and time adjusted to reflect pump duration. The raw data have been plotted and shown in Appendix I. The experiments are referred to according to experimental date and parameter values.

4.1   Setup verifications and definitions

The experimental setup was based on the work done by Nergaard (2011). Some procedural changes were made to this setup in addition to the modifications used in the specialization project work of fall 2012 (Hyllestad, 2012). Some initial tests have therefore been used to verify it.

4.1.1 Definition of experimental parameters

The calculated supersaturation levels (S) used in the experimental section is the initial supersaturation of the bulk solution directly after the reactants have been mixed. It is based on a bulk temperature of 30°C and the formation of pure calcite. This supersaturation will henceforth be referred to as the inlet supersaturation and given with one decimal. Different surface growth site conditions; consumption of reactants; and their effect on this parameter will be further discussed in Section 4.1.3 and 4.3. The setpoint for temperature on the inside of the U-tube will be symbolized with T_{Tube} and the concentration of MEG will be given in terms of weight percentage.

4.1.2 Parameter control

Carbonate ions can precipitate as $CaCO_3$, form bicarbonate ions, or evaporate as CO_2 (shown in equations (18)-(21)). A stable pH in bulk solution throughout the experiment indicates that the level of carbonate ions in the reactor is constant (see Figure 2.5). Calcium will only be present as ions or solid calcium carbonate in this system and is therefore directly related to consumption of carbonate ions.

With a constant level of calcium and carbonate ions, the activities of ions in the bulk solution are expected to remain stable for a given temperature. From the expression in equation (24) it is understood that the supersaturation in bulk will remain constant with a stable pH. The effect of temperature on supersaturation will be further discussed in Section 4.1.3 and 4.3.1.

Fluctuating pH-levels were observed in the project experiments of fall 2012 (Hyllestad, 2012). Additional stirring of reactant reservoirs was therefore included in the experimental procedure to ensure uniform mixing. The effect of this can be observed in Figure 4.1. The vertical line in the graph represents a change in batch reservoir.

The experimental procedure was changed to include a step with continuous flow of water through the system before the pumping of reactants was initiated. This was done to give more accurate pH-signals as the temperature compensation in the pH-meter is slow. A similar overshoot was seen in the logged temperature data and disappeared after introducing this step, shown in Figure 4.1.
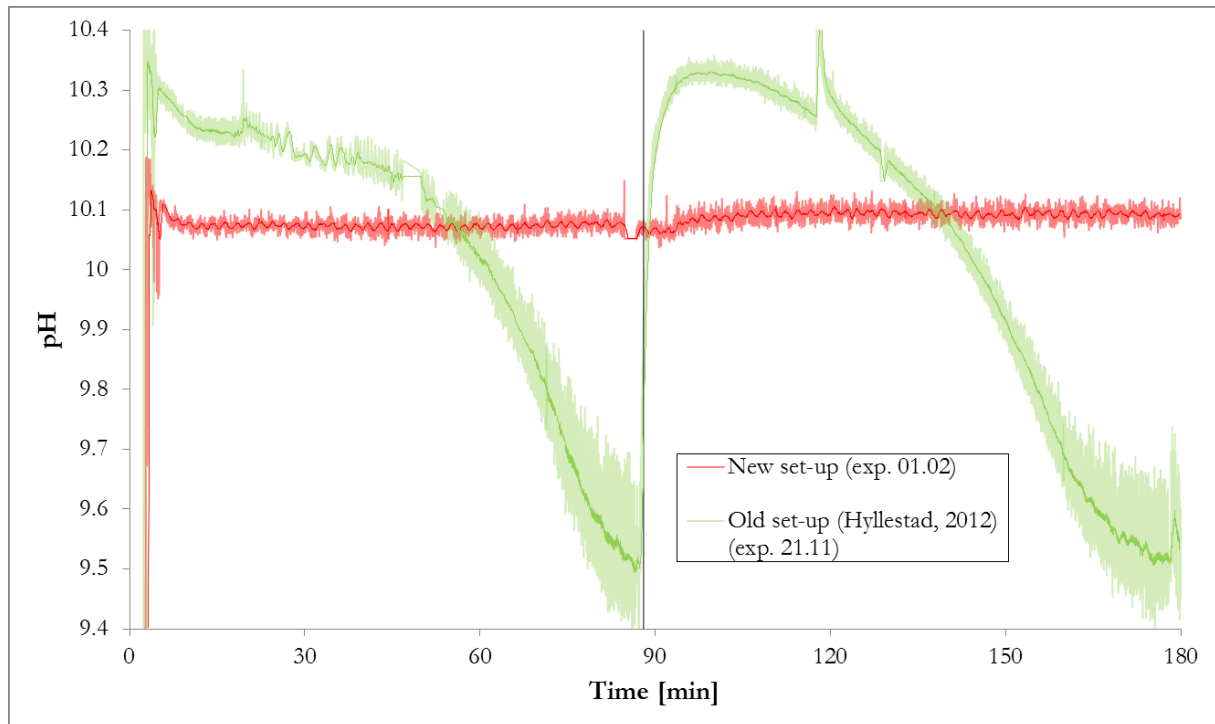
Figure 4.1: Graphical plot of pH data from bulk solution with old and new experimental procedure (S=4.5, T_{Tube}=90°C).

To ensure constant supersaturation, nucleation in the bulk solution should also be avoided. The formation of solid particles in bulk will consume ions from the solution and reduce parameter control on the tube growth site.

It is highly probable that the supersaturation level of the bulk solution was reduced in the start of the experiments due to residence time distribution, as discussed in Section 2.8. The average bulk residence time in these experiments were calculated to be 5.2 minutes as shown in Appendix C.2. Steady-state conditions involve constant parameters over time, which were expected to be achieved shortly after one residence time. This can be seen in Figure 4.1, were a constant pH was observed after approximately 7.0 minutes.

4.1.3 Referred supersaturation

The calculated inlet supersaturation was, as previously discussed, based on an approximate temperature of the bulk solution (30°C) and the formation of pure calcite. The temperature at the growth site on the tube surface (skin-temperature) would, however, be much closer to the tube set-point of 50/90°C.

With the skin-temperature and the quantity of polymorphism being different from the values used for bulk supersaturation calculations, the referred supersaturation

level on the crystal growth site would be different from the levels referred to in the experimental section. The supersaturation in the bulk solution would also be influenced by the consumption of ions per time in the reactor.

Equations (28)-(31) have been used with calculated MultiScale data to find supersaturation levels for calcite, aragonite and vaterite at different temperatures, shown in Table 4.1. The reduced supersaturation at elevated temperatures can possibly be explained from the complete system of equilibrium equations impacting the calcium carbonate system (shown in Section 2.6). Kinetics are changed by an increase in temperature, which might cause a different set of reactions to be significant at elevated temperatures.

The scaled layers will rarely consist of only one polymorph. Calculation of actual supersaturation levels, without knowing the exact skin-temperature and quantity of polymorphs, will therefore remain simplified estimates.

Table 4.1: Supersaturation level at a point based on temperature and polymorphism

Temperature [°C]	$S_{Calcite}$	$S_{Aragonite}$	$S_{Vaterite}$
30	6.0	5.1	3.2
40	5.9	5.0	3.2
50	5.7	4.9	3.2
70	5.5	4.8	3.2
90	5.5	4.8	3.3

The morphology of the different polymorphs is very different. Aragonite forms needle shaped tree-like structures (illustrated in Figure 4.3), calcite forms cube-shaped particles and vaterite normally forms plates or spherulites.

The large difference in structure of the various polymorphs could correspond to significant variation in physical properties of the scaled layer. For example, aragonite forms a more open structure than calcite which therefore results in a higher porosity. This open structure can contain an amount of stagnant water which reduces the heat transfer from tube to bulk and therefore skin-temperature. The growth rates of the different polymorphs also vary which makes it difficult to compare overall growth rates of scale layers composed of more than one polymorph. Comparison of the overall growth rate of scale layers with variable polymorphic quantity is therefore complicated.

4.2 Experimental approach with MEG as solvent

MEG was introduced to the system after several preliminary experiments with de-ionized water as solvent. Two important visual observations were made in the first MEG experiments: The bulk solution appeared turbid when MEG was introduced and no scale appeared to deposit on the heated U-tube surface.

4.2.1 Initial experiments with MEG solvent

The first two experiments were done with a supersaturation level of 6.0, tube temperature of 90°C and MEG concentrations of 50wt% and 70wt%.

Samples were extracted from the bulk of these experiments both before and after the addition of MEG to investigate for bulk nucleation. Analysis with SEM indicated that no solid particles had precipitated in the solution (included in Appendix G, Figure G.1). It was therefore concluded that at an inlet supersaturation level of 6.0, bulk nucleation is negligible with these solvent compositions.

Bulk nucleation makes it harder to control actual supersaturation level at the growth site, and is therefore undesirable in such experiments. The appearance of turbidity in MEG containing solutions can be explained from the solvents mixing with air and the physical properties of MEG. This was based on the observation that the effect disappeared when the agitator was turned off.

The heated U-tubes from these experiments were then investigated with SEM. This analysis showed no deposition of solid particles with a MEG concentration of 50wt% (Figure 4.2a). An increased concentration of MEG (70wt%) resulted in the formation of a few crystals of vaterite (Figure 4.2b). However, the majority of the tube did appear to be non-scaled. It should be noted that particles of nano-size would not be observable with this apparatus.
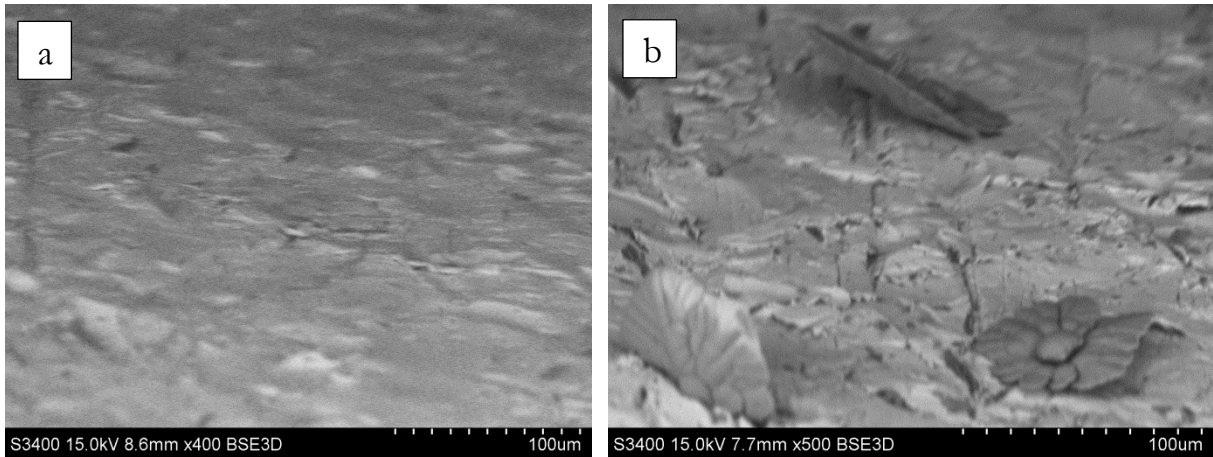
Figure 4.2: SEM pictures: a) S=6.0, T_{Tube}=90°C, 90 min, MEG=50wt%, x400 enlargement (exp.: 05.03) b) S=6.0, T_{Tube}=90°C, 90 min, MEG=70wt%, x500 enlargement (exp.: 26.02).

An experiment with increased inlet supersaturation (S=12.3) showed that scale can form on a non-scaled metal surface with solutions containing MEG. At this elevated level of supersaturation there was, however, a degree of bulk precipitation observed in the reactor at the end of the experiment.

4.2.2 Combined approach

Precipitation and growth of scale is often separated into regions/steps in literature (Bott, 1995, Rankin and Adamson, 1973). The formation of an initial uniform layer on which subsequent growth can continue was discussed in Section 2.7. The lack of scale formation in the presented MEG experiments indicates a long initiation period at a supersaturation level of 6.0. This does not necessarily involve a reduced growth rate on top of this initial layer.

It was therefore decided to create an initial uniform layer of scale from a solution without MEG. This pre-scaled tube would then be used as a basis for further growth. The initial period of scaling in a supersaturated water solution will be referred to as the pre-scale period when the objective of this formation is to create a layer for further growth with different parameters.

Initial experiments with a solution supersaturation level of 6.0 and a tube temperature of 90°C gave a uniform layer of almost exclusively aragonite after 90 minutes (Figure 4.3). The results from XRD-analysis have been included in Figure H.1, Appendix H. Quantification of polymorphism in this layer proved difficult, but a purity of 99.4% aragonite was found with similar parameters in the work done by Nergaard (2011). This result has been shown in Table H.1, Appendix H.

The introduced sets of parameters were selected based on negligible bulk nucleation and a complete surface coverage after a relatively short period of time. They were then selected as a reasonable set of parameters to form a pre-scale layer in later experiments. Formation of a pure aragonite layer also made it possible to calculate growth rate of this polymorph.

The tube was not dried between the pre-scale period and the subsequent growth period. The process of drying a scaled tube and then reinserting it into an agitated solution could make some of this initial layer undesirably peel off from the surface. A group of experiments were therefore used to determine the mass deposit per area of the pre-scaled layer with the previously discussed parameters. Reproducibility was sought in these experiments as the results would later be applied in the calculations of growth rates in the MEG solutions. Average weight data from four experiments were used to estimate an overall growth rate of scale in the pre-scaling period to $5.36\pm0.18\cdot10^{-6}$ kg/m$^2\cdot$s and a mass deposition per area of $2.90\pm0.10\cdot10^{-3}$ g/cm^2. The results have been given with a double standard deviation as calculated in Appendix D.
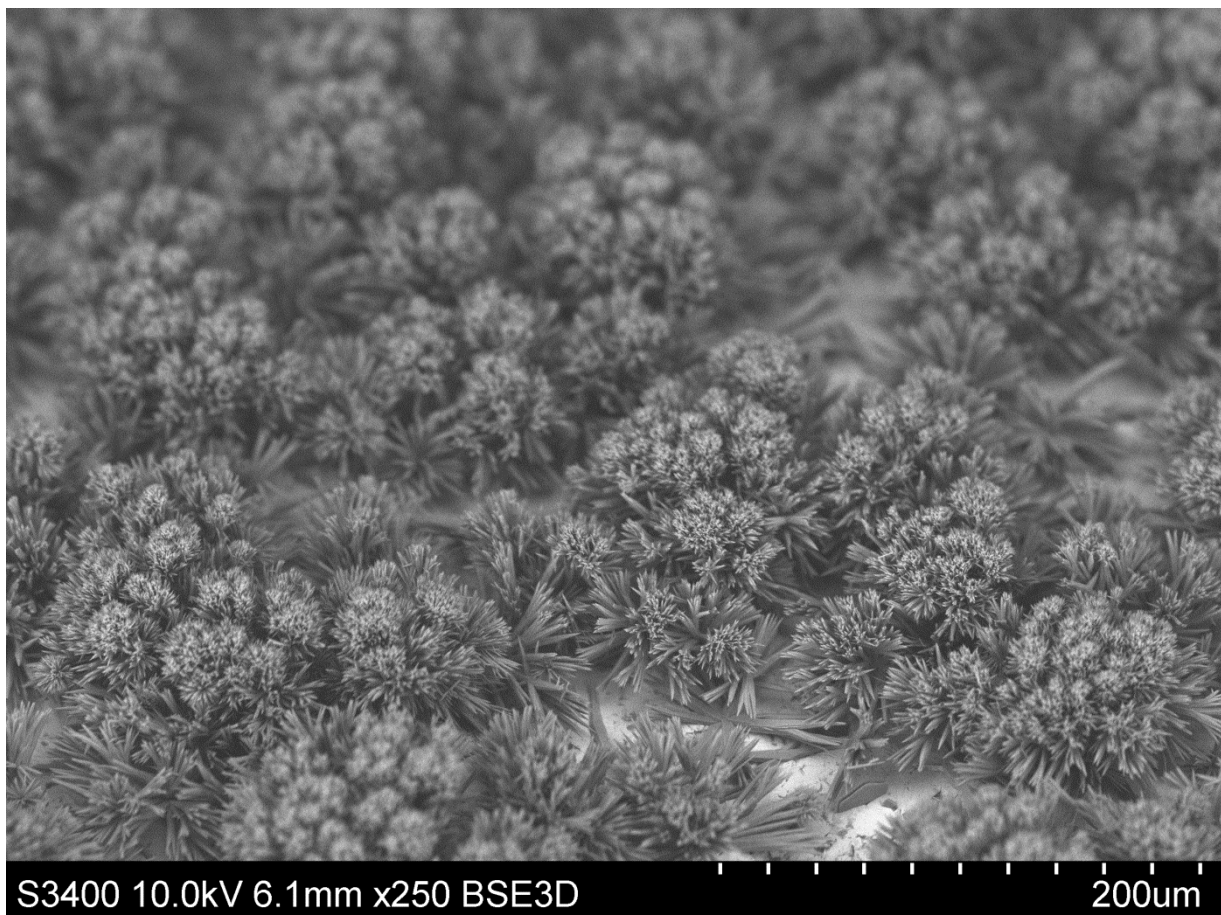
Figure 4.3: Formation of a uniform pre-scale layer of mainly aragonite from a supersaturated solution with water as solvent, S=6.0, T$_{Tube}$=90°C, 90min.

Experiments with crystal growth in a MEG solution on top of a pre-scaled layer indicated reduced growth. This will be further discussed in Section 4.4. The growth was not negligible opposed to the experiments without a pre-scale period. This confirms a long initiation period in MEG solutions at an inlet supersaturation level of 6.0.

The increased period can be explained from the differences in physical properties of MEG and water. The initiation period of a scale layer on a heated surface is associated with the heterogeneous nucleation and therefore the supersaturation, temperature, interfacial tension and viscosity of the solvent (as discussed in Section 2.7). When reduced growth was observed in experiments with variable solvent composition but constant temperature and supersaturation, it was therefore concluded that the differences of viscosity and surface tension of MEG and water (shown in Appendix B, Table B.2) increases the initiation period of scale in solvent solutions with MEG. The influence of physical properties of the solvent has been discussed further in Section 4.4.

4.3   Experiments in water

Supersaturation is, as described in Section 2.3, the driving force of crystallization. Thermodynamically, growth of crystals can be expected at supersaturation levels above 1. Kinetically, a further increase in this parameter is expected to elevate the rate of deposition. This will be studied in this section along with the insulative capabilities of the generated scale layer.

The supersaturation levels referred to in the experimental section are different from the levels experienced at the growth site. The effect of variation in temperature and polymorphism was briefly introduced in Section 4.1.3, and will be discussed further throughout this section. Variations in flow rate of reactants also had an effect on actual supersaturation. This did, however, prove to be very small, as shown in Appendix C.2.

4.3.1 Insulating effect of the scale deposit

The heated U-tubes in the experiments were placed in a supersaturated bulk solution. The temperature on the inside of this tube was higher than on the outside resulting in a heat transfer from tube to bulk, as discussed in Section 2.8. Temperature was logged as it entered and returned from the U-tube and the insulating effect of a scaled layer can be observed from the experimental data.

Two different levels of inlet supersaturation were studied for effect on scale growth, 4.5 and 6.0. The temperature data from these experiments have been compared with a control test of pure water as shown in Figure 4.4. The inlet temperature of pure water was not included in the graph for easier readability.
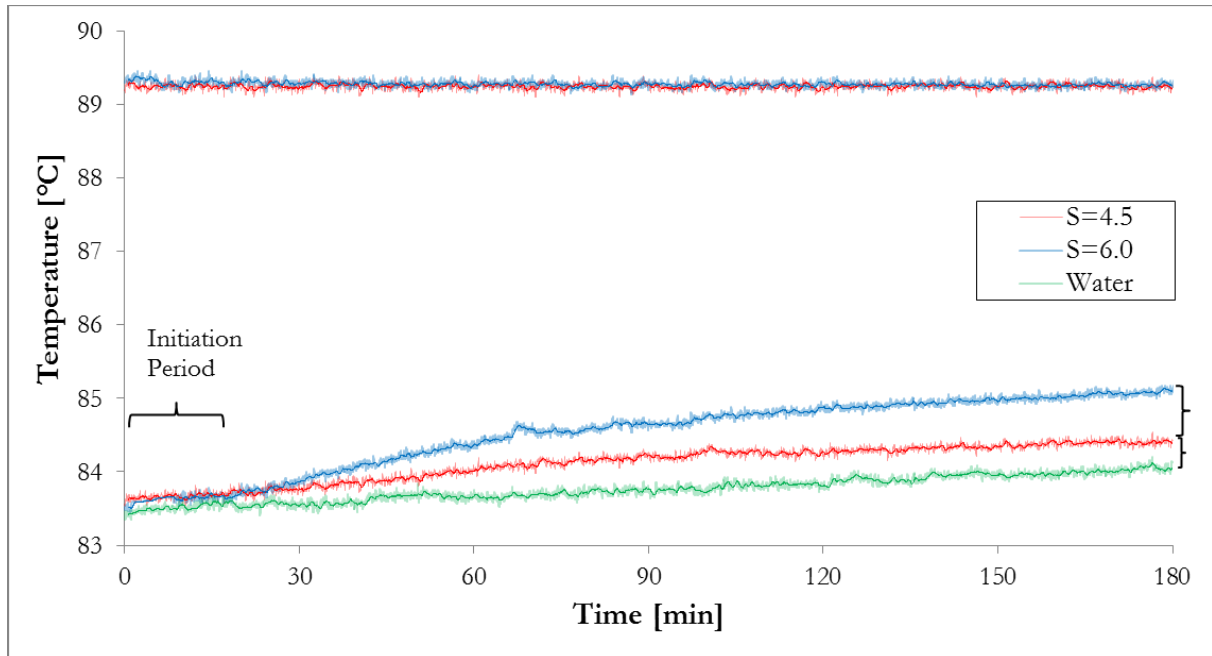
Figure 4.4: Temperature inlet/outlet of U-tube for solutions of S=4.5, S=6.0 and water without added salt at T$_{Tube}$=90°C, (exp.: 22.02, 13.03 and 14.05).

Figure 4.4 shows how an increased supersaturation results in a higher return temperature from the heated tube, due to a reduced heat transfer. This indicates a thicker scale layer, which was confirmed through SEM analysis (Appendix G, Table G.1). The figure also illustrate how it takes some time before the effect of a supersaturated solution becomes visible compared to flow of pure water (no scale). This delay could possibly be an indication of the initiation period with pure water as solvent. From Figure 4.4 this appears to be approximately 15 minutes, with the parameters and experimental setup of this work, but additional testing is required before a conclusion can be made.

The insulative effect of a scaled layer can also be observed in the bulk temperature data. A reduced heat transfer from the tube also lowers the temperature of this solution. A graphical plot comparing solutions of variable inlet supersaturations with flow of pure water has been included in Figure 4.5. The vertical lines in the graph represent change of batch reservoir.
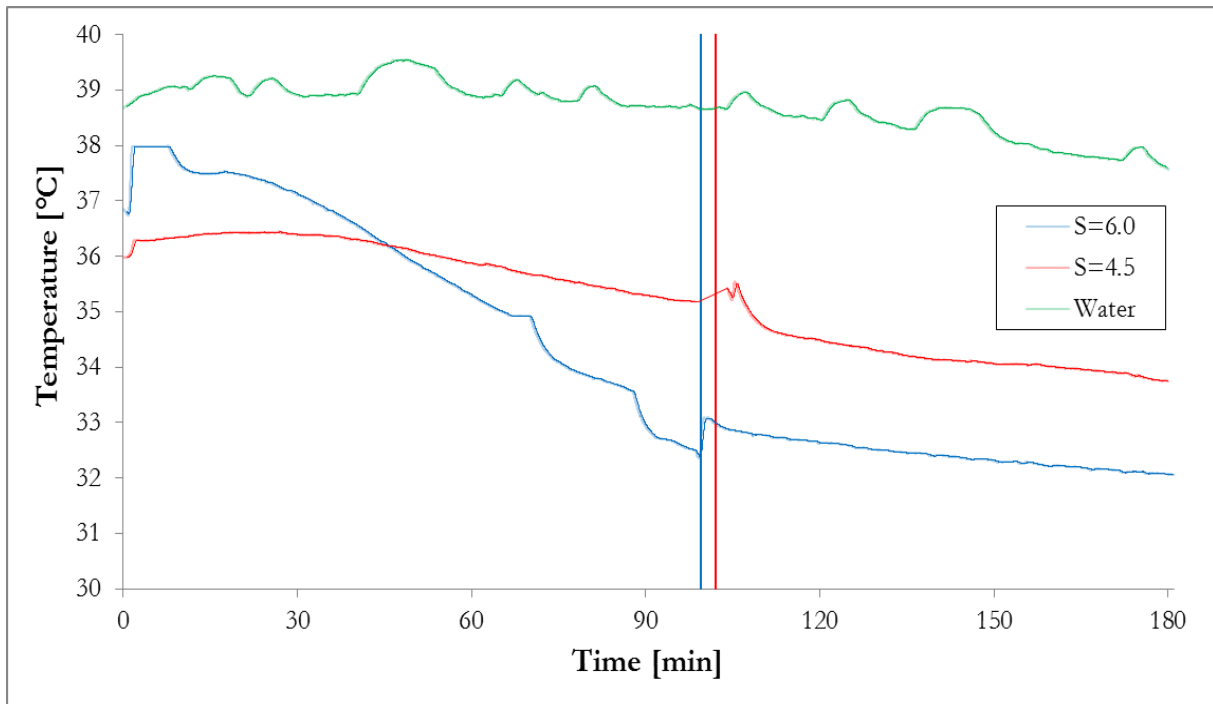
Figure 4.5: Graphical plot of bulk temperatures with solutions of S=4.5, S=6.0 and water without added salt at T$_{Tube}$=90°C, (exp.: 22.02, 13.03 and 14.05). The vertical lines represent change of batch reservoir.

Figure 4.5 confirms the observation of reduced heat transfer with increased inlet supersaturation as shown in Figure 4.4. The temperature peaks observed directly after changing the batch reservoirs are a result of a short stop in reactant flow into the reactor. This results in a momentarily increase of residence time and therefore more contact time with the heated surface.

An increased return temperature of the U-tube and a reduced bulk temperature was also observed in the test with pure water. This can be explained from the effect of several heat contributions into the system. The heat transfer from the U-tube into the bulk will approach a steady-state value with time, but this is influenced by the temperature of the surrounding environment and regulation of temperature in the reactor jacket/U-tube.

It has been shown how an increased supersaturation results in a reduced bulk temperature and an increased return temperature of the metal tube. This is believed to be caused by the formation of a thicker scale layer with insulative properties. The reduced heat transfer will also lower the temperature on the surface of the scaled layer (skin-temperature), which is where crystal growth takes place.

The reduced skin-temperature affects the growth rate in two different ways. The growth constant in the expression for growth rate (equation (15)) is a function of

40

temperature on the growth site. When this temperature is reduced, the rate of growth is also reduced.

Growth rate is also a function of supersaturation. The deposited layers in these experiments mainly consist of calcite and aragonite. The actual supersaturation on the growth site is therefore elevated with reduced surface temperature as shown in Table 4.1.

As the thickness of the layer increases, the two effects described above oppose each other at the pH level studied. The reduced skin-temperature decreases the growth rate directly, but increases it indirectly through increasing the supersaturation. Weight data should therefore be used to conclude on the effect of a thicker layer.

4.3.2 Overall growth rate

To investigate how a thicker scale layer affects the overall growth rate, experiments were done with a time magnitude of both 90 and 180 minutes at an inlet supersaturation level of 6.0 and an inside tube temperature of 90°C. With an increased experimental length and constant parameters, more solids would deposit on the surface and the effect of a thicker scale layer on further growth could be measured.

Overall growth rate describes the mass deposited per area and time and is assumed to be constant all over the surface at any given moment. Results showed that the average overall growth rate decreased by 3.8% when the experimental length was adjusted from 90 to 180 minutes (from $5.36\pm0.18\cdot10^{-6}$ kg/m$^2\cdot$s to $5.16\pm0.12\cdot10^{-6}$ kg/m$^2\cdot$s). These results are compared graphically with MEG solvent data in Section 4.4.3.

Nergaard (2011) observed an average and constant overall growth rate of $3.5\cdot10^{-6}$ kg/m$^2\cdot$s with approximately the same bulk temperature, inlet supersaturation and tube temperature. The average residence time was significantly shorter (3.2 min compared to 5.2 min in this work). Increased residence time should normally have the opposite effect as actual supersaturation is expected to be reduced with the increased consumption of ions this implies. However, the pumping of reactants was more unstable in the work done by Nergaard (2011), which could explain the difference.

The presented results indicated an effect of scale thickness on overall growth rate of scale at an inlet supersaturation of 6.0 and a tube temperature of 90°C. Further research on this is recommended before a definite conclusion can be made.

4.3.3 Effect of increased supersaturation

The solubility product of calcium carbonate is constant for a given temperature. An increase in supersaturation will therefore result in more available reactants in the solution, and more scale formed. An increased overall growth rate is expected with elevated supersaturation from equation (15).

Temperature data and SEM analysis have indicated how increasing the inlet supersaturation from 4.5 to 6.0 creates a thicker scale layer with insulative properties. Weight data confirmed this trend as illustrated in Figure 4.6. Experimental results showed how the overall growth rate increased from $2.6 \pm 0.3 \cdot 10^{-6}$ kg/m$^2 \cdot$s to $5.16 \pm 0.12 \cdot 10^{-6}$ kg/m$^2 \cdot$s with an experimental length of 180 minutes and the parameters mentioned above. This represents an increase of 95%.

Reproducibility was important in these experiments; several parallels with the same set of parameters were therefore completed. The overall growth rates included in this section reflects an average value from such a set of experiments with a double standard deviation as calculated in Appendix D. The error bars in the graphical plot indicates maximum and minimum values from the data sets. The results from the experiments with an inlet supersaturation level of 6.0 were, however, so similar that the error bars are not visible in the plot.

The scaled layer covered the entire surface of the tube after 180 minutes both at S=4.5 and S=6.0. With de-ionized water as solvent and an inside tube temperature of 90°C, this layer consisted of almost exclusively aragonite, as discussed in Section 4.2.2. This was necessary for a comparison of the overall growth results. A complete collection of growth rates calculated has been included in Appendix C.3. No significant differences in morphology/polymorphism were observed for this change in inlet supersaturation, but the quality of the SEM images were also quite poor for the experiments at S=4.5 (as shown in Figure G.2, Appendix G).
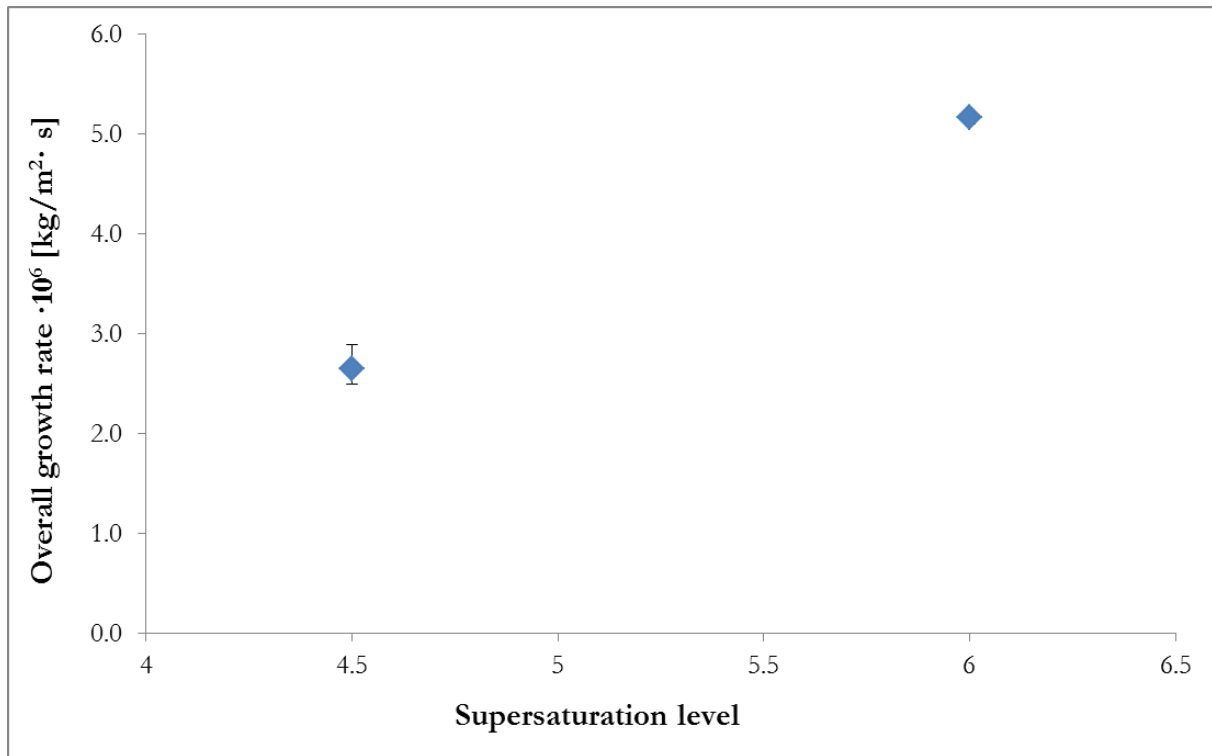
Figure 4.6: Calculated average overall growth rates as a function of inlet supersaturation at T_{Tube}=90°C and an experimental duration of 180 minutes. Error bars marks the maximum and minimum growth rates found in the series of experiments.

Similar studies in literature have also concluded on a general increase in growth rate of scale with supersaturation, when the solvent consists of pure water (Hasson et al., 1968, Nergaard, 2011). The overall growth rate observed at an inlet supersaturation of 6.0 was compared with literature values in Section 4.3.2 (Nergaard, 2011).

From the presented results it can be concluded that increasing the inlet supersaturation level from 4.5 to 6.0 at T_{Tube}=90°C results in an elevated growth rate and the formation of a thicker scale layer. Increased thickness then lowers the heat transfer from the inside of the tube which makes equipment such as heat exchangers less efficient.

4.3.4 Impact of heating medium temperature

The effect of a temperature change on the growth site of the scale surface was discussed in Section 4.1.3 and 4.3. In this section, the impact of changing the temperature setpoint of the tube will be focused.

Literature has found that calcite is more likely to form at low temperatures and aragonite at high temperatures (Ogino et al., 1987). A decreased tube temperature also leads to a reduced surface temperature which is therefore expected to change the polymorphism of the scaled layer. Experiments with a set temperature of 50°C and 90°C have been used in this work to study the effect of a temperature change on the growth of scale.

The formation of almost exclusively aragonite at a tube temperature of 90°C was briefly discussed in Section 4.2.2 and 4.3. This can be explained from kinetic control and the higher growth rates of aragonite compared to calcite/vaterite (Flaten et al., 2009). Figure 4.7 illustrates how the polymorphism of the scale layer is affected by a change in temperature of the heated surface.
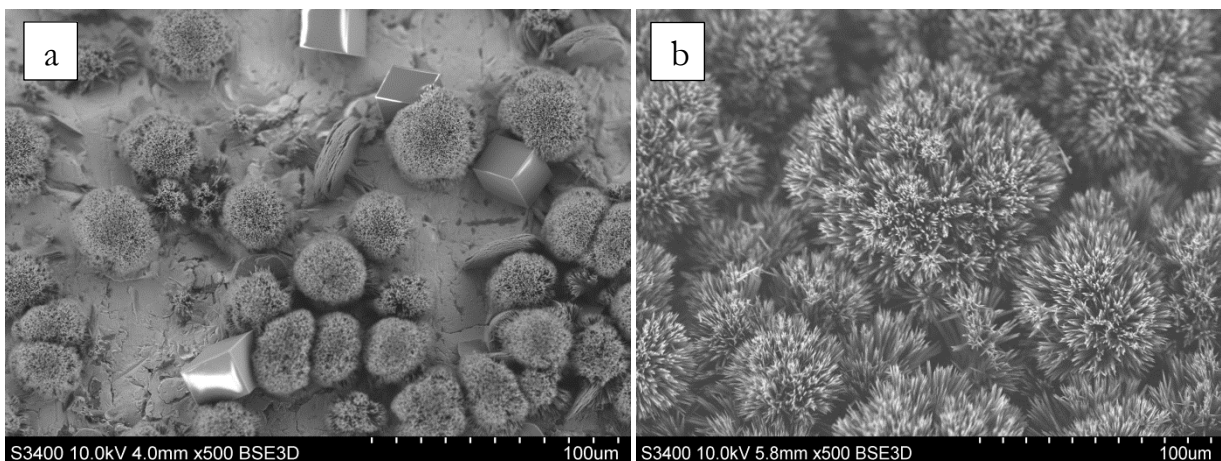
Figure 4.7: SEM pictures at an inlet supersaturation of 6.0 and an experimental length of 180 minutes: a) T_{Tube}=50°C b) T_{Tube}=90°C.

The SEM pictures clearly show how aragonite (needle shaped), calcite (cube) and vaterite (plate) can all be found with a tube temperature of 50°C, while almost exclusively aragonite is formed at 90°C.

The XRD data confirmed the observations made with SEM analysis. Formation of a uniform layer of aragonite at 90°C and a more mixed composition at 50°C was also found in literature (Ogino et al., 1987, Nergaard, 2011). The X-ray diffraction analysis data from this work was then compared with literature values to illustrate reproducibility (shown in Appendix H, Figure H.2 and Figure H.3). Quantitative

analysis of the polymorphic distribution proved to be too difficult with the samples collected from these experiments, but the results obtained by Nergaard (2011) at similar conditions have been included in Table H.1, Appendix H.

The growth rate of calcium carbonate will be affected in several ways when the tube temperature (and therefore also skin/bulk temperature) is reduced. The solubility product increases (shown in Section 2.6.3, Figure 2.7); the growth constant (K_g) in the growth rate expression (equation (15)) decreases; and the actual supersaturation on the growth site will be increased. The first two effects have a reducing effect on scale growth, while the latter will elevate growth rate as discussed in Section 4.2.

The overall growth rate of scale with different polymorphs cannot be directly compared due to differences in heat transfer and growth rates as discussed in Section 4.1.3. Significant differences were observed in polymorphism of the scale at the two different temperatures. The experiment with a tube temperature of 50°C did not achieve complete surface coverage as shown in Figure 4.7 and comparisons of growth rates for the two different tube temperatures were therefore not possible.

However, it can be concluded that a reduced tube temperature decreases the mass deposit of scale. Figure 4.8 illustrates the effect of tube temperature on the deposition of solid material. The deposition per area was observed to decrease by 79% when the tube temperature was changed from 90°C to 50°C at an inlet supersaturation level of 6.0 and an experimental length of 180 minutes (from $5.58 \pm 0.13 \cdot 10^{-3}$ g/cm^2 to $1.19 \cdot 10^{-3}$ g/cm^2). It was therefore concluded that the contributions to a decreased growth are larger than the opposite when the temperature is reduced from 90°C to 50°C at this supersaturation level.
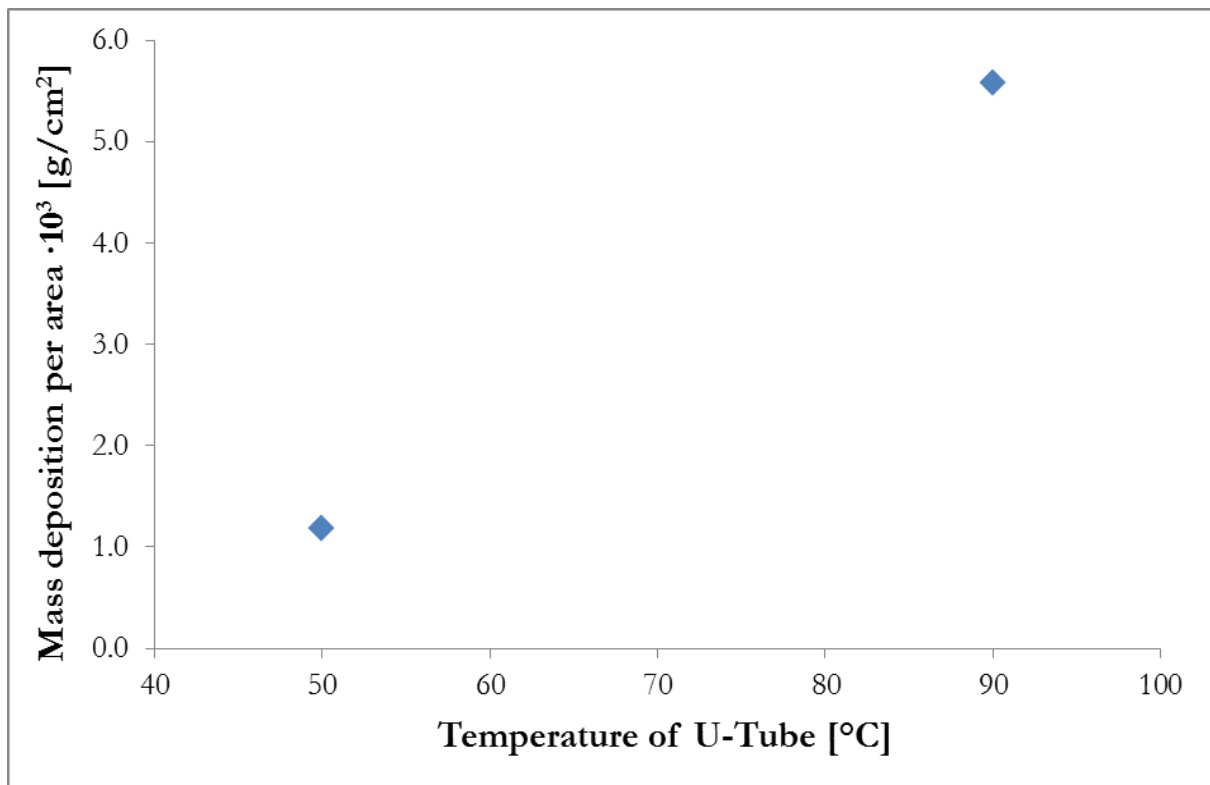
Figure 4.8: Mass deposition of solids per area as a function of temperature of the heated surface. Error bars have been included for the experiment at 90°C, but these where to small to be visible on the graph.

4.4 Experiments with variable solvent composition of water/MEG

The impact of supersaturation and temperature on scale growth rate and polymorphism for solutions with de-ionized water as solvent has been discussed in previous sections. In this section, experiments with MEG will be presented and the concentration varied to study its effect on growth and polymorphism of scale.

The time required for nucleation and crystal growth until a uniform scale layer developed has been defined as the initiation period. In Section 4.2 the addition of MEG to a system was shown to increase the induction period. In order to compare growth rates of subsequent layers independently, a pre-scaled layer of aragonite growth was first formed and subsequently used to compare the effect of varying MEG concentration on further crystal growth.

4.4.1 Heat transfer from tube to bulk solution

In Section 2.8 and 4.3.1 it was discussed how heat is transferred from the inside of the U-tube into the bulk solution due to a difference in temperature, with constant mass and heat capacity of the heating fluid (water). In this section, the effect of solvent composition on heat transfer rate will be discussed.

Figure 4.9 shows a graphical representation of the return temperature from the U-tube in experiments with variable solvent composition. The heat transfer from the tube surface to the bulk was visibly reduced with increasing concentration of MEG. This can be explained from the heat transfer equations (34) and (35) and the increased viscosity of MEG compared to water (shown in Table B.2, Appendix B). The heat transfer coefficient of the bulk solution (h_{bulk}) is influenced by the bulk viscosity (η_{bulk}), as shown in equation (35). Increased concentrations of MEG will increase the viscosity of the bulk solution and therefore decrease the overall heat transfer from the tube, as shown in equation (34). The heat is then reflected back into the tube which increases the return temperature as observed in Figure 4.9. The increased resistance to convective heat transfer with MEG concentration also results in an elevated skin-temperature.
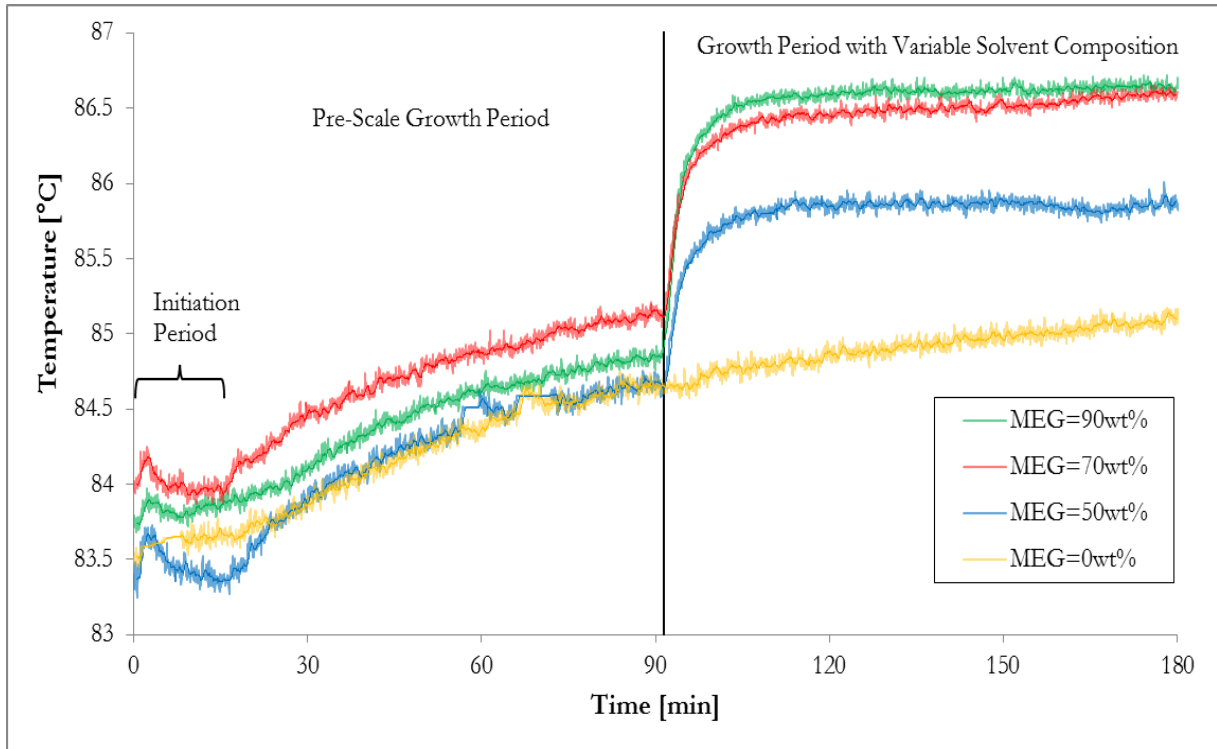
Figure 4.9: Graphical plot of return temperature from the U-tube in experiments with variable solvent composition (S=6.0, T_{Tube}=90°C). The first 90 minutes were done with pre-scale conditions, while the solvent was varied in the next 90 minutes as indicated in the figure legend. The vertical line represents the change in batch reservoir.

Variable initial temperature was observed in Figure 4.9. It was assumed that a relative comparison between the experiments could still be made since a vertical shift to an identical start-temperature would give the same trends with solvent composition as previously discussed.

The initial peaks in return tube temperature graphs indicate a temperature overshoot and the time needed to reach steady state in the bulk solution, as discussed in Section 4.1.2. This is then followed by an initiation period which is indicated by the horizontal trend in the figure. The following gradual increase in return temperature throughout the pre-scale period corresponds to a growing thickness of the scale layer which affects the thermal conductivity k_d (shown in equation (34)) and therefore the overall heat transfer from the tube to the bulk solution.

The vertical step in Figure 4.9 directly after changing from water to a MEG/water solvent can be explained from a different heat transfer coefficient in the bulk solution with variable solvent composition. The reduced slope after this period corresponds to the reduced growth rate of scale and heat transfer to the bulk phase in MEG solutions.

48

4.4.2 Mass deposition per area

Based on the literature, injection of MEG is generally expected to increase the scale growth rate and therefore also form thicker layers as the concentration increases. This is caused by a decrease in solubility with MEG addition, which then elevates the supersaturation level of the solution. This effect was counteracted by adjusting the concentration of reactants to study the separate effect of solvent composition.

At comparable supersaturation levels, the growth rate of scale is expected to decrease with weight percentage of MEG, as discussed in Section 2.7 (Flaten et al., 2010). The reactants were adjusted stoichiometrically to prevent the possibility of reagent limitation.

A graphical representation of the effect of increased MEG concentration on the growth of scale has been included in Figure 4.10. An average value has been calculated in the experiments with several parallels. Error bars are used to illustrate maximum and minimum results from the respective set of data. A comprehensive collection of calculated results has been included in Appendix C.3.

The portion of mass deposit in the pre-scale period was estimated from four separate experiments which were terminated after 90 minutes. This calculated mass deposit per area of $2.90 \pm 0.10 \cdot 10^{-3}$ g/cm^2 was then used to determine the portions of total scale deposit that corresponded to the water and mixed solvents part of the experiment, respectively. It should be noted that the error propagation of the entire experiment will therefore be at least the added error bars of the two periods combined.
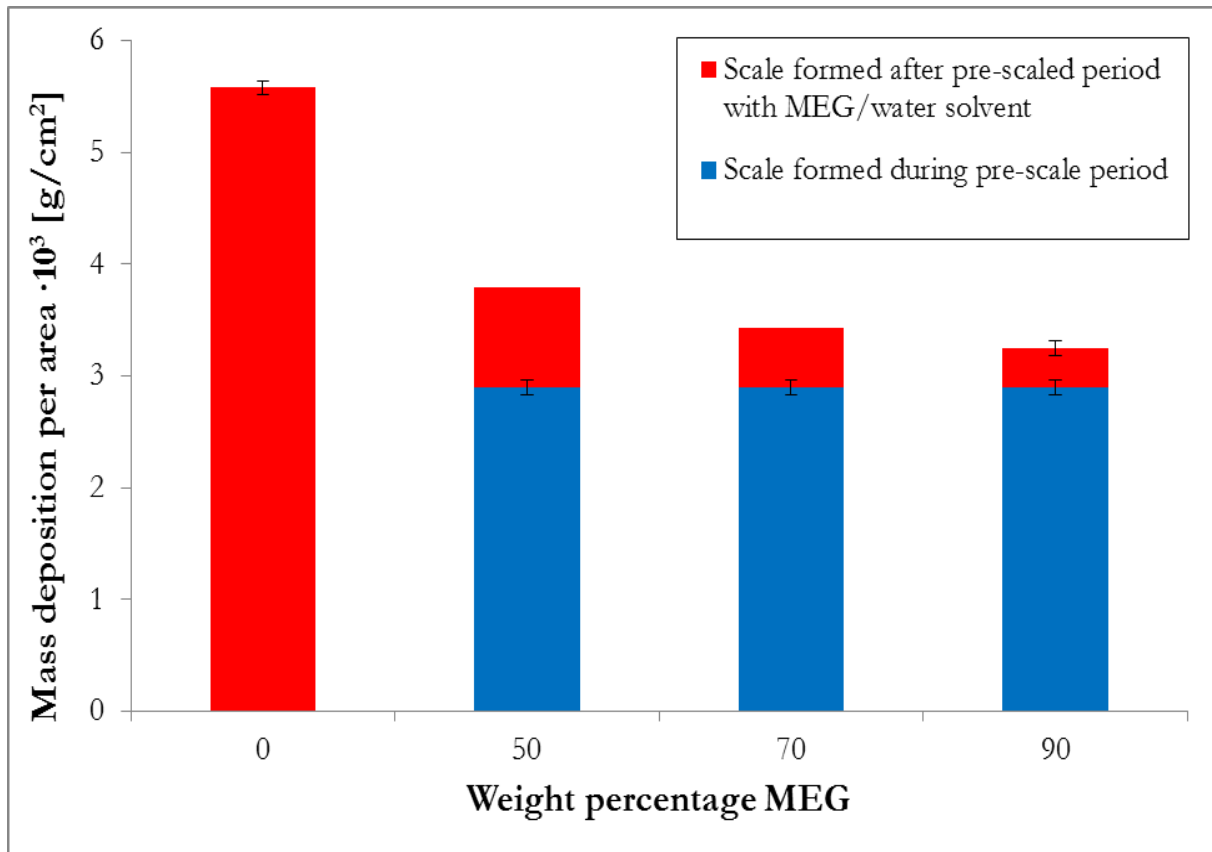
Figure 4.10: Graphical representation of mass deposition per area split into growth during pre-scale period and growth in solution with water/MEG solvent (S=6.0, T_{Tube}=90°C, 90+90 min). The abscissa shows the solvent mixture during the last 90 minutes of the experiments. The plot with 0wt% MEG represents the average of the two experiments with duration of 180 min and pre-scale conditions.

Figure 4.10 illustrates how the growth of scale was reduced with increasing concentration of MEG at an inlet supersaturation level of 6.0 and a tube temperature of 90°C. The mass depositions per area were measured to 0.90 mg/cm² (50wt% MEG), 0.53 mg/cm² (70wt% MEG) and 0.36 mg/cm² (90wt% MEG) after the pre-scale period. Reduction of calcium carbonate growth in solution with increased presence of MEG has also been observed in literature (Flaten et al., 2010, Beck et al., 2013).

The overall growth rate of scale per unit time could not be compared directly for the different solvent compositions, as the polymorphism of the layer varied with MEG concentration. This has been discussed further in Section 4.4.4.

The increased skin-temperature on the growth site with elevated MEG-concentration (showed in Section 4.4.1), at comparable supersaturation levels, should result in a higher growth rate of scale. The opposite observation was made

in this work, indicating a separate effect of the solvent on growth kinetics and/or growth mechanism.

The growth decrease can be explained from the physical properties of the solvent. The growth of scale is controlled by nucleation rate and growth rate as shown in equations (11) and (15). When the level of supersaturation, temperatures and agitation are kept at a constant comparable level, the physical properties viscosity and interfacial tension of the solvent become the main variable parameters.

MEG has a higher viscosity than water as shown in Table B.2, Appendix B. The viscosity of the bulk solution will therefore increase with concentration of MEG and decrease the diffusivity of ions. The impact on growth of scale depends on the determining growth mechanism in the respective solvent. The reaction/integration controlled (growth order of two) and diffusivity controlled mechanisms (growth order of one) were introduced in Section 2.5.2. From literature it has been shown that the growth order (symbolized with g in equation (15)) is approximately two in calcium carbonate solutions with pure water solvent, while it approaches a level of one in MEG-water solutions (Beck et al., 2013). This indicates that diffusion of ions from the bulk solution is the rate determining mechanism in experiments with MEG, which can explain the reduced scale growth with an elevated concentration of this co-solvent.

The increased viscosity in MEG can also affect the rate of growth through the growth rate constant K_g in equation (15). Flaten and co-workers (2010) showed that K_g declines with an elevated viscosity as shown in Figure 4.11. A higher viscosity will also decrease the rate of nucleation through the kinetic parameter Ω in equation (11). Reduced growth rate with MEG concentration can therefore possibly be explained from the change in viscosity.

It should be noted that the growth constant in Figure 4.11 is given in m/s, while it is referred to in terms of $kg/m^2 \cdot s$ in the rest of this work. The declining trend will, however, be the same.
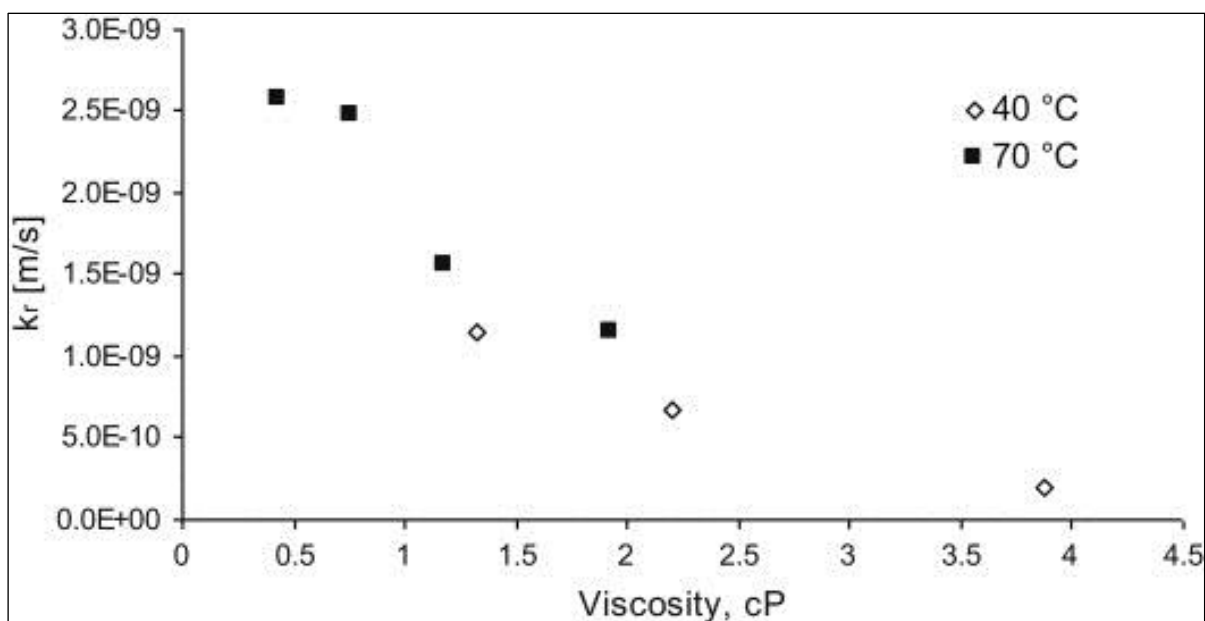
Figure 4.11: Growth rate constants as a function of viscosity (Flaten et al., 2010).

The effect of a change in interfacial tension with solvent composition has been discussed by Flaten and co-workers (2010). Contradicting results were found and it was concluded that the reduced growth in MEG could not be caused by changes in this parameter alone. Specific adsorption of solvent on the kink sites of the crystal surface could also be a possible explanation (Flaten et al., 2010). It is, however, beyond the scope of this work to investigate the specific behavior of MEG in the surface reaction.

Previous work has studied how the growth rate of calcium carbonate in the bulk of a batch reactor decreased with increasing concentration of MEG (Flaten et al., 2010, Beck et al., 2013). This work has showed how this trend is also observable on a heated surface in a continuous stirred-tank reactor. Polymorphism of the scaled layer will be discussed in Section 4.4.4.

4.4.3 Effect of scale thickness and heating medium temperature

A series of experiments were done with a MEG concentration of 50wt% and an inlet supersaturation of 6.0 to investigate the effect of scale layer thickness on growth in a MEG/water solvent. These experiments were done with a pre-scale period to overcome the prolonged initiation period in MEG.

With a comparable temperature and solvent composition, the polymorphic growth was assumed to be similar for the entire growth period. Based on the results from these investigations and the 90 minutes pre-scale experiments, the overall growth rate was therefore calculated for the time with a mixed MEG/water solvent. The

results are included in Figure 4.12 and show a steady decrease from the moment MEG was introduced into the system.
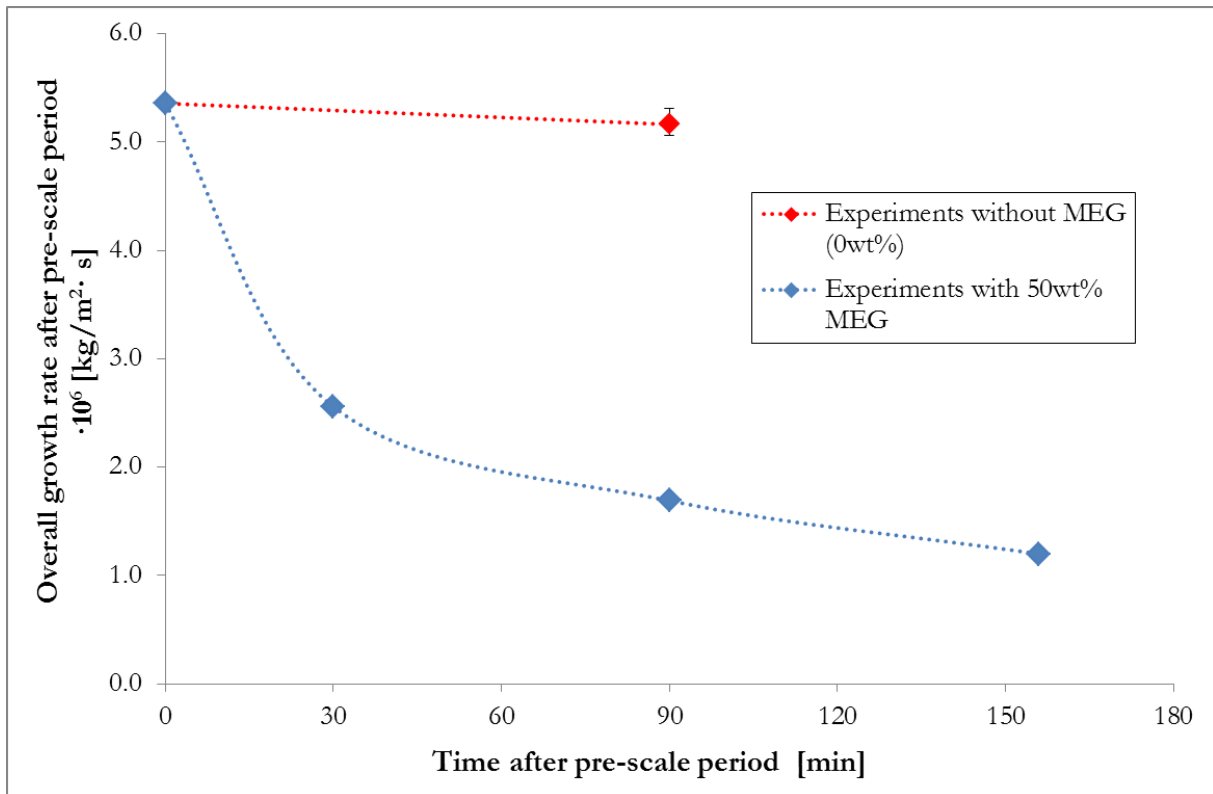
Figure 4.12: Schematic of overall growth rate as a function of time after the pre-scale period, S=6.0, T_{Tube}=90°C, MEG=50wt%/0wt%. The dotted lines are included for readability, but additional experiments could reveal a different trend.

The decline in overall growth rate was observably more pronounced in a MEG/water solvent than in experiments with pure de-ionized water. With comparable temperature and inlet supersaturation it is therefore likely that this can be explained from a change in the growth rate constant.

In Section 4.4.1 it was discussed how this constant is dependent on solvent viscosity, and equation (16) showed how it can be seen as an Arrhenius correlation with an exponential factor. It was also discussed how the skin-temperature increased in solutions with MEG. The exponential behavior with temperature could therefore result in a larger decrease in growth rate constant at the elevated skin-temperatures with a MEG solvent compared to a water solution.

A graphical representation of the tube set-temperature effect on the growth of scale in solutions with variable solvent composition has been included in Figure 4.13. Overall growth rate and mass deposit per area cannot be compared directly as the experiments with MEG solvent did not create a completely covered scale layer.
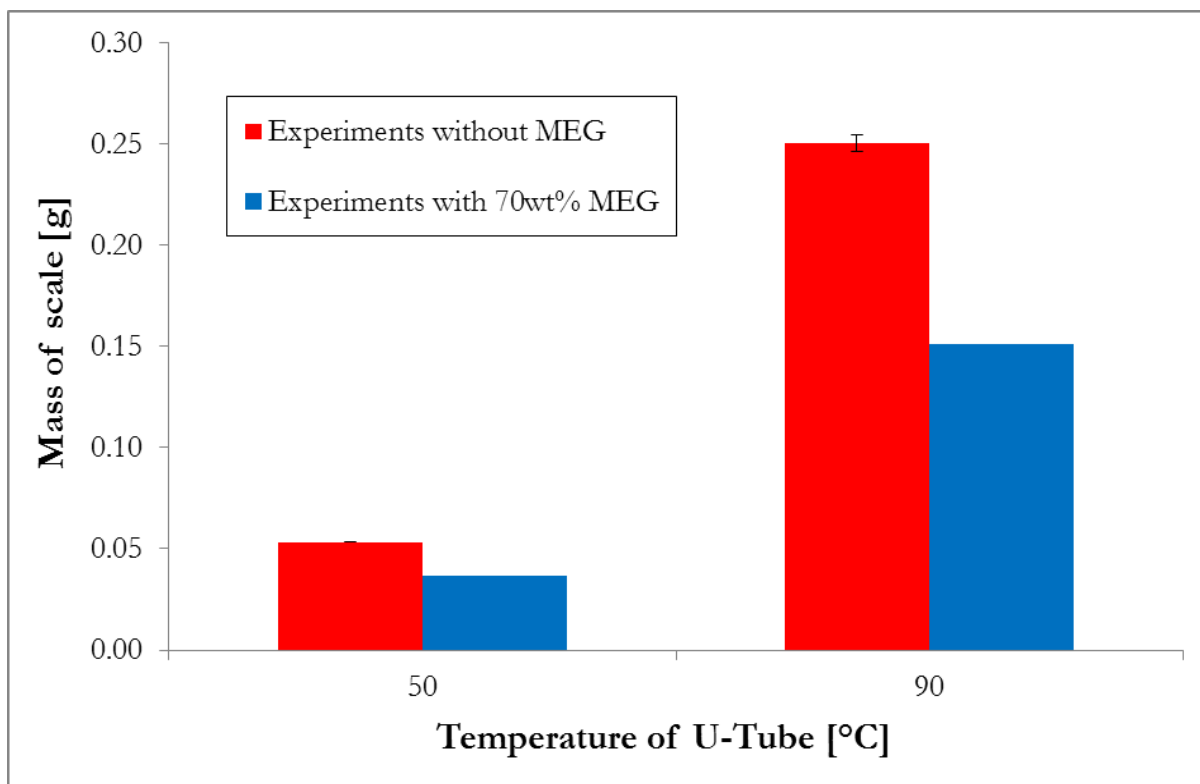
Figure 4.13: Mass of scale as a function of temperature on the heated surface in experiments with S=6.0 and an experimental duration of 180 minutes. The experiments with a MEG solvent have first had a pre-scale period of 90 minutes at 50/90°C before a period of 90 minutes with 70wt% MEG solvent at the same temperature.

Figure 4.13 shows how the growth of scale is reduced with temperature of the heating medium regardless of solvent composition. In Section 4.3.4 it was discussed that this can be explained from a decreased solubility and a reduced growth rate constant. It should be noted, when studying the effect in a MEG solvent, that the experiment at 90°C would have a much higher mass deposit in the pre-scale period than the experiment at 50°C.

4.4.4 Impact of MEG on polymorphism and morphology

The concentration of MEG in solution was observed to have an impact on both polymorphism and morphology of the scaled layer. In this section, the effect of solvent composition will be studied at two different temperatures of the heating medium.

A graphical representation of an XRD analysis comparing polymorphism of samples with and without MEG at a tube temperature of 90°C has been plotted in Figure 4.14. The concentration of MEG in the included experiment was 90wt%.

Results from the XRD analysis of experiments at 50°C with and without MEG (70wt%) has been graphically represented in Figure 4.15.
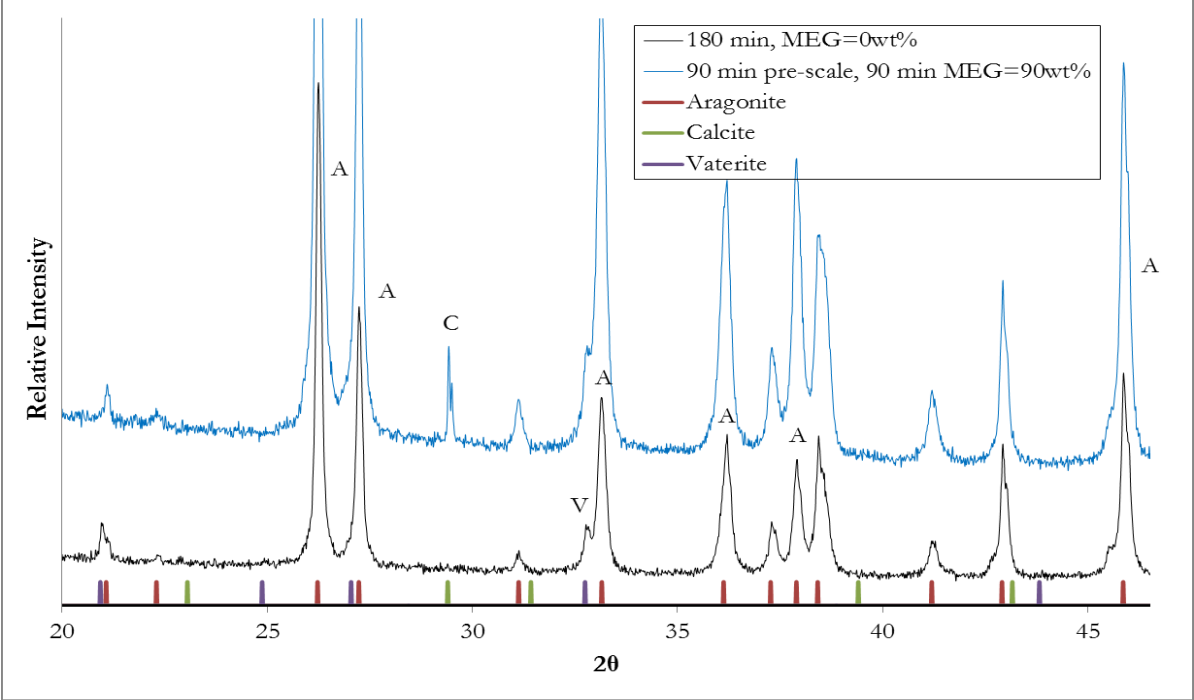
Figure 4.14: Graphical representation of results from XRD analysis of experiments with S=6.0, T_{Tube}=90°C at MEG=0wt% and MEG=90wt%.
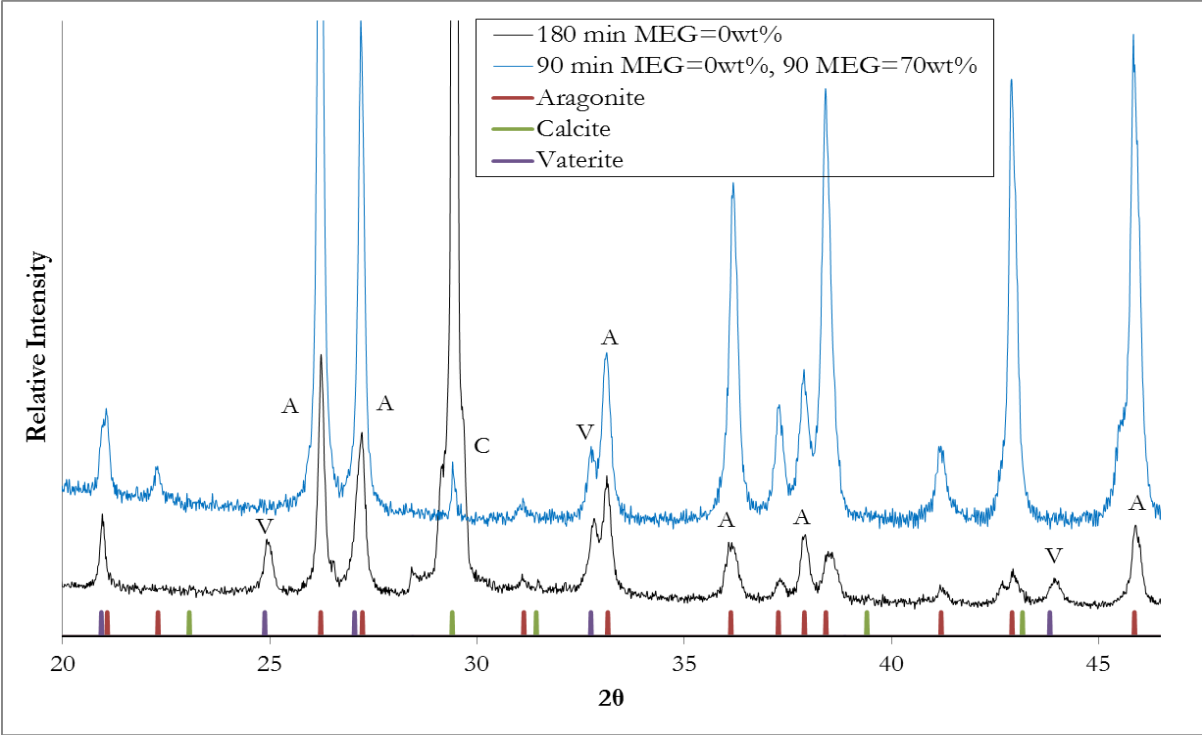
Figure 4.15: Graphical representation of results from XRD analysis of experiments with S=6.0, T_{Tube}=50°C at MEG=0wt% and MEG=70wt%.

In a water solution, aragonite and some vaterite were observed at a tube temperature of 90°C and an inlet supersaturation of 6.0. Calcite was not observed at these conditions. The same polymorphic composition was identified with a 50wt% MEG solvent (Figure H.6, Appendix H). However, when the concentration of MEG was increased to 90wt%, calcite was identified in the XRD analysis as illustrated in Figure 4.14.

The opposite trend was observed when the setpoint of the heated surface was set to 50°C. In these experiments the presence of calcite was decreased when MEG (70wt%, S=6.0) was injected into the system compared to a pure water solvent, as shown in Figure 4.15.

Analysis with SEM indicated that the identified calcite in a MEG solvent was only present in very small amounts at a tube temperature of 90°C. This has been shown in Figure 4.16. The sample was, however, not quantified, and it could therefore not be concluded whether there was additional calcite present near the tube surface or if the included SEM picture reflected the overall scale layer composition.
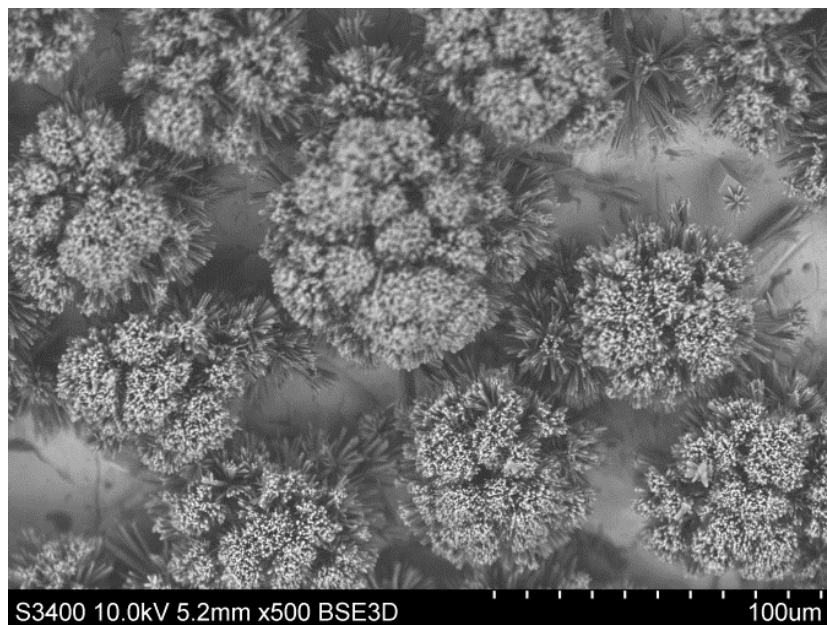
Figure 4.16: SEM pictures of experiment 09.04, S=6.0, T_{Tube}=90°C, 90+90 min, MEG=90wt% x500 enlargement.

SEM-analyses of the experiments with a temperature of 50°C in the heated medium confirmed the observations made with XRD. Growth of calcite was notably inhibited in the MEG solvent. The size of aragonite crystals were also reduced in the solution with MEG, which indicates a large impact on growth kinetics at this temperature. The photos have been included in Figure 4.17.

56
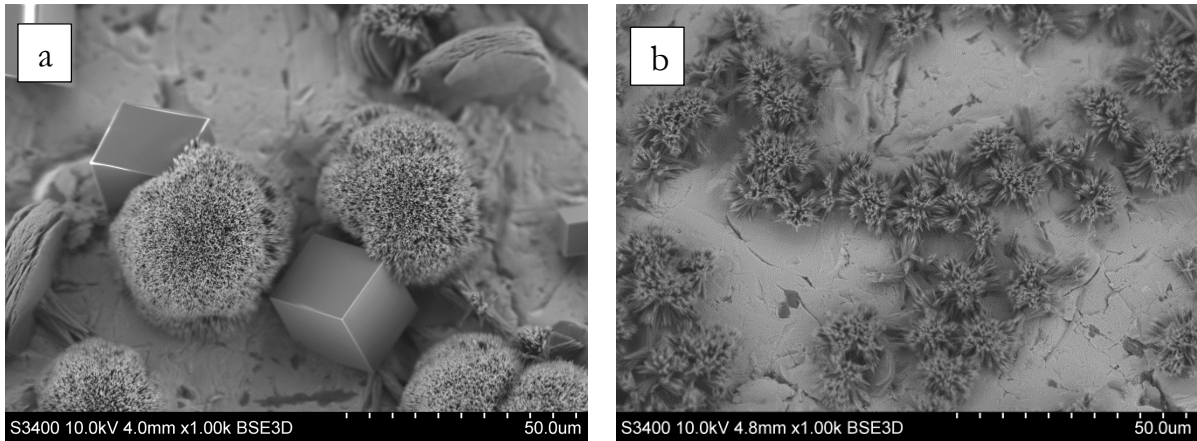
Figure 4.17: SEM analysis of experiments with S=6.0 and T_{Tube}=50°C, x1000 enlargement: a) 180 min MEG=0wt% b) 90 min MEG=0wt%, 90 min MEG=70wt%.

From the XRD- (Figure 4.15) and SEM-analyses (Figure 4.17) it appears like the formation of vaterite is decreased in solutions with MEG at a temperature of 50°C and an inlet supersaturation of 6.0. Flaten and co-workers (2010) argued that the hexagonal vaterite plates formed in water were not observed on crystals grown in solutions at 70wt% MEG. These experiments were done at temperatures of 40/70°C and correspond well with the results from this work at 50°C.

When the tube temperature was elevated to 90°C, vaterite was not identified with XRD-analyses of the experiments, regardless of solvent composition (Figure 4.14). SEM-analyses supported this observation, but indicated a change in scale morphology when the batch reservoir was changed from pre-scale conditions to MEG solvent. This has been shown in Figure 4.18.
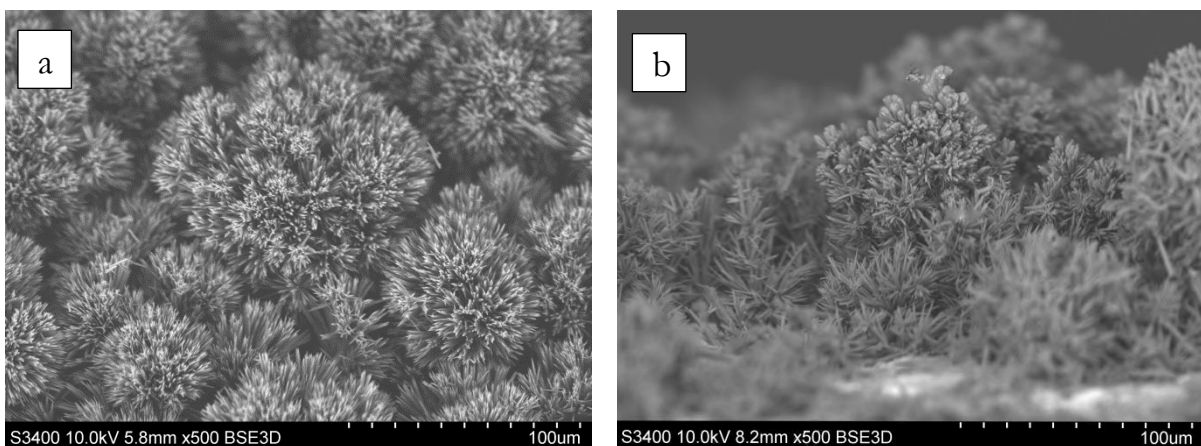
Figure 4.18: SEM analysis of experiments with S=6.0 and T_{Tube}=90°C, x500 enlargement: a) 180 min MEG=0wt% b) 90 min MEG=0wt%, 90 min MEG=70wt%.

57

Flaten and co-workers (2009) reported an increase in vaterite formation with bulk concentration of MEG at all temperatures in a batch reactor. However, the results obtained in this work indicate that there might be a more complex relationship between the growth of vaterite and solvent composition/tube temperature on a heated surface in a flow through system.

5   Conclusions

In this work, deposition of calcium carbonate scale on a heated surface was studied in a flow through system with MEG-water solvent. Inlet supersaturation, temperature of the heating medium and solvent concentration were varied to study the effect on overall growth rate, polymorphism and morphology of the scaled layer.

Results showed that the overall growth rate of aragonite decreased by 3.8% from $5.36 \pm 0.18 \cdot 10^{-6}$ kg/m$^2 \cdot$s to $5.16 \pm 0.12 \cdot 10^{-6}$ kg/m$^2 \cdot$s when the experimental duration was changed from 90 to 180 minutes in a water solvent. These experiments were done at an inlet supersaturation of 6.0 and a temperature of 90°C in the heated U-Tube.

An average overall growth rate of $2.6 \pm 0.3 \cdot 10^{-6}$ kg/m$^2 \cdot$s was measured using an inlet supersaturation of 4.5, tube temperature of 90°C, and an experimental duration of 180 minutes in a water solvent. Analysis with XRD and SEM identified a change from almost exclusively aragonite to a mixed polymorphic composition when the tube temperature was changed from 90°C to 50°C.

Experimental results showed that scale growth has a prolonged initiation period in monoethylene glycol solutions compared to a pure de-ionized water solvent. A decrease in heat transfer to the bulk solution was observed with a higher presence of MEG in the solvent, which elevated the skin-temperature. The reduction in growth rate with scale thickness was notably higher in a combined water/MEG solvent than in pure water. This could be explained by a more sensitive growth rate constant with a higher skin-temperature.

The mass deposited scale was observably reduced with an elevated concentration of MEG. Mass deposits per area after the pre-scale period were 0.90 mg/cm^2 (50wt% MEG), 0.53 mg/cm^2 (70wt% MEG) and 0.36 mg/cm^2 (90wt% MEG) at an inlet supersaturation of 6.0 and a tube temperature of 90°C. The reduced deposit at comparable levels of supersaturation could possibly be caused by a lower growth rate constant due to the increased solvent viscosity with MEG.

The introduction of MEG was observed to decrease the formation of calcite and vaterite at a tube temperature of 50°C. At a higher heating medium temperature (90°C), vaterite was not identified regardless of solvent composition.

Recommendations for Further Work

In the oil and gas industry, flows will not consist of a pure mix of MEG, water and calcium carbonate. The effect of impurities (such as alginates) on morphology, polymorphism and growth rates could therefore be of interest for further research.

Heat transfer through the scaled layer and variable skin-temperatures has been discussed, but without an accurate model this temperature will remain unknown. Such a model based on empirical temperature data would make it possible to study the growth of scale with knowledge of actual growth site conditions at any given time.

The range of temperatures, MEG concentrations and inlet supersaturation levels are limited in this work. It is recommended to extend these ranges and also to identify the impact of an even thicker scale layer on the overall growth rate.

Possible conditions that ensure the growth of uniform vaterite and calcite layers should be identified. Knowledge of growth rates for all the polymorphs at different regimes could be compared with industrial conditions to create a comprehensive model for scale growth. A quantitative analysis with XRD should also be conducted to achieve results with a MEG/water solvent because analyses with SEM only give simplified indications of polymorphism in the scaled layer.

Other possible considerations for research include impact of surface material and roughness, effect of residence time, scale inhibitor injection, influence of polymorphism on the crystal solubility in acid (scale removal), and the application of seeding to control scale formation.

This work has identified some experimental improvements, which could further ensure control of parameters and constant supersaturation in reactor. The pumping of reactants should be initialized when the bulk temperature reaches a certain level after the initial step with pure water flow. By doing so, possible variations in the initial bulk temperature could be minimized. Furthermore, the logging of reservoir pH would yield information on the effect of CO_2 from the atmosphere and remedial steps to close the system should also be considered.

References

ANDREASSEN, J.-P. 2005. Formation mechanism and morphology in precipitation of vaterite - nano aggregation or crystal growth? *Journal of Crystal Growth,* 274**,** pp. 256-264.

ANDREASSEN, J.-P., BECK, R. & NERGAARD, M. 2012. Biomimetic type morphologies of calcium carbonate grown in absence of additives. *Faraday Discussions,* 159**,** pp. 247-261.

ANDREASSEN, J.-P. & HOUNSLOW, M. J. 2004. Growth and aggregation of vaterite in seeded batch experiments *AIChE J.,* 50**,** pp. 2772-2782.

AYLWARD, G. & FINLAY, T., 2008. *SI Chemical Data,* 6th edition*,* Australia, John Wiley & Sons.

BECK, R., NERGAARD, M. & ANDREASSEN, J.-P. 2013. Crystal Growth of Calcite at Conditions of Gas Processing in Solvent Mixtures of Monoethylene Glycol and Water. *Transactions of Tianjin proceedings* 19**,** pp. 79-85.

BERTHOUD, A. 1912. Theorie de la formation des faces d'un crystal. *Journal de Chimique Physique,* 10**,** pp. 624-635.

BOTT, T. R., 1995. *Fouling of heat exchangers.*

BRECEVIC, L. & NIELSEN, A. E. 1989. *J. Cryst. Growth,* 98**,** pp. 504-510.

CALLISTER, W. D., JR. & RETHWISCH, D. G., 2010. *Materials Science and Engineering: An introduction,* 8th edition*,* New York, John Wiley & Sons, Inc.

CAO, G., 2004. *Nanostructures & Nanomaterials: Synthesis, Properties and Applications*, Imperial College Press.

CHEN, T., NEVILLE, A. & YUAN, M. 2005. Calcium carbonate scale formation - assesing the initial stages of precipitation and deposition. *Journal of Petroleum Science and Engineering,* 46**,** pp. 185-194.

CLARKSON, J. R., PRICE, T. J. & ADAMS, C. J. 1992. *J. Chem. Soc., Faraday Trans.,* 88**,** pp. 243-249.

COWAN, J. C. & WEINTRITT, D. J., 1976. *Water-Formed Scale Deposits,* 98, Knovel.

FLATEN, E. M., SEIERSTEN, M. & ANDREASSEN, J.-P. 2009. Polymorphism and morphology of calcium carbonate precipitated in mixed solvents of ethylene glycol and water. *Journal of Crystal Growth,* 311**,** pp. 3533-3538.

FLATEN, E. M., SEIERSTEN, M. & ANDREASSEN, J.-P. 2010. Growth of the calcium carbonate polymorph vaterite in mixtures of water and ethylene glycol at conditions of gas processing. *Journal of Crystal Growth,* 312**,** pp. 953-960.

FOGLER, H. S., 2005. *Elements of chemical reaction engineering,* N.J., Prentice-Hall PTR.

GEANKOPOLIS, C. J., 2003. *Transport Processes and Separation Process Principles,* 4th edition*,* New Jersey, Prentice Hall.

HASSON, D., AVRIEL, M. R., WILLIAM, ROZENMAN, T. & WINDREICH, S. 1968. Calcium carbonate scale deposition on heat transfer surfaces. *Desalination,* 5**,** pp. 107-119.

HAUG-WARBERG, T., 2006. *Den Termodynamiske Arbeidsboken,* 2nd edition*,* Fornebu, Kolofon Forlag AS.

HAYDEN, H. W., MOFFATT, W. G. & WULFF, J., 1965. *The Structure and Properties of Materials,* **3,** p. 70.

HELBÆK, M. & KJELSTRUP, S., 2006. *Fysikalsk Kjemi,* 2nd edition, Fagbokforlaget.

HYLLESTAD, K. 2012. Scaling of calcium carbonate on heated surfaces in a flow through system. NTNU: Department of Chemical Engineering.

JACOB, D. J., 1999. *Introduction to Atmospheric Chemistry*, Princeton University Press.

JAKOBSEN, H. A. 2008. Chemical reactor modeling: multiphase reactive flows.

KAASA, B. 1998. *PhD Thesis.* NTNU.

KAASA, B., SANDENGEN, K. & ØSTVOLD, T. 2004. Thermodynamic Predictions of Scale Potential, pH and Gas Solubility in Glycol Containing Systems.

KAN, A. T., FU, G., WATSON, M. A. & TOMSON, M. B. 2002. Effect of hydrate inhibitors on oilfield scale formation and inhibition. *Proceedings of 2002 Oilfield Scale Symposium.*

KASHCHIEV, D. & VAN ROSMALEN, G. M. 2003. Review: Nucleation in solutions revisited. *Cryst. Res. Technol.,* 38**,** pp. 555-574.

LIESEGANG, R. E. 1911. Über die Reifung von Silberhaloidemulsionen. *Zeitschrift für Physikalische Chemie,* 75**,** pp. 374-377.

LIU, C., LI, Y., XU, Y., MINARI, T., LI, S., TAKIMIYA, K. & TSUKAGOSHI, K. 2012. Controlling the crystal formation in solution-process for organic field-effect transistors with high-performance. *Organic Electronics.*

MEGLOBAL. 2008. *Ethylene Glycol, Product Guide* [Online]. Available: http://www.meglobal.biz/media/product_guides/MEGlobal_MEG.pdf [Accessed 30.05 2013].

MIERS, H. A. & ISAAC, F. 1906. Refractive indices of crystallization solutions. *Journal of the Chemical Society,* 89**,** pp. 413-454.

MIERS, H. A. & ISAAC, F. 1907. The spontanous crystallization pf binary mixtures. *Proceedings of the Royal Society,* A79**,** pp. 322-351.

MULLIN, J. W., 2001. *Crystallization,* 4th edition*,* Oxford, Butterworth Heinemann.

NERGAARD, M. 2011. *Scaling of calcium carbonate on heated surfaces in a continuous system.* Master Thesis, NTNU.

NERGAARD, M. 2012. Scaling of $CaCO_3$ on heated surfaces. Unpublished work.

NIELSEN, A. E. 1964. *Kinetics of Precipitation.*

NIELSEN, A. E. & TOFT, J. M. 1983. Electrolyte Crystal Growth Kinetics. *Journal of Crystal Growth,* 67**,** pp. 278-288.

O'HARA, M. & REID, R. C. 1973. *Modelling Crystal Growth Rates from Solution.*

OGINO, T., SUZUKI, T. & SAWADA, K. 1987. *Geochim. Cosmochim. Acta,* 51.

OLDERØY, M. Ø., XIE, M., STRAND, B. L., FLATEN, E. M., SIKORSKI, P. & ANDREASSEN, J.-P. 2009. Growth and Nucleation of Calcium Carbonate Vaterite Crystals in Presence of Alginate. *Crystal Growth & Design,* 9**,** pp. 5176-5183.

PEYGHAMBARZADEH, S. M., VATANI, A. & JAMIALAHMADI, M. 2011. Influences of bubble formation on different types of heat exchanger fouling. *Applied Thermal Engineering,* 50**,** pp. 848-856.

PITZER, K. S. 1973. Thermodynamics of electrolytes. I. Theoretical basis and general equation. *J. Phys. Chem.,* 77**,** pp. 268-277.

PITZER, K. S. 1986. Theoretical considerations of solubility with ephasis on mixed aqueous electrolytes. *Pure Appl. Chem. ,* 58**,** pp. 1599-1610.

PLUMMER, L. N. & BUSENBERG, E. 1981. The solubilities of calcite, aragonite and vaterite in CO_2-H_2O solutions between 0 and 90ºC, and an evaluation of the aqueous model for the system $CaCO_3$-CO_2-H_2O. *Geochimica et Cosmochimica Acta,* 46**,** pp. 1011-1040.

RANKIN, B. H. & ADAMSON, W. L. 1973. Scale Formation as Related to Evaporator Surface Conditions. *Desalination,* 13**,** pp. 63-87.

REITZER, B. J. 1964. Rate of Scale Formation in Tubular Heat Exchangers.

SANDENGEN, K. 2006. *Prediction of mineral scale formation in wet gas condensate pipelines and in MEG (Mono Ethylene Glycol) regeneration plants.* Doctoral thesis, NTNU.

SKOGESTAD, S., 2009. *Chemical and Energy Process Engineering,* Taylor & Francis Group, LLC.

SUNAGWA, I., 2005. *Crystals: Growth, Morphology and Perfection,* 1st edition*,* Cambridge, UK, Cambridge University Press.

VALETON, J. P. P. 1924. Wachstum und Auflösung der Kristalle. *Zeitschrift für Kristallographie,* 59**,** pp. 483.

VOLMER, M. 1939. *Kinetic der Phasenbildung.*

Appendices

A   Derivations

A.1   Chemical potential

The differential of Gibbs energy has been stated in literature for thermodynamic relations (Haug-Warberg, 2006).

$$dG(\tau_T, \pi, \mu) = -S_E \cdot d\tau_T - V \cdot d\pi + \mu \cdot dN$$

When assuming constant pressure and temperature, which is valid considering the experimental conditions, the expression can be simplified.

$$dG = \left(\sum \mu_i \cdot dn_i \right)_{\tau, \pi}$$

$$dG = \mu_{Solution} dn_i + \mu_{Crystal} dn_i^{Crystal}$$

The rate of dissolution is the same as formation, however opposite in sign. When this is used with the equations above it gives an expression for the difference in chemical potential in a solution with a liquid and a solid state. This was used in Section 2.3 to find an expression for the supersolubility.

$$dn_i^{Crystal} = -dn_i$$

$$dG = 0 \rightarrow \mu_{Crystal} = \mu_{Solution}$$

$$\Delta\mu = \mu_{Crystal} - \mu_{Solution}$$

A.2 Alkalinity of calcium carbonate system

In the studies which were covered in this paper, Na_2CO_3 and $Ca(NO_3)_2$ were used as reactants. An electron neutrality balance for this system and a mass balance for calcium were derived in order to find the total alkalinity of the system.

$$2 \cdot \widetilde{M}_{Ca^{2+}} + \widetilde{M}_{Na^+} + \widetilde{M}_{H^+} + \widetilde{M}_{CaHCO_3^+}$$
$$= 2 \cdot \widetilde{M}_{CO_3^{2-}} + \widetilde{M}_{HCO_3^-} + \widetilde{M}_{NO_3^-} + \widetilde{M}_{OH^-}$$

$$\widetilde{M}_{Ca_{Tot}} = \widetilde{M}_{Ca^{2+}} + \widetilde{M}_{CaHCO_3^+} + \widetilde{M}_{CaCO_3^0(aq)}$$

$$2 \cdot \widetilde{M}_{Ca_{Tot}} - \widetilde{M}_{CaHCO_3^+} - 2 \cdot \widetilde{M}_{CaCO_3^0(aq)} + \widetilde{M}_{Na^+} + \widetilde{M}_{H^+}$$
$$= 2 \cdot \widetilde{M}_{CO_3^{2-}} + \widetilde{M}_{HCO_3^-} + \widetilde{M}_{NO_3^-} + \widetilde{M}_{OH^-}$$

Applying the definition for total alkalinity (sum of titratable bases) gives the total alkalinity for the calcium carbonate system with the applied reactants, as shown below.

$$Alk_T = \widetilde{M}_{CaHCO_3^+} + 2 \cdot \widetilde{M}_{CaCO_3^0(aq)} - \widetilde{M}_{H^+} + \widetilde{M}_{OH^-} + 2 \cdot \widetilde{M}_{CO_3^{2-}}$$
$$+ \widetilde{M}_{HCO_3^-}$$

B Chemicals and Solvents

Table B.1 lists all the chemicals utilized in the experiments as well as relevant information about them. Chemicals not mentioned in the experimental methods have typically been used in electrodes. Some physical data for the solvents water and MEG have been listed in Table B.2.

Table B.1: Chemicals applied in experiments

Chemical	Formula	Purity [%]	State	Supplier
Ammonia	NH_3	>25.0	L	VWR
Ammonium chloride	NH_4Cl	>99.8	S	Merck
Calcium nitrate tetra hydrate	$Ca(NO_3)_2 \cdot 4H_2O$	>99.0	S	Sigma-Aldrich
Ethylenediamine tetra acetic acid	$C_{10}H_{16}N_2 \cdot 2H_2O$	Titrisol (III)	Aq	Merck
Ethanol	C_2H_5OH	96.0	Aq	VWR
Hydrochloric acid	HCl	37.0 (fuming)	L	Merck
Mono ethylene glycol (MEG)	$C_2H_6O_2$	>99.0	L	Univar
Potassium chloride	KCl	>99.5	S	Merck
Silver chloride	AgCl	>99.0	S	Fluka
Sodium carbonate (anhydrous)	Na_2CO_3	>99.0	S	VWR

Table B.2: Physical properties of water and MEG (MEGlobal, 2008, Aylward and Finlay, 2008)

	Water	MEG
Viscosity (20°C) [mPas]	1.0	21
Surface tension (25°C) [mN/m]	72.0	48.0
Solubility in water (20°C) [wt%]	-	100

C Experimental Calculations

C.1 Preparation of reactant solutions

The molality needed to give a desired supersaturation was calculated iteratively in the simulation program MultiScale 7.0®. The results from these calculations have been presented in Table C.1.

Table C.1: Results from MultiScale calculations of molality needed to give desired inlet supersaturation in solution

S	MEG [wt %]	MEG [kg]	Na_2CO_3 [mmol/kg]	$Ca(NO_3)_2$ [mmol/kg]
4.5	0	0	0.5614	0.5614
6.0	0	0	0.7910	0.7910
6.0	50	12.60	0.6918	0.6918
6.0	70	17.64	0.7030	0.7030
6.0	90	22.68	0.8235	0.8235
12.3	50	12.60	3.499	3.499

The reactant solutions were prepared in batches of 25.2 kg. Firstly, the required amount of MEG was added to a clean and empty container followed by 0.2 kg of a concentrated solution of the required salt. Lastly, distilled water was used to make up a total weight of 25.2 kg. The reservoir batch was closed and shaken adequately to mix the reactants. A calculation example has been included underneath for Na_2CO_3 at an inlet supersaturation of S=6.0. The molar amount is doubled in the calculation due to the mixing from two equally sized reservoirs into a shared reactor.

$$n_{Na_2CO_3,Batch} = C_{Batch} \cdot 2 \cdot m_{Tot,Batch} = 0.791 \frac{mmol}{kg} \cdot 2 \cdot 25.2\ kg$$
$$= 39.8664\ mmol$$

The concentrated solutions were prepared in 1.0 kg containers out of which 0.2 kg was used per 25.2 kg batch. A sample calculation for one of these solution preparations of Na_2CO_3 at S=6.0 follows. The results of all calculations have been summarized in Table C.2. Calcium nitrate tetra hydrate was used as source for calcium ions after some concerns about the possible influence of precipitated NaCl when using $CaCl_2$. The effect of hydrate ions on the concentration was neglected. This simplification is motivated after calculations showed that their overall

71

contribution to total volume was very low. All the experimental sodium carbonate utilized was anhydrous.

$$
\begin{aligned}
m_{Na_2CO_3,upconcentrated\ solution} \\
= \frac{n_{Na_2CO_3,Batch}}{m_{Solution\ used\ in\ Batch}} \\
\cdot m_{Tot,\ upconcentrated\ solution} \cdot M_{m,Na_2CO_3} \\
= \frac{39.8664\ mmol}{0.200\ kg} \cdot 1.00\ kg \cdot 0.1060\ \frac{g}{mmol} \\
= 21.13\ g
\end{aligned}
$$

Table C.2: Mass of salts used in preparation of up concentrated solutions used in reservoirs

Supersaturation	MEG [wt %]	Na_2CO_3 [g]	$Ca(NO_3)_2 \cdot 4H_2O$ [g]
4.5	0	14.99	33.41
6.0	0	21.13	47.07
6.0	50	18.48	41.17
6.0	70	18.78	41.84
6.0	90	21.99	49.01
12.3	50	-[a]	-

[a] **The experiment with S=12.3 was done after a miscalculation and it was therefore not prepared in the same manner as the other experiments.**

C.2 Calculation of residence time and effect of flow rate on supersaturation

The flow of reservoir solution into the reactor was monitored continuously and the total consumption was recorded at the end of each experiment. The actual flow was then used along with the actual bulk temperature to calculate the supersaturation level in the reactor using Multiscale 7.0®. Table C.3 shows the calculated value for some of the experiments. Temperature information was collected from the graphs in Appendix I.

Table C.3: Calculated actual supersaturation in the reactor

Exp.	MEG [wt%]	Mass Na_2CO_3 [kg]	Mass $Ca(NO_3)_2$ [kg]	T_{Bulk} [°C]	$S_{Prepared}$	$S_{Calculated}$
22.04	0+90[a]	19.2+19.9	19.2+18.4	33+32	6.0	6.0+5.9
16.04	0	20.1	17.7	37	6.0	5.9
12.04	0+50	40.4	34.3	32	6.0	6.0
21.03	0+70	18.4+19.4	15.2+16.0	34+32	6.0	5.9+6.0
14.03	0+50	20.6+19.9	15.6+20.6	35+33	6.0	6.0+5.9
22.02	0	38.9	39.1	35	4.5	4.4

[a] **Experiments marked with two added time intervals describes an initial period without MEG (pre-scale period) and then a continuation with the same supersaturation level and temperature for a new time interval with MEG.**

Table C.3 illustrates how small variations in bulk temperature and flow rate of reactants have a small effect on supersaturation level. It should, however, be noted that these calculations only represent overall values for the entire experimental duration. Fluctuations in pumping rates of the two reactant pumps and bulk temperature could make the supersaturation level of the bulk liquid deviate from this level during the experiments. A discussion of the effects of skin-temperature and polymorphism on referred supersaturation at the growth site has been included in Section 4.1.3 of the report.

The residence time of the reactor can be calculated according to equation (36) as reproduced below. An average mass flow rate of the two reactant flows was used with the measured mass volume of 2.2 kg in the reactor after agitation was turned on.

$$\tau \equiv \frac{V}{v_0} = \frac{2200 \ g}{420 \ g/min} = 5.24 \ min$$

C.3 Overall growth rate of scaling

Surface areas of the U-tubes were calculated based on the outer diameter (provided by manufacturer) and the total length. The length was measured through putting the tube on the inside of a silicon tube and then finding the length of the silicon tube. This was done due to the curvature of the tube. The area marked as not scaled in the surface area calculations are the areas covered with silicon tube. This silicon tube (approximately 0.50 cm long on each side) was used to keep the U-tube in position inside the reactor. The exact area covered with silicon tube was measured and calculated for each individual experiment.

$$A_{Surface,Tube} = D_{Outside} \cdot \pi \cdot L_{Tube} - A_{Not\ Scaled}$$
$$= 0.635\ cm \cdot \pi \ \cdot 23.9\ cm - 1.99\ cm^2 = \ 45.7\ cm^2$$

Tube areas not scaled in the experiments or damaged before weighing were accounted for in the calculation of the scale rates. The weight of scale was measured by weighing the tube before and after the experiments. Surface areas of the tubes were assumed to be approximately the same since the weight of them differed by no more than 3.43 % (approximately 28.7 g).

The overall growth rates in the experiments were calculated according to equation (14) as revisited below. Table C.4 and Table C.5 shows the experimental parameter values, weight data and calculated growth rates for the experiments used in the report. Experiments 12.03, 01.02 and 04.02 were used to test the setup. Weight data was not collected from these tests.

$$Overall\ growth\ rate = \frac{1}{A} \cdot \frac{dm}{dt} \left[\frac{kg}{m^2 \cdot s} \right]$$
$$= \frac{m[g]}{A[cm^2] \cdot t[min]} \cdot \frac{\frac{kg}{1.00e3\ g}}{\frac{m^2}{1.00e4\ cm^2}} \cdot \frac{60\ s}{min}$$

Table C.4: Parameter values for experiments used in the report

Experiment	S	T_{Tube} [°C]	Duration [min]	MEG [wt%]	Tube (Nr.)
26.apr (2)	6.0	50	90+90[a]	0+70	H
26.apr	6.0	50	180	0	K
22.apr	6.0	90	90+90	0+90	H
16.apr(2)	6.0	90	90	0	L
16.apr	6.0	90	90	0	K
15.apr	6.0	90	90	0	F
12.apr	6.0	90	180	0	E
10.apr	6.0	90	90	0	C
09.apr	6.0	90	90+90	0+90	J
06.apr	6.0	90	90+30	0+50	H
04.apr	12.3	90	30	50	D
02.apr	6.0	90	90+155	0+50	C
21.mar	6.0	90	90+90	0+70	H
14.mar	6.0	90	90+90	0+50	J
13.mar	6.0	90	180	0	H
12.mar	6.0	90	90	0	D
05.mar	6.0	90	180	50	F
26.feb	6.0	90	180	70	C
22.feb	4.5	90	180	0	H
19.feb	4.5	90	180	0	F
18.feb	4.5	90	180	0	D
15.feb	4.5	90	180	0	C
08.feb	4.5	90	180	0	I
04.feb	4.5	90	180	0	B
01.feb	4.5	90	180	0	A

[a] **Experiments marked with two added time intervals describes an initial period without MEG (pre-scale period) and then a continuation with the same supersaturation level and temperature for a new time interval with MEG.**

The calculated growth rate (kg/m²·s) in Table C.5 represents overall growth rate for the entire experiment. Table C.6 includes the calculated average mass deposition per area and average overall growth rate for three sets of experiments with more than one repeat:

Table C.7 shows calculated growth rates for the period after pre-scale. The calculations of these values were based on the calculated average mass deposition per area of the pre-scale layer (as shown in Table C.6). Calculated standard deviation of these values has been included in Appendix D.

Table C.5: Measured weight data and calculated growth rate for experiments used in the report

Exp.	Scale [g]	Mass deposition per area [g/cm²]	[g/cm²·min]	Overall growth rate [kg/m²·s]
26.apr(2)	0.0369	0.0008	$4.61 \cdot 10^{-6}$	$7.68 \cdot 10^{-7}$
26.apr	0.0533	0.0012	$6.60 \cdot 10^{-6}$	$1.10 \cdot 10^{-6}$
22.apr	0.1487	0.0033	$1.84 \cdot 10^{-5}$	$3.07 \cdot 10^{-6}$
16.apr(2)	0.1295	0.0029	$3.21 \cdot 10^{-5}$	$5.34 \cdot 10^{-6}$
16.apr	0.1282	0.0029	$3.20 \cdot 10^{-5}$	$5.33 \cdot 10^{-6}$
15.apr	0.1261	0.0028	$3.15 \cdot 10^{-5}$	$5.25 \cdot 10^{-6}$
12.apr	0.2544	0.0056	$3.13 \cdot 10^{-5}$	$5.22 \cdot 10^{-6}$
10.apr	0.1335	0.0030	$3.30 \cdot 10^{-5}$	$5.51 \cdot 10^{-6}$
09.apr	0.1430	0.0032	$1.76 \cdot 10^{-5}$	$2.93 \cdot 10^{-6}$
06.apr	0.1496	0.0033	$2.78 \cdot 10^{-5}$	$4.63 \cdot 10^{-6}$
04.apr	0.0165	0.0004	$1.23 \cdot 10^{-5}$	$2.05 \cdot 10^{-6}$
02.apr	0.1788	0.0040	$1.64 \cdot 10^{-5}$	$2.73 \cdot 10^{-6}$
21.mar	0.1512	0.0034	$1.90 \cdot 10^{-5}$	$3.17 \cdot 10^{-6}$
14.mar	0.1702	0.0038	$2.08 \cdot 10^{-5}$	$3.47 \cdot 10^{-6}$
13.mar	0.2464	0.0055	$3.06 \cdot 10^{-5}$	$5.10 \cdot 10^{-6}$
05.mar	0.0090	0.0002	$1.13 \cdot 10^{-6}$	$1.88 \cdot 10^{-7}$
26.feb	0.0068	0.0002	$8.53 \cdot 10^{-7}$	$1.42 \cdot 10^{-7}$
22.feb	0.1197	0.0027	$1.50 \cdot 10^{-5}$	$2.49 \cdot 10^{-6}$
19.feb	0.1273	0.0029	$1.60 \cdot 10^{-5}$	$2.67 \cdot 10^{-6}$
18.feb	0.1259	0.0028	$1.57 \cdot 10^{-5}$	$2.62 \cdot 10^{-6}$

15.feb	0.1224	0.0028	$1.53 \cdot 10^{-5}$	$2.56 \cdot 10^{-6}$
08.feb	0.1402	0.0031	$1.74 \cdot 10^{-5}$	$2.89 \cdot 10^{-6}$

Table C.6: Calculated average mass deposition per area and overall growth rate for pre-scale period experiments and 180 min experiments with S=4.5/6.0

S	Time [min]	Mass deposition per area [g/cm^2]	Overall growth rate [kg/m$^2 \cdot$s]
6.0	90	0.0029	$5.36 \cdot 10^{-6}$
6.0	180	0.0056	$5.16 \cdot 10^{-6}$
4.5	180	0.0029	$2.65 \cdot 10^{-6}$

Table C.7: Calculated overall growth rates for time period after pre-scale

Experiment	Weight percentage MEG	Overall growth rate after pre-scale period [kg/m$^2 \cdot$s]
22.apr	90	$7.89 \cdot 10^{-7}$
12.apr	0	$5.17 \cdot 10^{-6}$
09.apr	90	$5.44 \cdot 10^{-7}$
06.apr	50	$2.56 \cdot 10^{-6}$
02.apr	50	$1.20 \cdot 10^{-6}$
21.apr	70	$9.97 \cdot 10^{-7}$
14apr	50	$1.69 \cdot 10^{-6}$
13.apr	0	$4.92 \cdot 10^{-6}$

D Experimental Uncertainty

With laboratory experiments and measurements there will always be a certain degree of uncertainty in the reported values. This can for example be caused by poor calibration, lack of sensitivity, error in mechanical transfer or inaccurate reading of the measurement.

Several of the experiments were done with more than one repeat to account for reproducibility. Average overall growth rates and mass depositions per area have been calculated from these results and referred to in the report. The raw data can be found in Appendix C.3.

The double standard deviation (2σ) was calculated and included in Table D.1 and Table D.2. The equation used for these calculations has been shown underneath and is acquired from the standard set of functions in Microsoft Excel. Standard rules for number of significant digits have been applied.

$$2 \cdot \sigma = 2 \cdot \sqrt{\frac{\sum_{i=1}^{n}(x_i - \bar{x})^2}{n}}$$

Table D.1: Average overall growth rate and double standard deviation from experiments with more than one parallel

S	T_{Tube} [°C]	Duration [min]	MEG [wt%]	Average growth rate [kg/m²·s]	$2 \cdot \sigma$ [kg/m²·s]
4.5	90	180	0	$2.6 \cdot 10^{-6}$	$0.3 \cdot 10^{-6}$
6.0	90	90	0	$5.36 \cdot 10^{-6}$	$0.18 \cdot 10^{-6}$
6.0	90	180	0	$5.16 \cdot 10^{-6}$	$0.12 \cdot 10^{-6}$
6.0	90	90	90	$6.7 \cdot 10^{-7}$ [a]	$2.4 \cdot 10^{-7}$

[a] The calculated growth rate in the experiment with MEG reflects growth after the end of the pre-scale period

Table D.2: Average mass deposition per area and double standard deviation from experiments with more than one parallel

S	T_{Tube} [°C]	Duration [min]	MEG [wt%]	Mass deposition [g/cm²]	$2 \cdot \sigma$ [g/cm²]
4.5	90	180	0	$2.9 \cdot 10^{-3}$	$0.3 \cdot 10^{-3}$
6.0	90	90	0	$2.90 \cdot 10^{-3}$	$0.10 \cdot 10^{-3}$
6.0	90	180	0	$5.58 \cdot 10^{-3}$	$0.13 \cdot 10^{-3}$

At the end of each experiment, the used U-tube was dried and weighed. The resulting weight data was used in the calculations of growth rate and mass deposition per area.

A drying period of approximately 48 hours was used in the experiments. This period was based on when the tube weight had approached a stable value, as shown in Figure D.1.
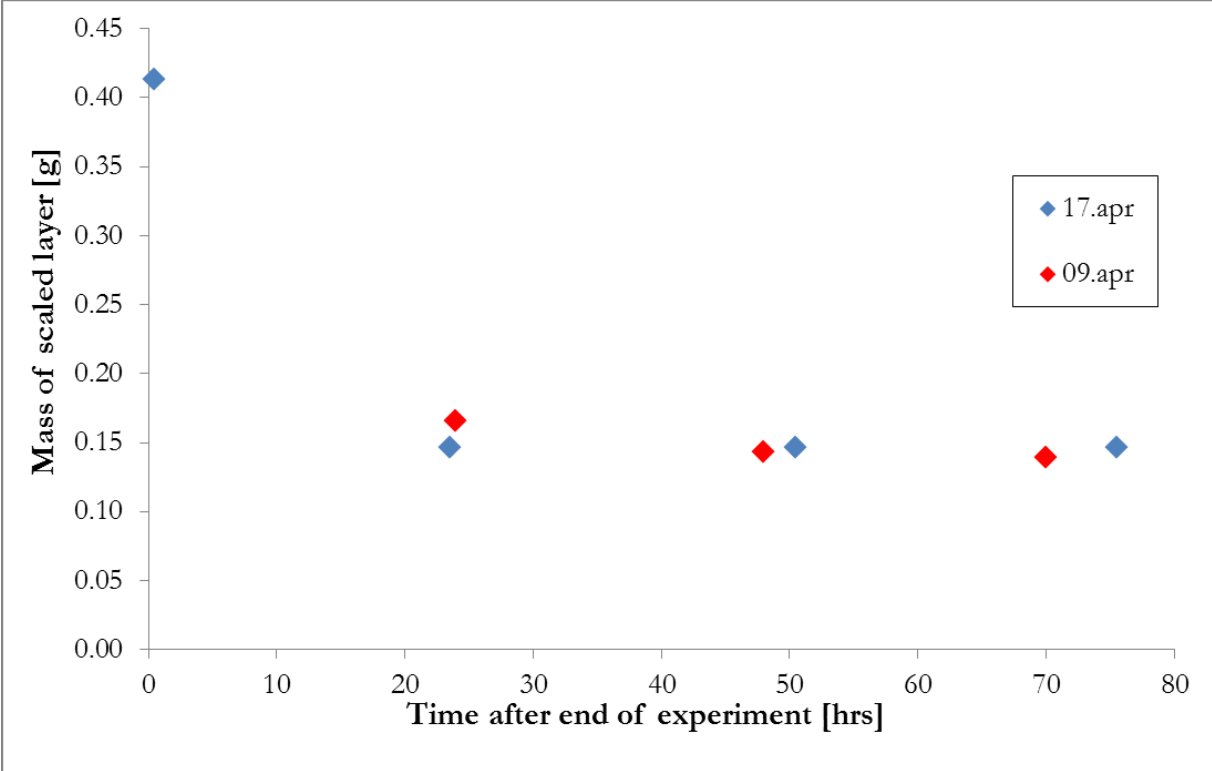
Figure D.1: Graphical representation of data from test of drying period.

E   Images of U-tube, Experimental Setup and Reactor

Figure E.1 shows an example of the sandblasted stainless steel (TP316L) U-tubes used in the experiments, while the reactor is presented in Figure E.2. The U-tube is not included in the reactor picture, but it is normally placed in the middle of the reactor with the lowest part approximately 1.00 cm underneath the bottom of the impeller. A total of 13 tubes were used. They had all been weighed in advance. Figure E.3 shows a picture of the entire experimental setup and a this setup has been shown as a schematic in Figure E.4.

Figure E.1: Sandblasted stainless steel tube used in experiments.
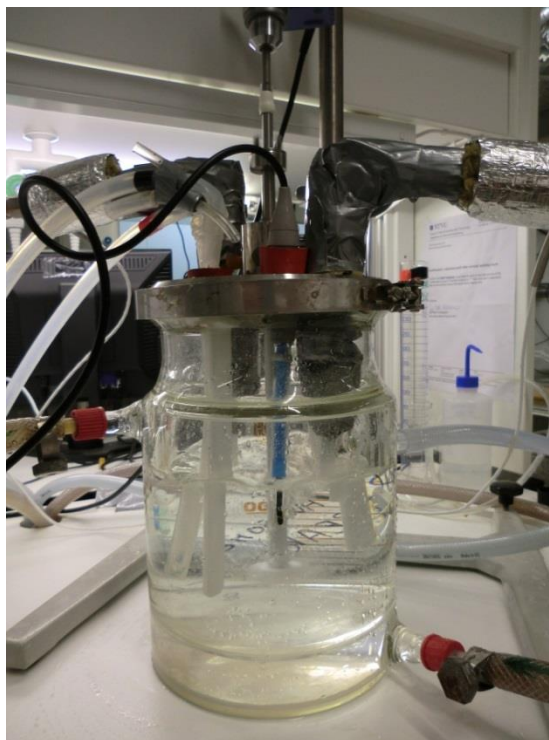
Figure E.2: Jacked glass reactor used in experiments.

Figure E.3: Experimental setup with pre-coolers, logging, pump, reactor and thermostatic units.

Reactor Setup

A   Temperature probe connected to PT-100 element
B   pH-probe connected to a Mettler Toledo pH-meter
C   Impeller (4-blade)
D   Reactant supply tube
E   U-tube (Sandblaste stainless steel)
F   Jacked glass reactor (2.0 L) with two fixed baffles
G   Y-shaped reactant mixer
H   IKA stirrer (variable speed control)

I   Julabo F33 Thermostatic unit
J   Lauda RE205 Thermostatic unit
K   PT-100 Element Temperature logging unit
L   Masterflex peristalic pump
M   Lauda RE205 Thermostatic unit
N   Reactant reservoirs (25.2 L)
O   Mettler Toledo scales

Reactant precooling units (two identical)

P   Jacked glass vessel (2.0 L)
Q   Impeller (2-blade)
R   Glass spiral
S   IKA stirrer (variable speed control)
T   Cooling jacket of reactor

Figure E.4: Schematic of the experimental setup.

83

F Health, Safety and Environment (HSE)

This section includes the HSE evaluation performed in advance of the experimental testing. Table F.1 shows the Hazardous activity identification process, Table F.2 includes the risk assessment form and the HSE action plan is given in Table F.3.

F.1 Hazardous activity identification process

NTNU		Risk Evaluation	Number	Date	
	Hazardous activity identification process	HSE-dep.	HMSRV2601		
		Approved by	Page		
HSE					

Unit: Chemical Engineering   Date: 18.01.2013

Line manager: Øyvind Gregersen

Participants in the identification process (including their function):

Ketil Hyllestad (Daily Manager of Apparatus) og Margrethe Nergaard (PhD-student)

Continuous flow scaling setup

Table F.1: Hazardous activity identification process form

ID no.	Activity/process	Responsible person	Existing documentation	Existing safety measures	Comment
1	Solution preparation of reactant solutions (Ca(NO3)2 and Na2CO3 in water/MEG-mixtures)	Ketil Hyllestad	MSDS (MEG, NaCO$_3$, Ca(NO$_3$)$_2$)		Solutions prepared on bench. Use safety glasses at all times, gloves and laboratory jacket when necessary (MEG). Depending on solution (Dilution of fuming HCl, ammonia buffer preparation), fume cupboard should be used.
2	Solution preparation of analytical solutions		HCl, NH$_3$		Use safety glasses and gloves at all times. Dilution of fuming HCl/ ammonia buffer preparation, fume cupboard should be used.
3	Storage of chemicals	Ketil Hyllestad	MEG, HCl (37%), NH$_3$, NaCO$_3$, Ca(NO$_3$)$_2$		Vapor pressure of MEG at room temperature is very low (0.09mmHg compared to 17.3 mmHG for H$_2$O). Close tank after withdrawal of chemical.
4	Running the experiment	Ketil Hyllestad	MSDS (MEG, NaCO$_3$, Ca(NO$_3$)$_2$)	Use safety glasses at all times, lab coat when handling MEG	
5	Emptying and cleaning	Ketil Hyllestad	HCl (0.50%)	Use safety glasses at all times, gloves.	

F.2 Risk assessment

NTNU		Risk Evaluation	Number	Date	
	Risk Assessment	HSE-dep.	HMSRV2601		
		Approved by	Page		
HSE					

Unit: Chemical Engineering   Date: 18.01.2013

Line manager: Øyvind Gregersen

Participants in the identification process (including their function):

Ketil Hyllestad (Daily Manager of Apparatus) og Margrethe Nergaard (PhD-student)

Continuous flow scaling setup

Table F.2: Risk assessment form

ID no.	Activity from the identification process form	Potential undesirable incident/strain	Likelihood: Likelihood (1-5)	Consequence: Human (A-E)	Environment (A-E)	Economy/ material (A-E)	Reputation (A-E)	Risk value Human	Comments/status Suggested measures
1	Solution preparation of reactant solutions ($Ca(NO_3)_2$ and Na_2CO_3 in water/MEG-mixtures)	Spill of solution on floor/bench	5	A	A	A	A	5A	Wash the bench after preparing solutions
2		Spill of solution on humans	4	A	A	A	A	4A	If contact: Remove contaminated cloths and wash skin
3		Spill of solutions into the eyes	2	B	A	A	A	2B	Wear safety glasses at all times, flush with water if contact
4		Swallowing the solutions when spilled in face	1	B	A	A	A	1B	Do not induce vomiting. Seek medical attention immediately. If person is fully conscious give 250mL of water. If medical advice is delayed and if an adult has swallowed several ounces of chemical, then give (90-120 ml) of hard liquor such as 40% whiskey

5	Solution preparation of analytical solutions	Spill of solution on floor/bench	5	A	A	A	A	5A	Wash the bench after preparing solutions
6		Spill of solution on humans	3	C	A	A	A	3C	Wear gloves at all times, if skin contact wash with plenty of water and remove contaminated clothing
7		Spill of solutions into the eyes	2	D	A	A	C	2D	Wear safety glasses at all times, if eye contact rinse out with plenty of water
8		Swallowing the solutions when spilled in face	1	E	A	A	D	1E	Do not induce vomiting. Seek medical attention immediately. Give plenty of water. Do not try to neutralize.
9	Storage of chemicals	Fume formation if MEG tank is left open on very hot days	1	A	A	A	A	1A	The tank should always be closed.
10	HCl (37%)	Stinging odour if container is not tightly closed	1	A	A	A	A	1A	Store in fume cupboard and close container firmly
11	NH$_3$	Inhalation	1	A	A	A	A	1A	Store closed at room temperature underneath eye height

12	$NaCO_3$	Inhalation of dust or eye contact	1	B	A	A	A	1B	Store closed and cool
13	$Ca(NO_3)_2$	Inhalation	1	A	A	A	A	1A	Store closed and dry
14	Running the experiment	Hair stuck in mechanical stirrers	2	D	A	D	D	2D	People with long hair should be careful
15		Spill of solution on floor/bench	5	A	A	A	A	5A	Wash the bench after preparing solutions, place electric components at elevated positions
16		Spill of solution on humans	3	B	A	A	A	3B	Wear safety glasses at all times, if eye contact rinse out with plenty of water
17		Fume formation from MEG in contact with hot surface	4	B	A	A	A	4B	Fume hood used above reactor
18		Injury from lifting of heavy units	3	C	A	C	B	3C	Safe lifting technique
19		Injury from falling of elevated equipment	3	B	A	C	C	3B	Equipment placed away from the edge

20	Emptying and cleaning	Spill of solution on floor/bench	5	A	A	A	A	5A	Wash the bench after preparing solutions
21		Spill of solution on humans	3	B	A	A	A	3B	Wear gloves when handling acidic solution
22		Spill of solutions into the eyes	2	C	A	B	B	2C	Wear safety glasses at all times, if eye contact rinse out with plenty of water
23		Swallowing the solutions when spilled in face	1	D	A	C	C	1D	

Likelihood, e.g.:
1. Minimal
2. Low
3. Medium
4. High
5. Very high

Consequence

A. *Safe*
B. *Relatively safe*
C. *Dangerous*
D. *Critical*
E. *Very critical*

Risk value (each one to be estimated separately):
Human = Likelihood x Human Consequence
Environmental = Likelihood x Environmental consequence
Financial/material = Likelihood x Consequence for Economy/materiel

F.3 HSE action plan

Unit : Chemical Engineering, Continuous flow scaling setup (K4.008)

Table F.3: HSE action plan form

What	Measure	Unit responsible	Priority	Current status
Solution preparation of reactant solutions ($Ca(NO_3)_2$ and Na_2CO_3 in water/MEG-mixtures)	Wear safety glasses and gloves, Lab coat used when handling MEG	Ketil Hyllestad	High	Complete
Solution preparation of analytical solutions	Wear safety glasses and gloves, use fume cupboard	Ketil Hyllestad	High	Complete
Storage of chemicals	Acids placed in fume cupboard, glass equipment stored below head level, chemicals stored in marked locker	Ketil Hyllestad	High	Complete
Running the experiment	Secure connections, electric equipment placed at distance, wear safety glasses, fume hood placed over reactor	Ketil Hyllestad	High	Complete
Emptying and cleaning	Wear safety glasses, lab coat and gloves	Ketil Hyllestad	High	Complete

Date: 18.01.2013   Line Manager: Øyvind Gregersen

G SEM Analysis Images and Results

The thickness of the scaled layers was found through SEM analysis. An area with solid deposit was scraped clean on the tube, which enabled measurement of thickness in the apparatus. This analysis was also used to give information on morphology and polymorphism of the scale.

Some experiments were not analyzed with SEM, especially when several parallels were done with the same set of parameters or when the experiment was used only to test the setup. Figure G.1 shows the results from a bulk sample test used to check for bulk nucleation in a solution with an inlet supersaturation of 6.0 and a MEG concentration of 50wt%. The same observation was made with a MEG concentration of 70wt%.

Figure G.2- Figure G.22 shows the results from the analysis. In most experiments there was a certain degree of non-uniformity. This has been accounted for in the thickness measurement by calculating an average value from several areas. It should be noted that this thickness measurement is not very accurate and should be considered an approximate value.

Table G.1 includes a summary of the polymorphs observed and measured layer thickness. When several polymorphs have been observed, the most abundant ones have been marked with bold writing. SEM apparatus settings have been briefly discussed in Section 3.5.
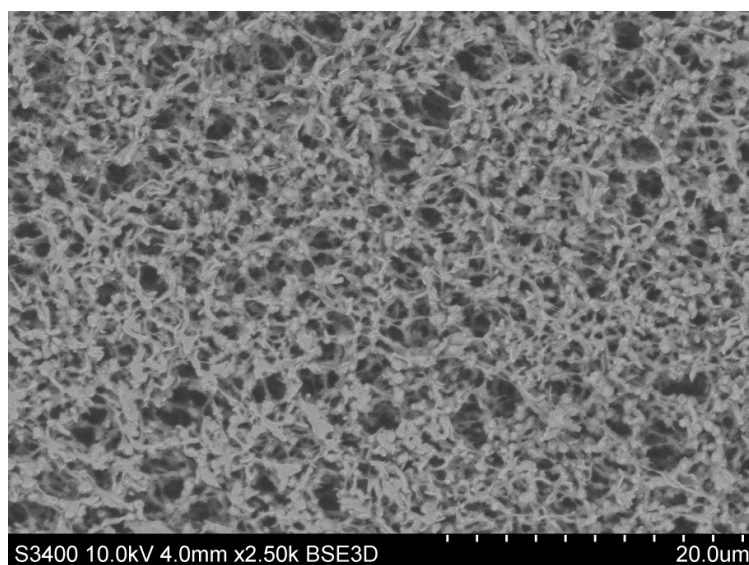
Figure G.1: SEM picture of 22 μm filter after filtration of bulk sample from experiment with S=6.0, T_{Tube}=90°C and 50wt% MEG (no particles observed).
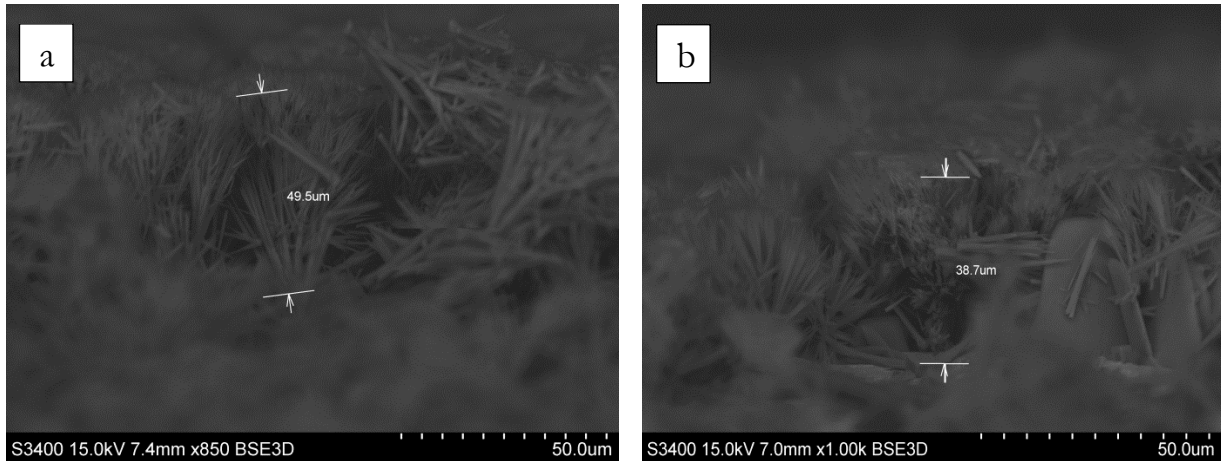
Figure G.2: SEM pictures: a) S=4.5, T_{Tube}=90°C, 180 min, experiment 15.02, x850 enlargement b) S=4.5, T_{Tube}=90°C, 180 min, experiment 22.02, x1000 enlargement.
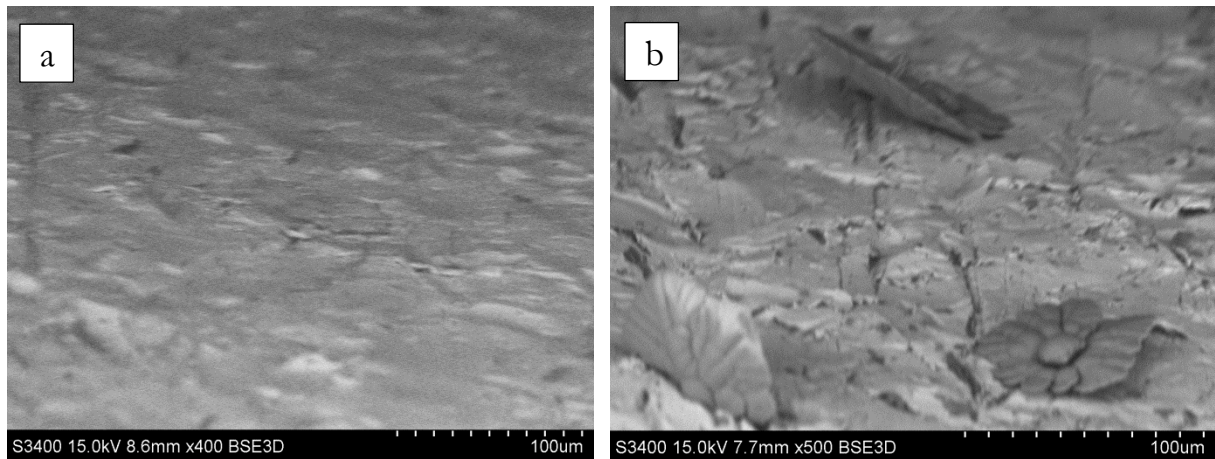
Figure G.3: SEM pictures: a) S=6.0, T_{Tube}=90°C, 90 min, MEG=50wt%, x400 enlargement (exp.: 05.03) b) S=6.0, T_{Tube}=90°C, 90 min, MEG=70wt%, x500 enlargement (exp.: 26.02).
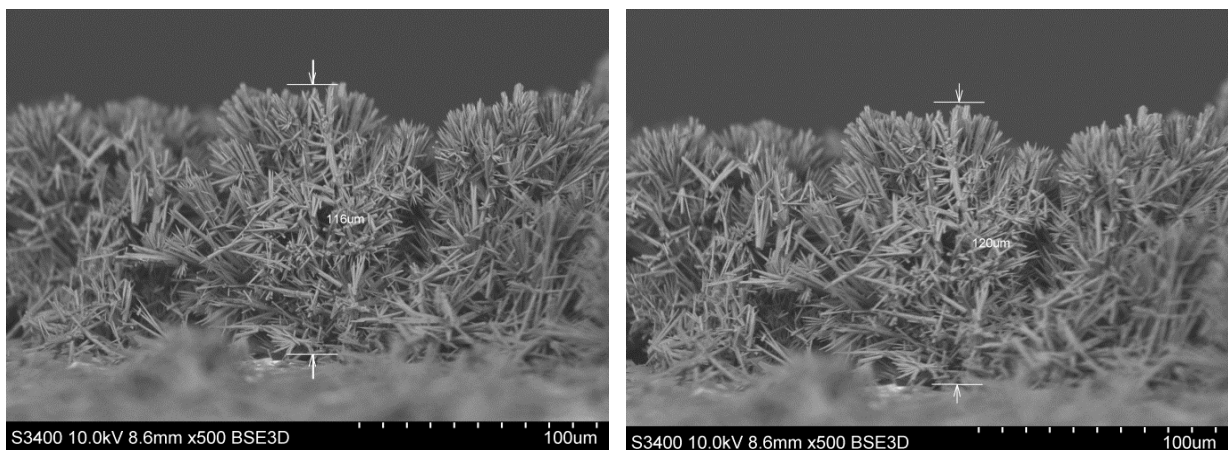
Figure G.4: SEM pictures of experiment 14.03, S=6.0, T_{Tube}=90°C, 90+90 min, MEG=50wt%, x500 enlargement.
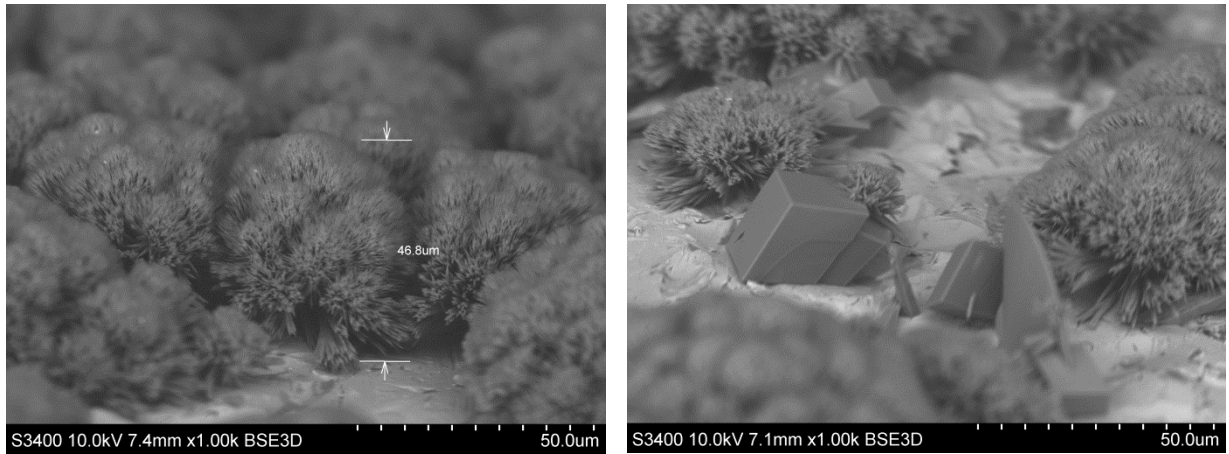
Figure G.5: SEM pictures of experiment 02.04, S=6.0, T_{Tube}=90°C, 90+155 min, MEG=50wt%, x1000 enlargement.
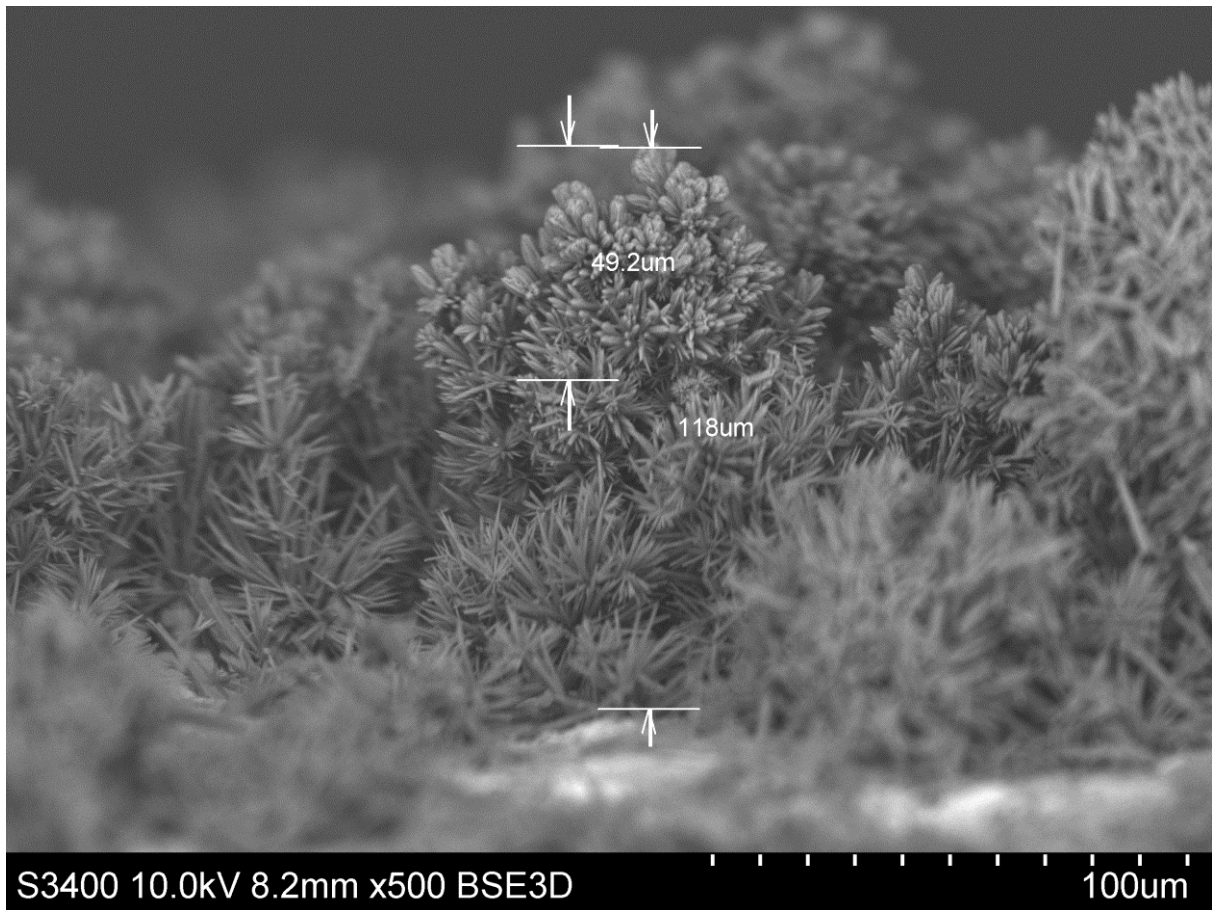
Figure G.6: 21.03: SEM picture of experiment 21.03, S=6.0, T_{Tube}=90°C, 90+90 min, MEG=70wt%, x500 enlargement.
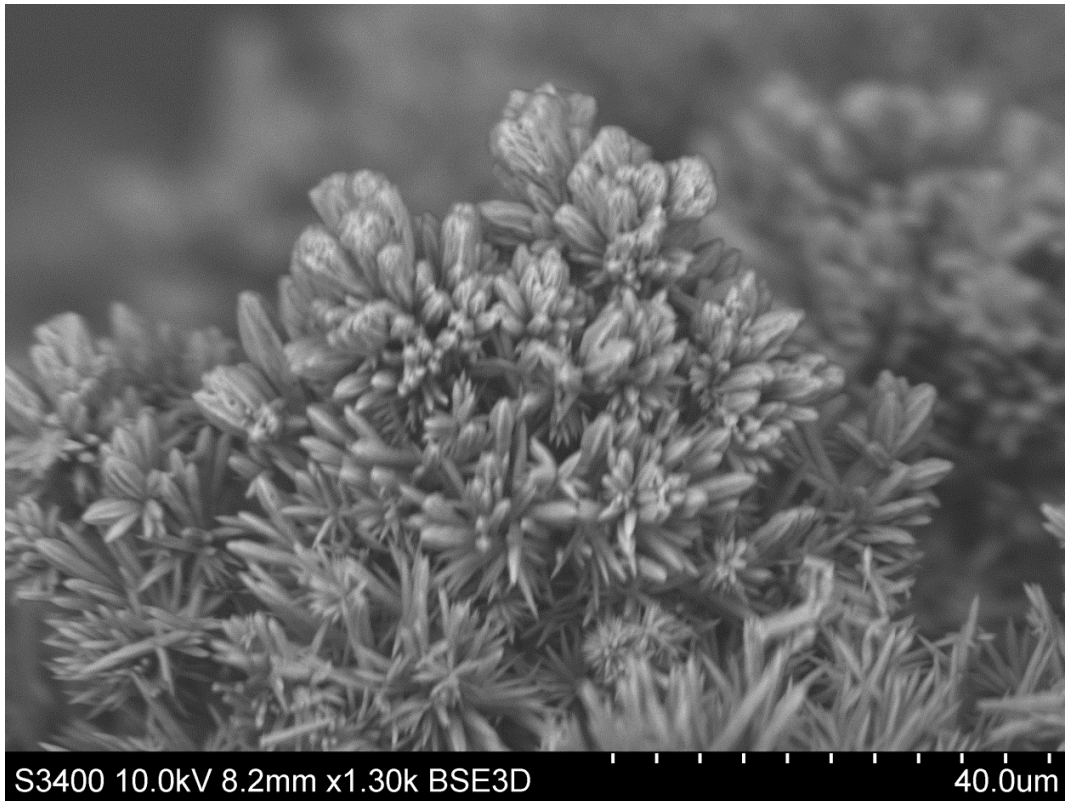
Figure G.7: SEM picture of experiment 21.03, S=6.0, T$_{Tube}$=90°C, 90+90 min, MEG=70wt%, x1300 enlargement.
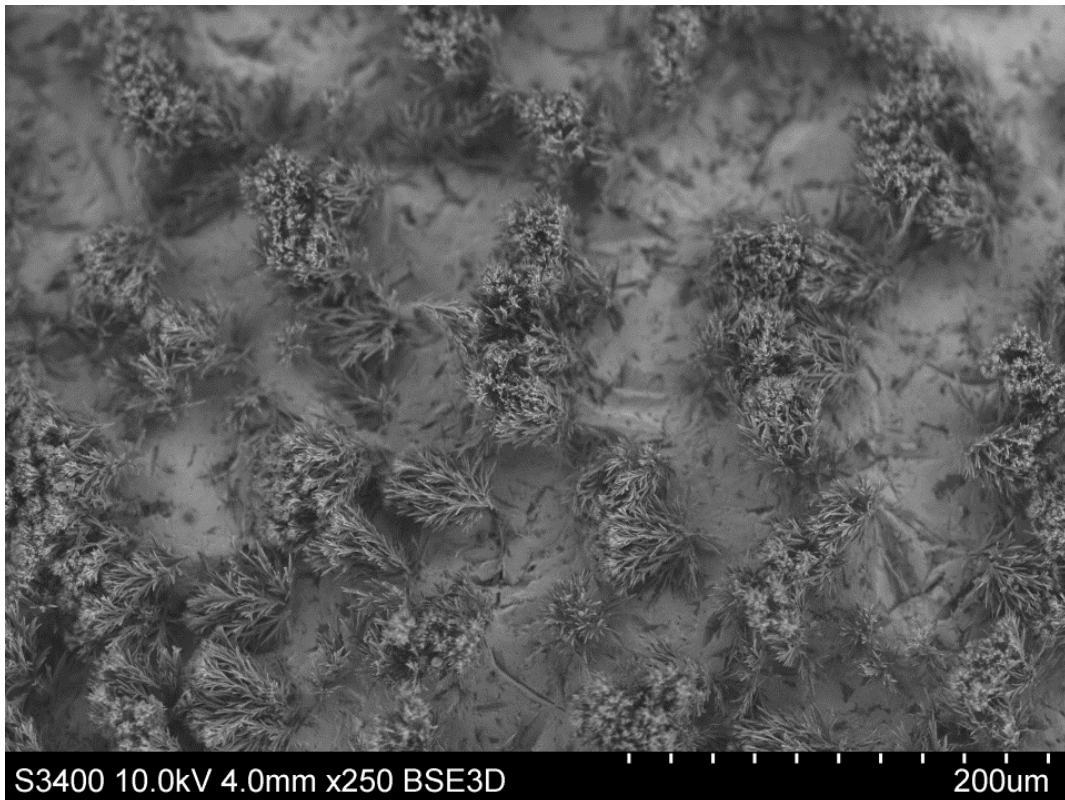
Figure G.8: SEM picture of experiment 04.04, S=12.3, T$_{Tube}$=90°C, 30 min, MEG=50wt%, x250 enlargement .
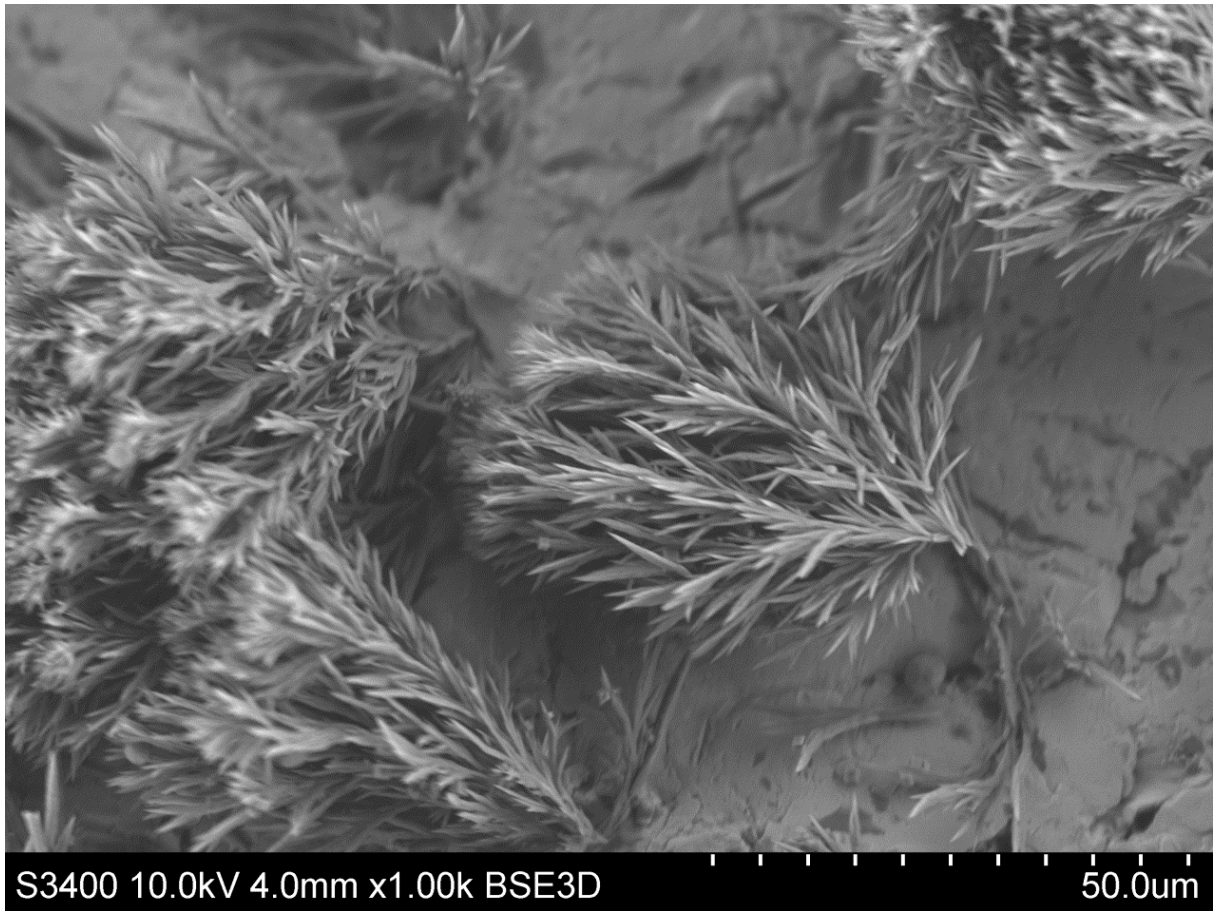
Figure G.9: SEM picture of experiment 04.04, S=12.3, T_{Tube}=90°C, 30 min, MEG=50wt%, x1000 enlargement.
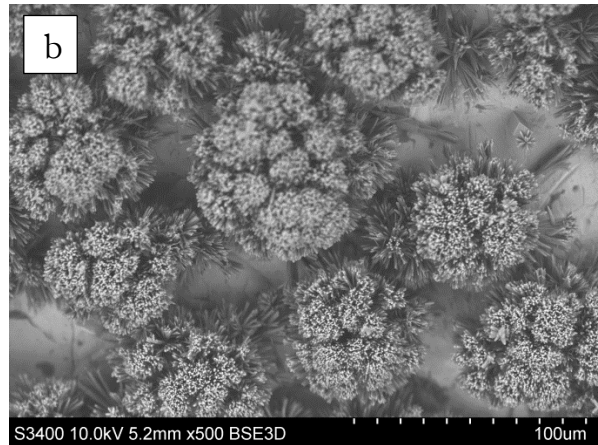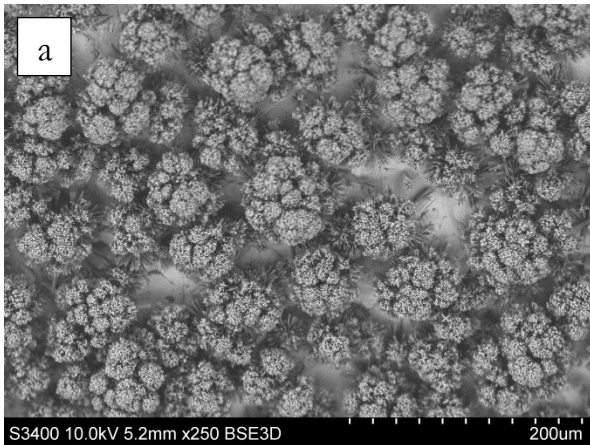
Figure G.10: SEM pictures of experiment 09.04, S=6.0, T_{Tube}=90°C, 90+90 min, MEG=90wt% a) x250 enlargement b) x500 enlargement.
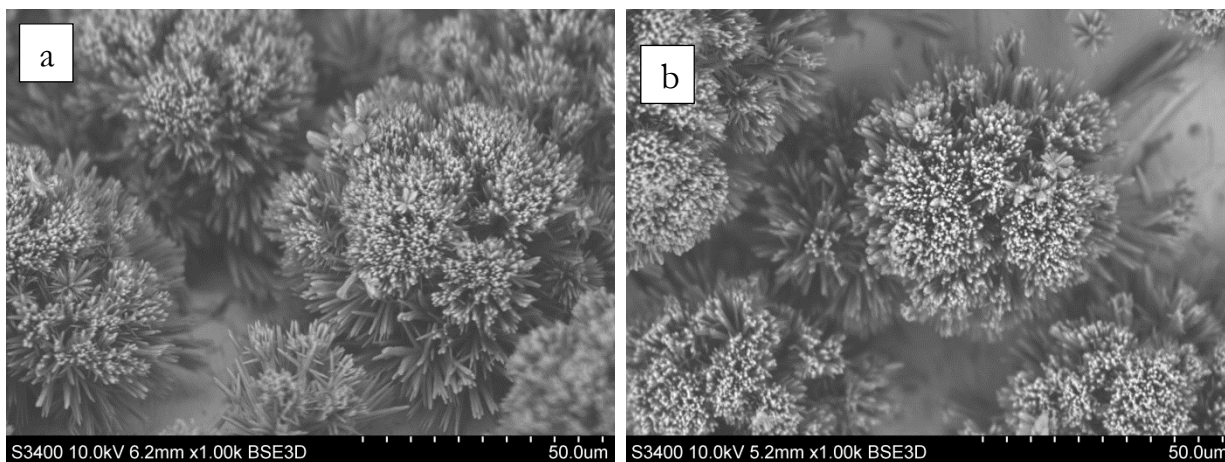
Figure G.11: SEM pictures of experiment 09.04, S=6.0, T_{Tube}=90°C, 90+90 min, MEG=90wt%, x1000 enlargement.
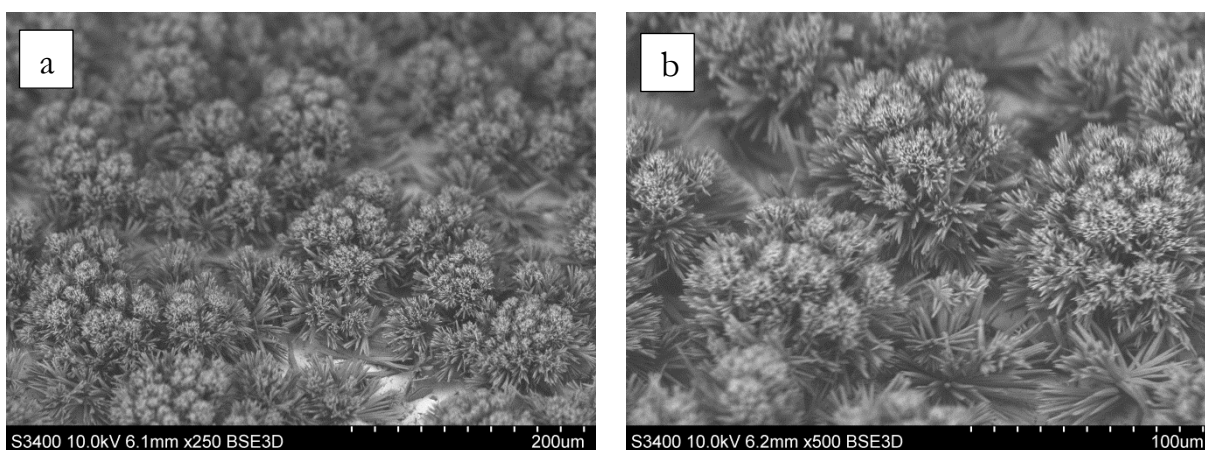
Figure G.12: SEM pictures of experiment 10.04, S=6.0, T_{Tube}=90°C, 90 min a) x250 enlargement b) x500 enlargement.
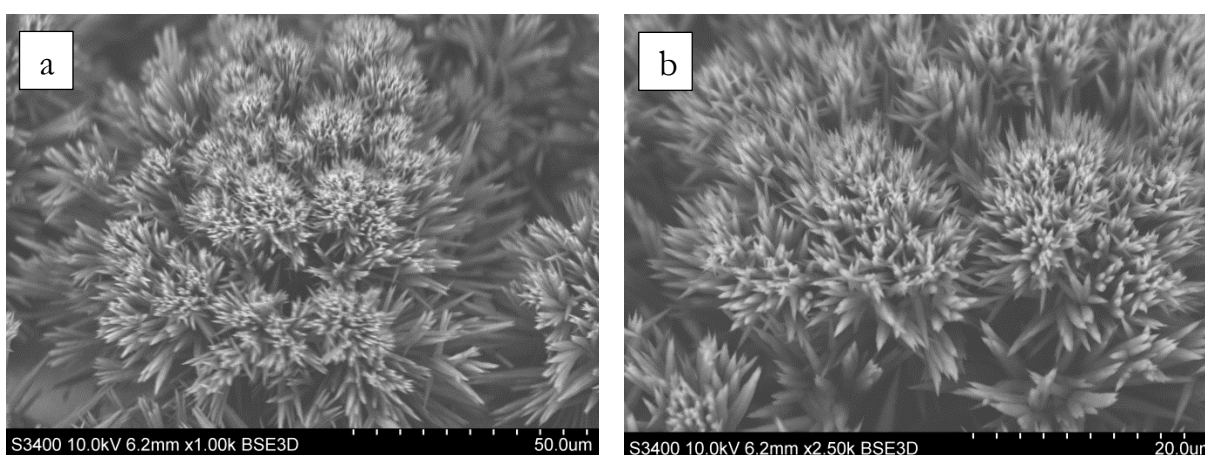
Figure G.13: SEM pictures of experiment 10.04, S=6.0, T_{Tube}=90°C, 90 min a) x1000 enlargement b) x2500 enlargement.
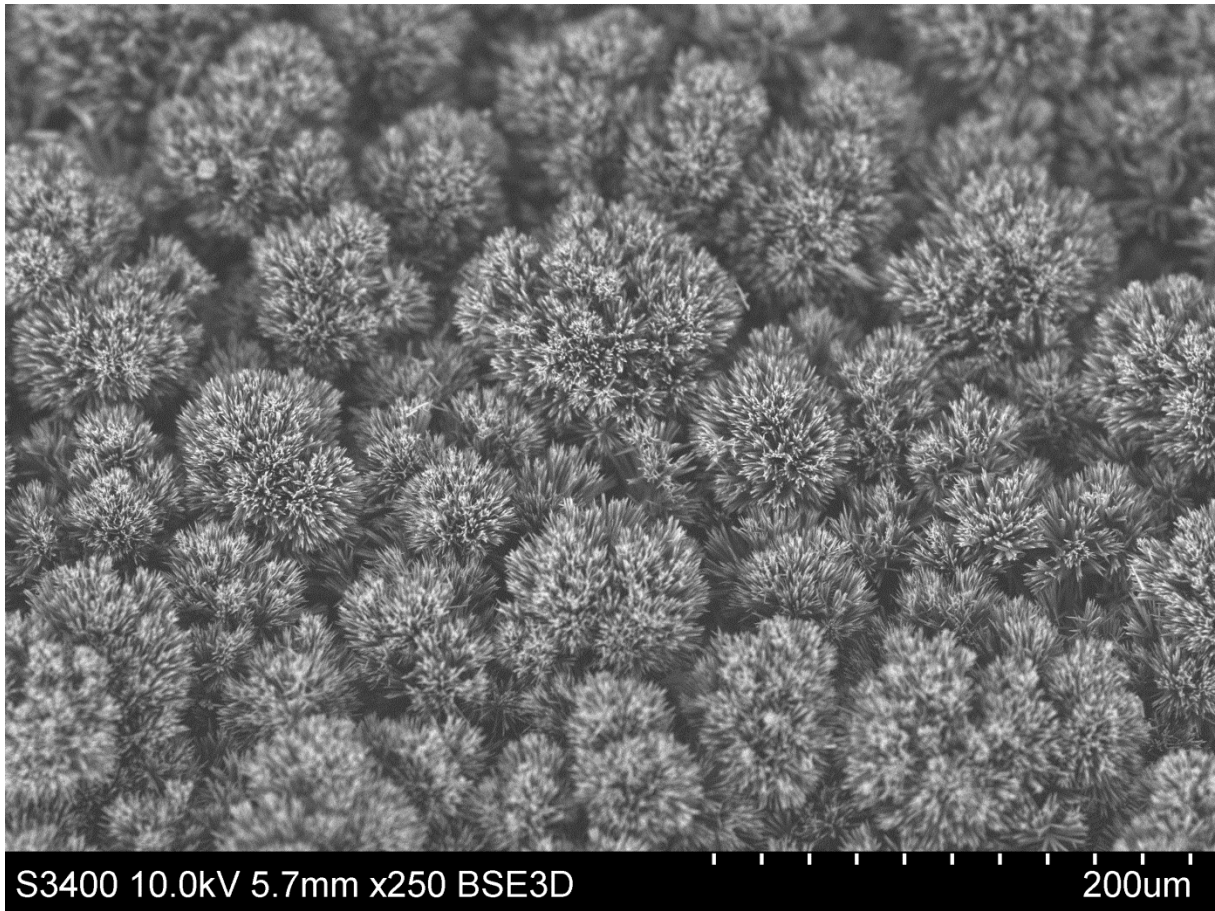
Figure G.14: SEM picture of experiment 12.04, S=6.0, T_{Tube}=90°C, 180 min, x250 enlargement.
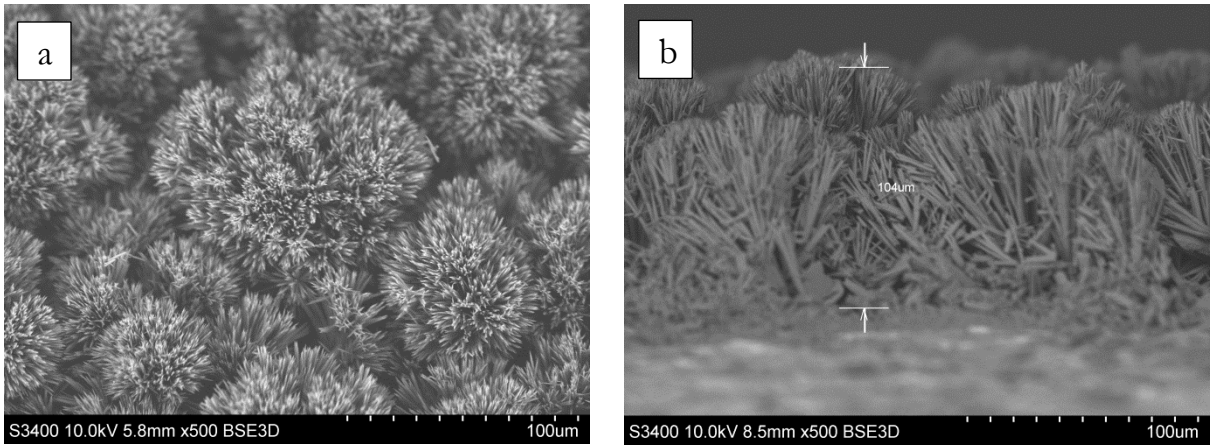
Figure G.15: SEM pictures of experiment 12.04, S=6.0, T_{Tube}=90°C, 180 min, x500 enlargement.

S3400 10.0kV 5.8mm x1.00k BSE3D   50.0um
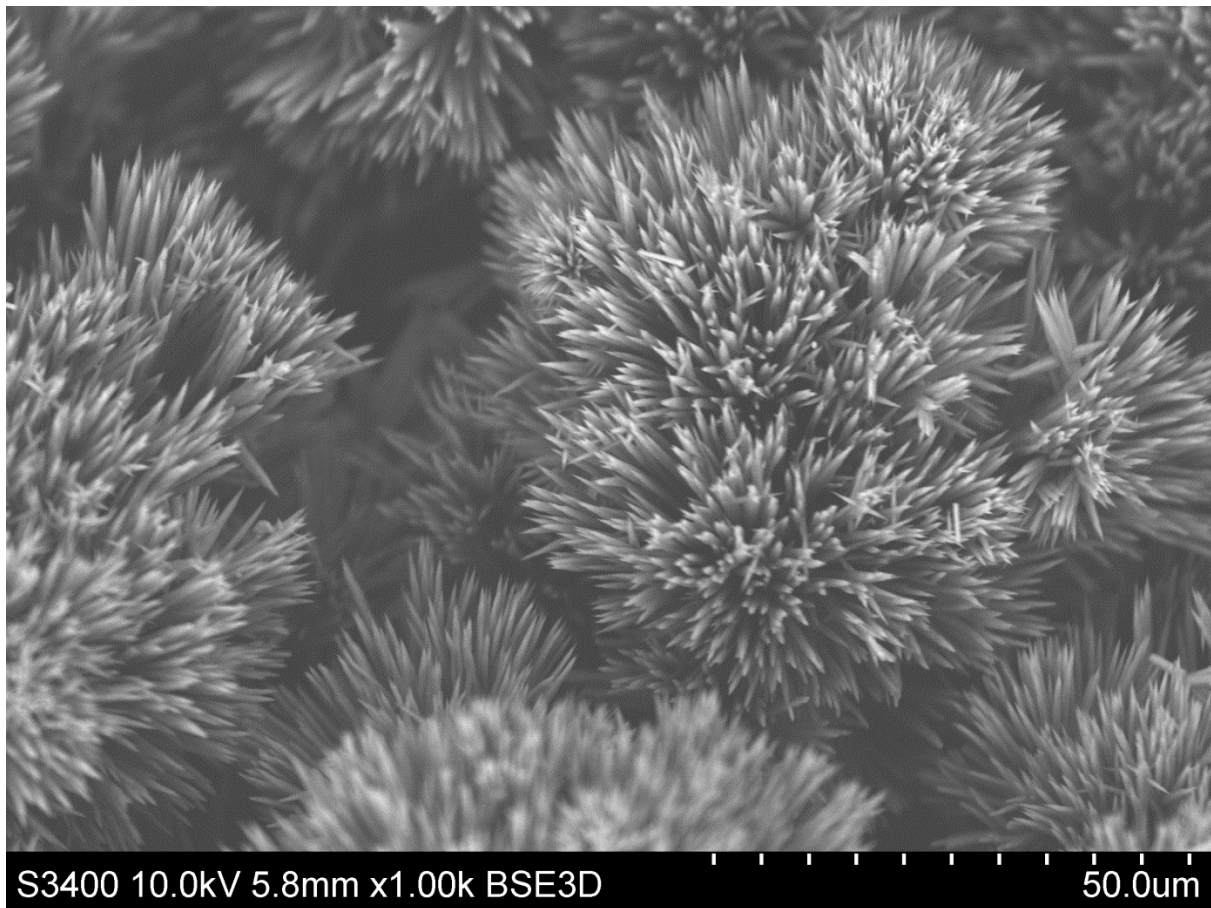
Figure G.16: SEM picture of experiment 12.04, S=6.0, T_{Tube}=90°C, 180 min, x1000 enlargement.

a

S3400 10.0kV 4.0mm x250 BSE3D   200um

b

S3400 10.0kV 4.0mm x500 BSE3D   100um
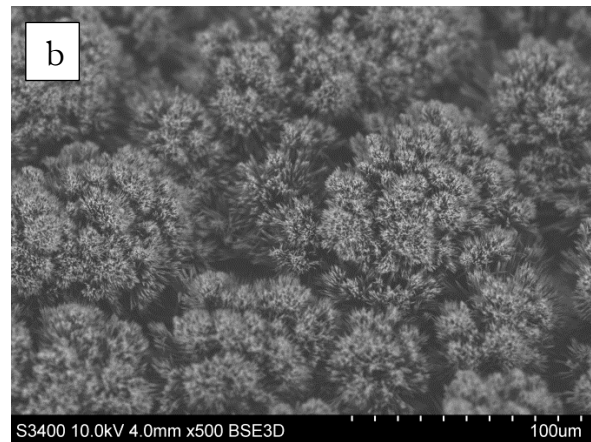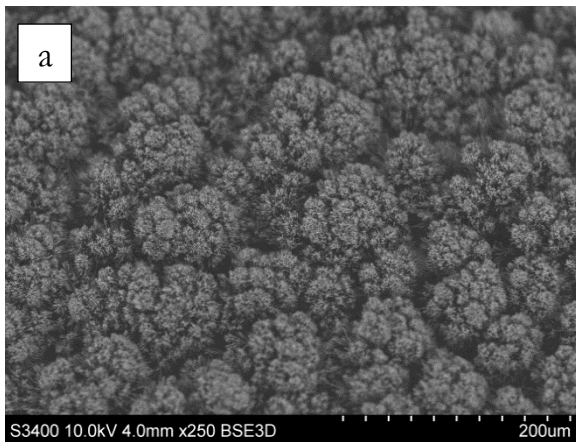
Figure G.17: SEM pictures of experiment 16.04, S=6.0, T_{Tube}=90°C, 90 min: a) x250 enlargement b) x500 enlargement.
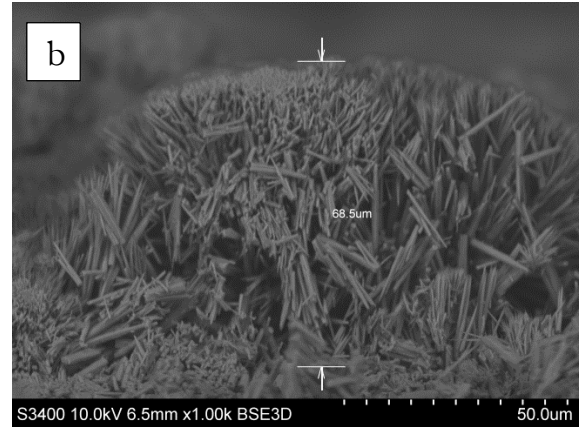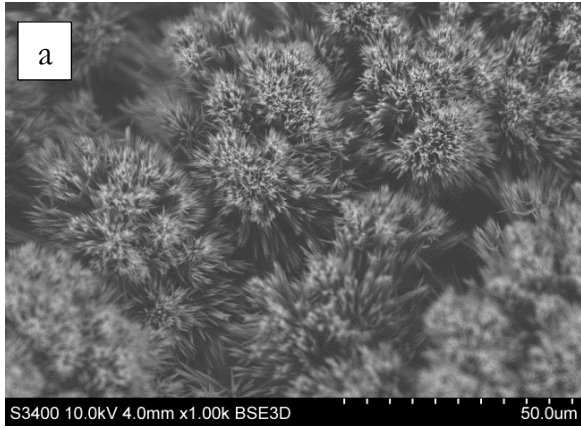
Figure G.18: SEM pictures of experiment 16.04, S=6.0, T_{Tube}=90°C, 90 min, x1000 enlargement.
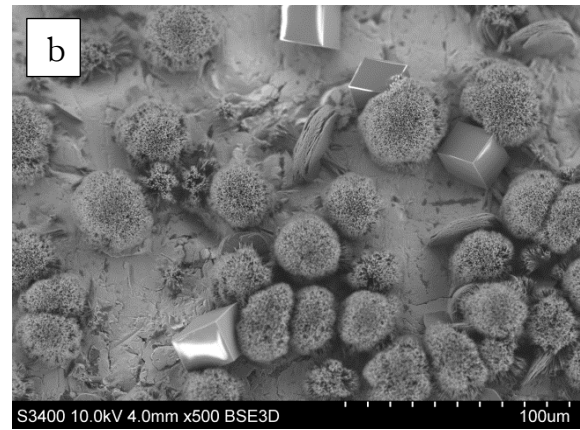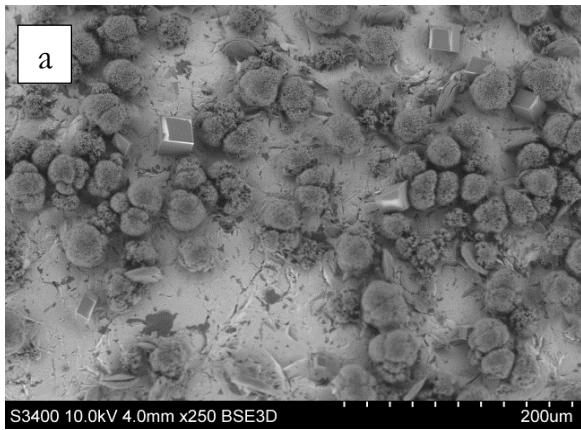
Figure G.19: SEM pictures of experiment 26.04, S=6.0, T_{Tube}=50°C, 180 min: a) x250 enlargement b) x500 enlargement.
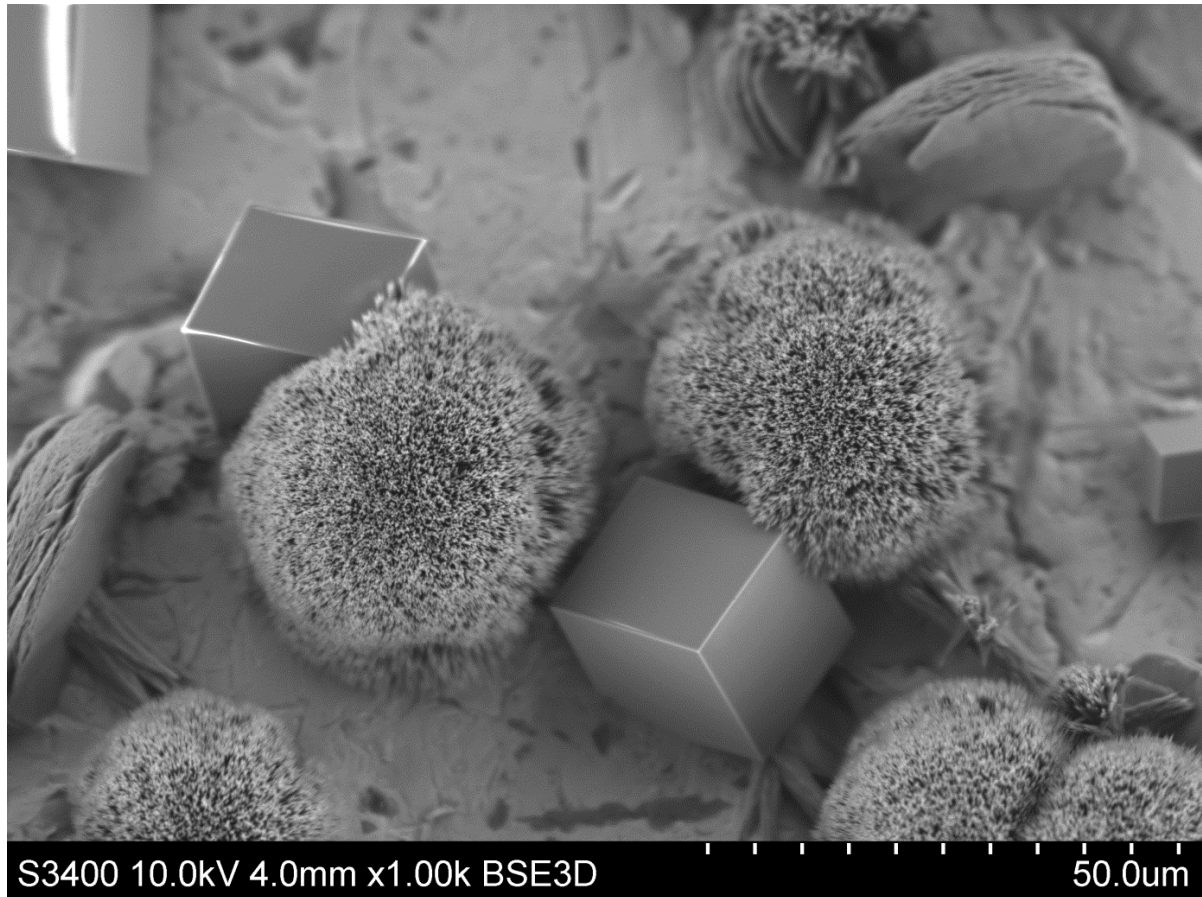
Figure G.20: SEM picture of experiment 26.04, S=6.0, T_{Tube}=50°C, 180 min, x1000 enlargement.
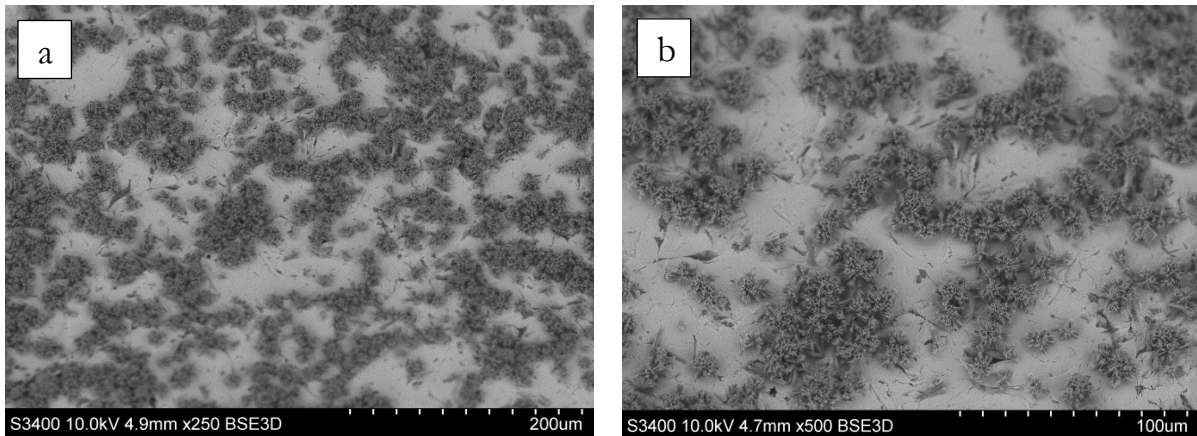
Figure G.21: SEM pictures of experiment 26.04(2), S=6.0, T_{Tube}=50°C, 90+90 min, MEG=70wt%: a) x250 enlargement b) x500 enlargement.
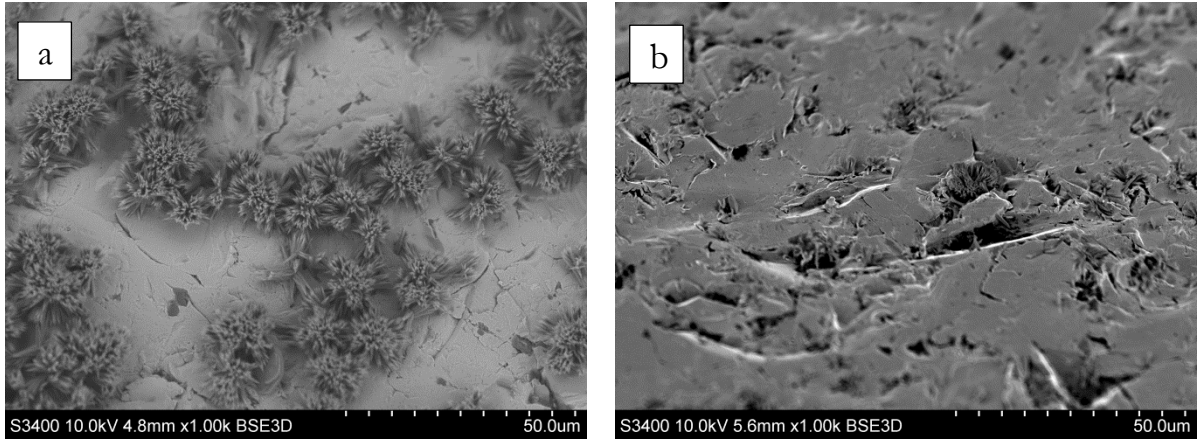
Figure G.22: SEM pictures of experiment 26.04(2), S=6.0, T_{Tube}=50°C, 90+90 min, MEG=70wt%, x1000 enlargement: a) semi-densely scaled-area b) area with scale only occurring in surface cracks.

Table G.1: Observed polymorphs and estimated average layer thickness from SEM analysis

Exp.	S	T_{Tube} [°C]	Duration [min]	MEG [wt%]	Average layer thickness [µm]	Polymorph(s) observed
26.04(2)	6.0	50	90+90[a]	0+70	-[b]	**Aragonite** (Calcite, Vaterite)[c]
26.04	6.0	50	180	0	-	**Aragonite**, Calcite, (Vaterite)
16.04	6.0	90	90	0	68.1	Aragonite
12.04	6.0	90	180	0	104	Aragonite
10.04	6.0	90	90	0	59.9	Aragonite
09.04	6.0	90	90+90	0+90	75.2	**Aragonite**, Vaterite, (Calcite)
04.04	12.3	90	30	50	-	Aragonite
02.04	6.0	90	90+155	0+50	46.8	**Aragonite**, Calcite, (Vaterite)
21.03	6.0	90	90+90	0+70	118	**Aragonite**, Vaterite
14.03	6.0	90	90+90	0+50	118	Aragonite
05.03	6.0	90	180	50	-	No crystals observed
26.02	6.0	90	180	70	-	(Vaterite)
22.02	4.5	90	180	0	36.7	Aragonite
15.02	4.5	90	180	0	49.5	Aragonite

[a] Experiments marked with two added time intervals describes an initial period without MEG (pre-scale period) and then a continuation with the same supersaturation level and tube temperature for a new time interval with MEG.

[b] Scaled layer not uniform enough to determine layer thickness is marked (-) in the table.

[c] Polymorphs only observed in very minor amounts are marked with brackets in the table. Bold writing marks most abundant polymorph in a given experiment.

H XRD Analysis

Samples from six experiments were collected and prepared for qualitative X-ray diffraction analysis (XRD). This was done through a process of scraping off as much scale as possible from the U-tubes and then mortaring it into a fine powder. In the end it was diluted with ethanol and a few drops of the solution were added to a silica holder. When the ethanol had evaporated the sample was ready for analysis.

The results of XRD analysis can be graphically represented. The position and intensity of the peaks in these plots are related to crystallographic orientation. This information can be used to qualitatively identify the polymorphs deposited in the different experiments. Figure H.2-Figure H.7 shows a graphical representation of the data collected from the XRD analysis. The most important and intense peaks have been identified and marked with the polymorph they represent: Aragonite (A), calcite (V) or vaterite (V).

Crystallographic data from the ICDD PDF4+ 2011 database were used in the identification process, including: 04-008-5421 (aragonite), 04-007-8659 (calcite) and 04-015-4788 (vaterite). The scanning angles expected to give peaks for the different polymorphs have been marked with bars underneath the graphs according to the mentioned dataset. When two polymorphs are expected to give peaks at very similar scanning angles, the identification process can be difficult and such peaks are therefore often regarded as non-unique.

All the samples have been scanned from 18 to 75° with a 1 mm opening slit and 0.5 seconds scanning time per step. A D8 Focus unit equipped with a LynxEye detector was used in the scanning process. This was run in Bragg Brentano mode with Cu-K alpha radiation.

The presented results have been edited and results from some scanning angles have been removed when no significant peaks were yielded or when this data was no longer relevant. The y-axis of these results shows the relative intensity at the different scanning angles. Due to a few very high peaks in some of the samples, the y-axes in all the experiments have been shortened to make the results more readable. This editing has been done in the same manner for all the graphs so it is possible to compare them to one another. The x-axis' are given in two times the Bragg angle (2θ).

Quantitative analysis of the samples can for example be done with the Rietveld method. However, it proved too difficult to apply it with this set of samples. This type of analysis is based on the knowledge that the area under a peak reflects amount of that specific crystal. Table H.1 shows the results from the quantitative analysis made by Nergaard (2011) with similar setup and experimental parameters as the ones used in this work.

Table H.1: Quantitative results from XRD-analysis in the work by Nergaard (2011) with similar setup

S	T_{Tube}[°C]	Duration [min]	Aragonite [%]	Calcite [%]	Vaterite [%]
6.0	90	270	99.39	0.42	0.19
6.0	50	270	55.92	42.77	1.30

Figure H.1 shows the results from the XRD-analysis of the pre-scaled layer. This result is important since it forms the basis for other experiments. The experimental setup and parameters used in these experiments were largely based on the work done by Nergaard (2011). Figure H.2 shows a comparison of the XRD analysis results from this work and the data obtained by Nergaard (2011) at a tube temperature of 50°C and S=6.0. More calcite peaks were found in the literature data, but this could be caused by poor sample preparation. Figure H.3 shows the same data at 90°C. The literature data has been shifted upwards in these graphs to make the data more readable.
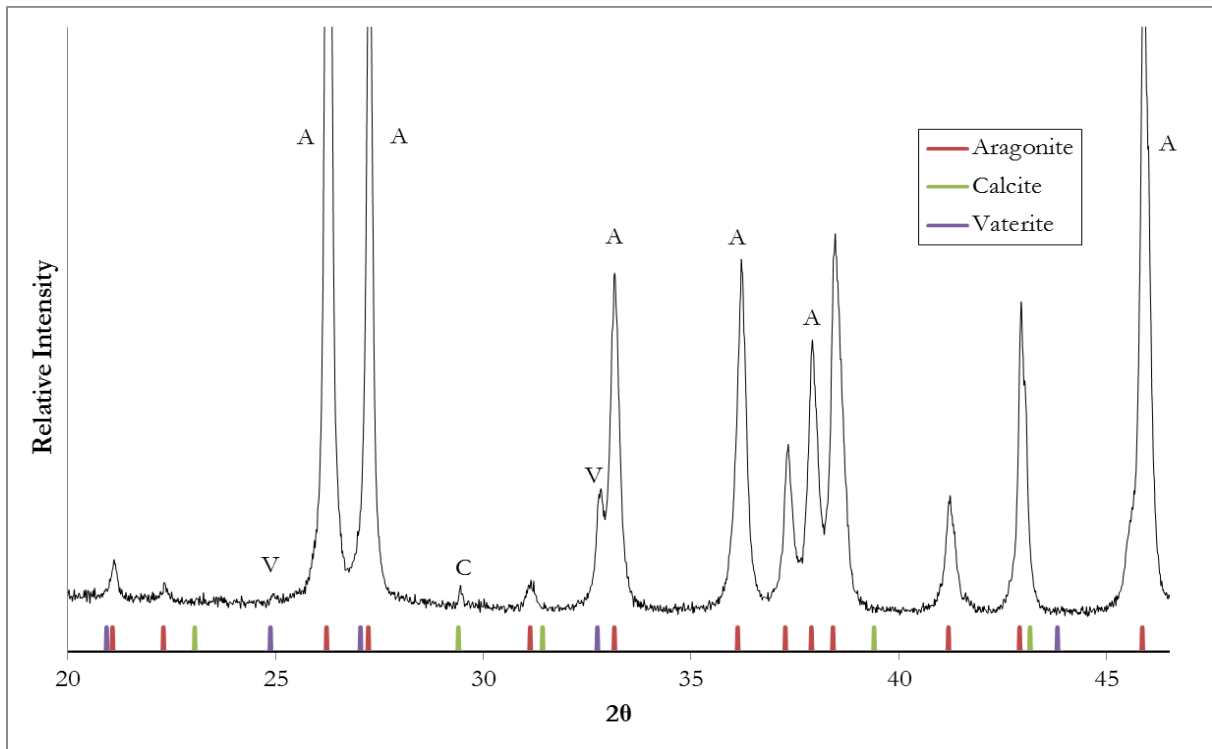
Figure H.1: Schematic of results from XRD analysis of experiment 16.04(2) with S=6.0, T_{Tube}=90°C and a time magnitude of 90 min (pre-scale test).
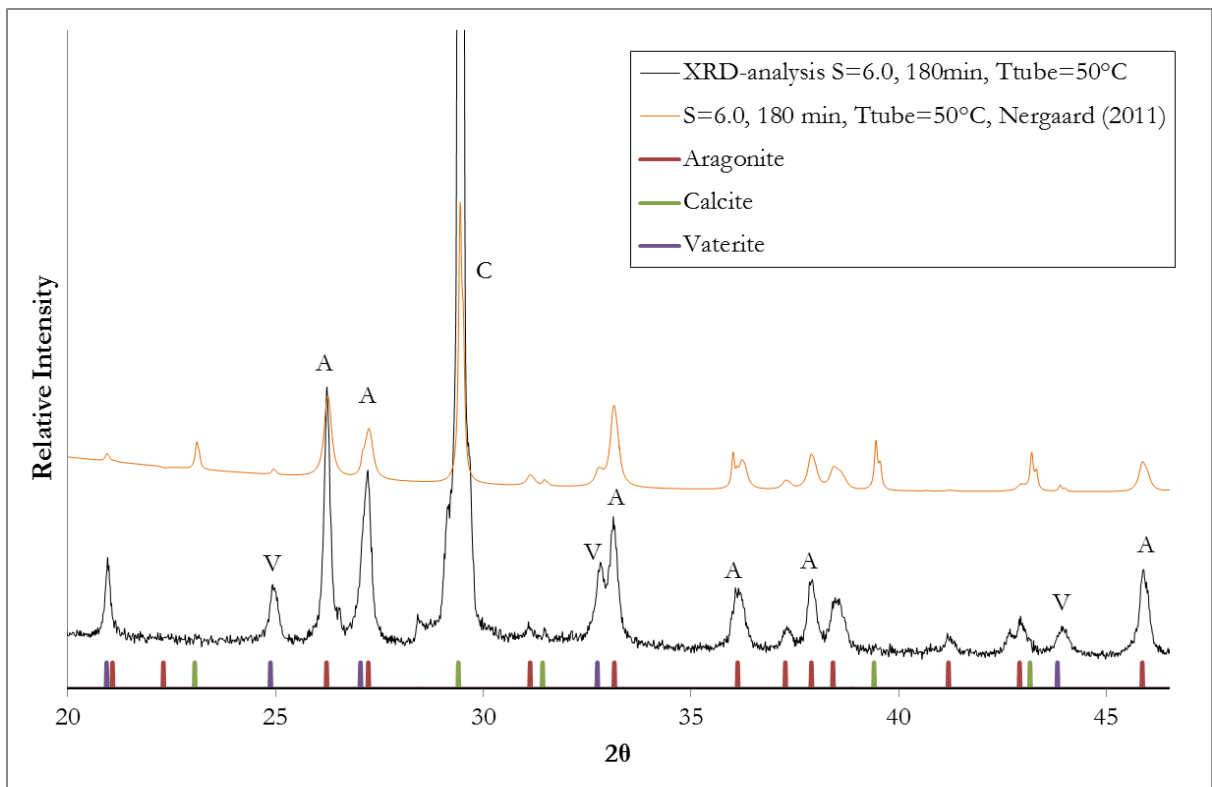
Figure H.2: Schematic of results from XRD analysis of experiment 26.04 with S=6.0, T_{Tube}=50°C and a time magnitude of 180 min compared with literature data (Nergaard, 2011).
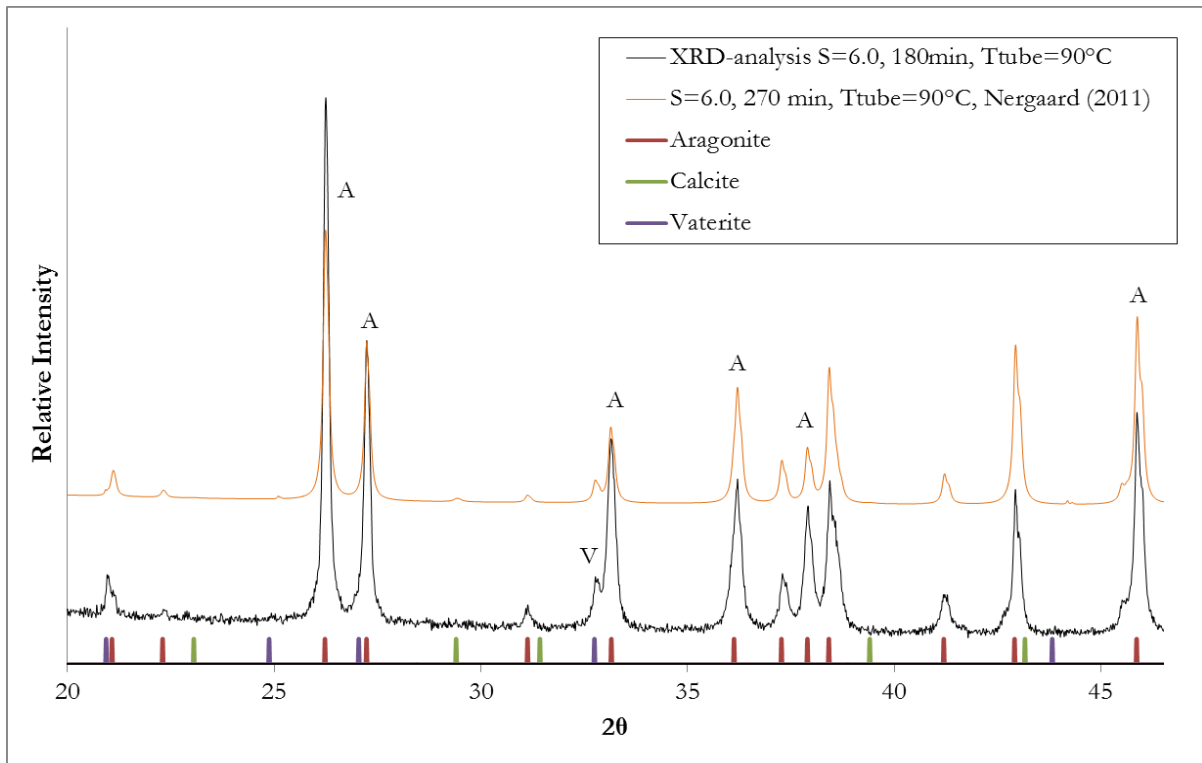
Figure H.3: Schematic of results from XRD analysis of experiment 12.04 with S=6.0, T_{Tube}=90°C and a time magnitude of 180 min compared with literature data (Nergaard, 2011).
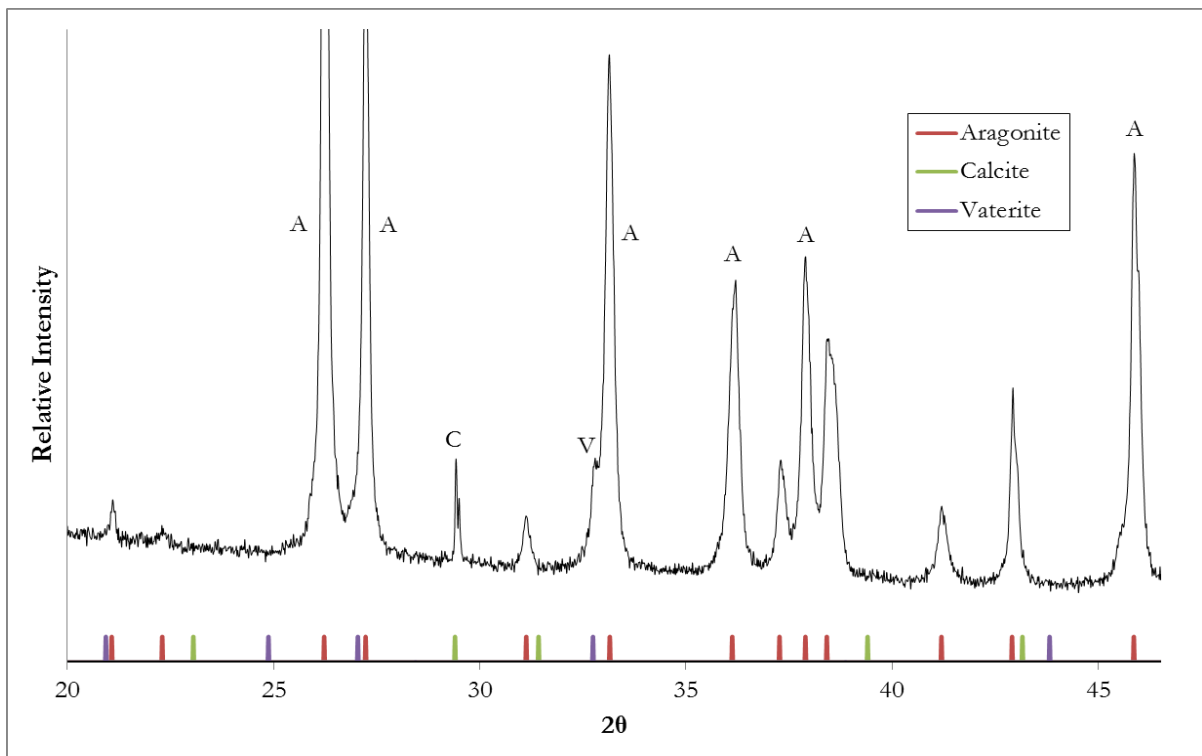
Figure H.4: Schematic of results from XRD analysis of experiment 09.04 with S=6.0 and T_{Tube}=90°C. First a pre-scale period without MEG for 90 min then 90 min with MEG=90wt%.
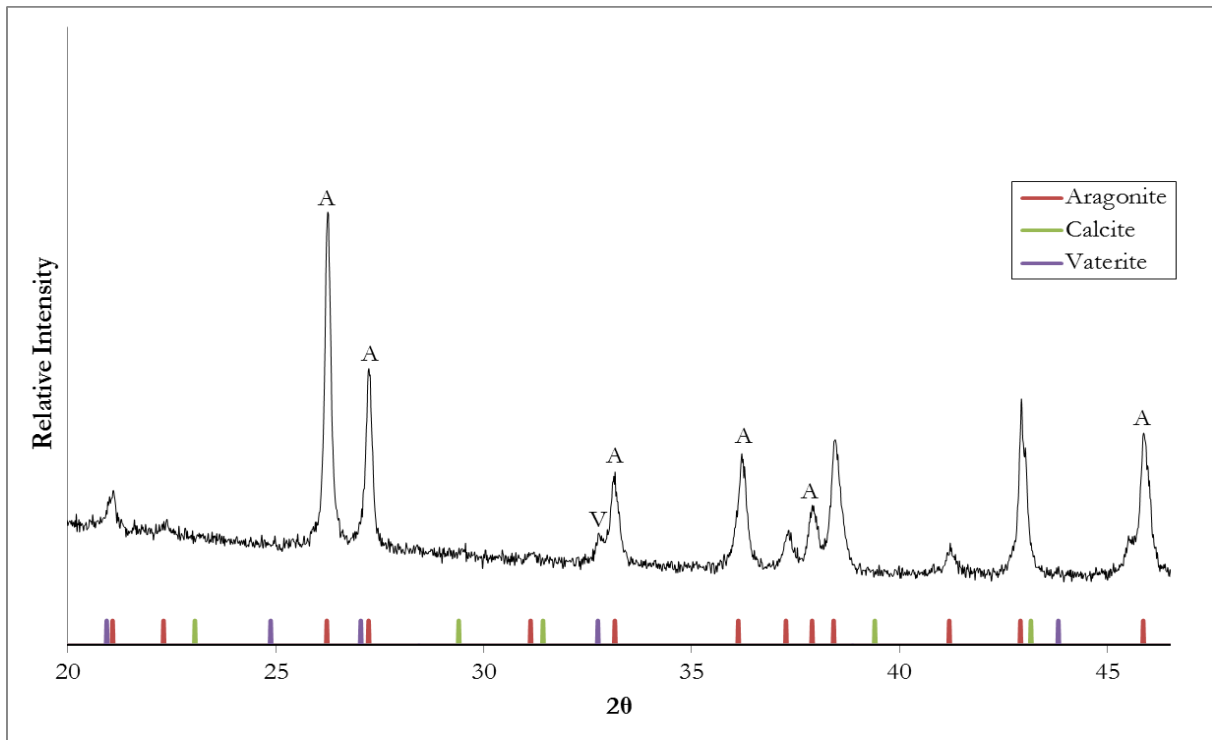
Figure H.5: Schematic of results from XRD analysis of experiment 14.03 with S=6.0 and T$_{Tube}$=90°C. First a pre-scale period without MEG for 90 min then 90 min with MEG=50wt%.
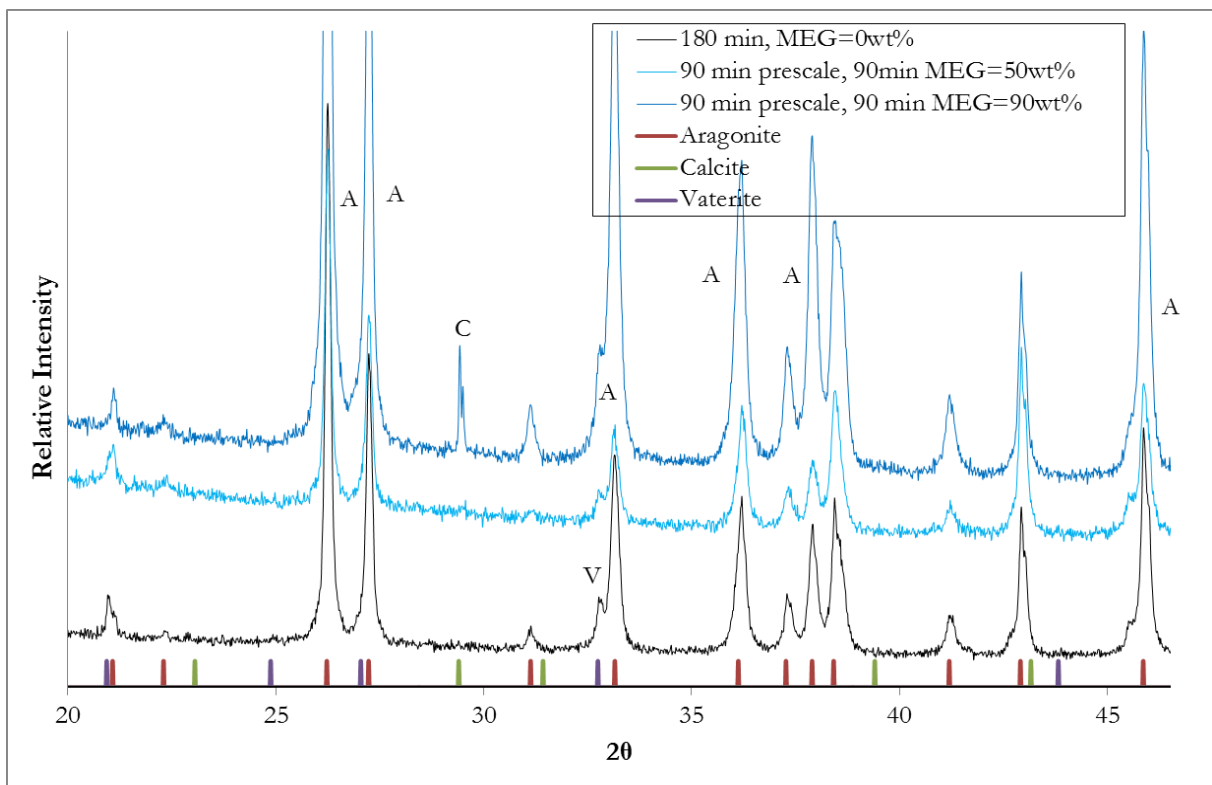
Figure H.6: Graphical representation of results from XRD analysis of experiments with S=6.0, T$_{Tube}$=90°C at MEG=0wt%, MEG=50wt% and MEG=90wt%.
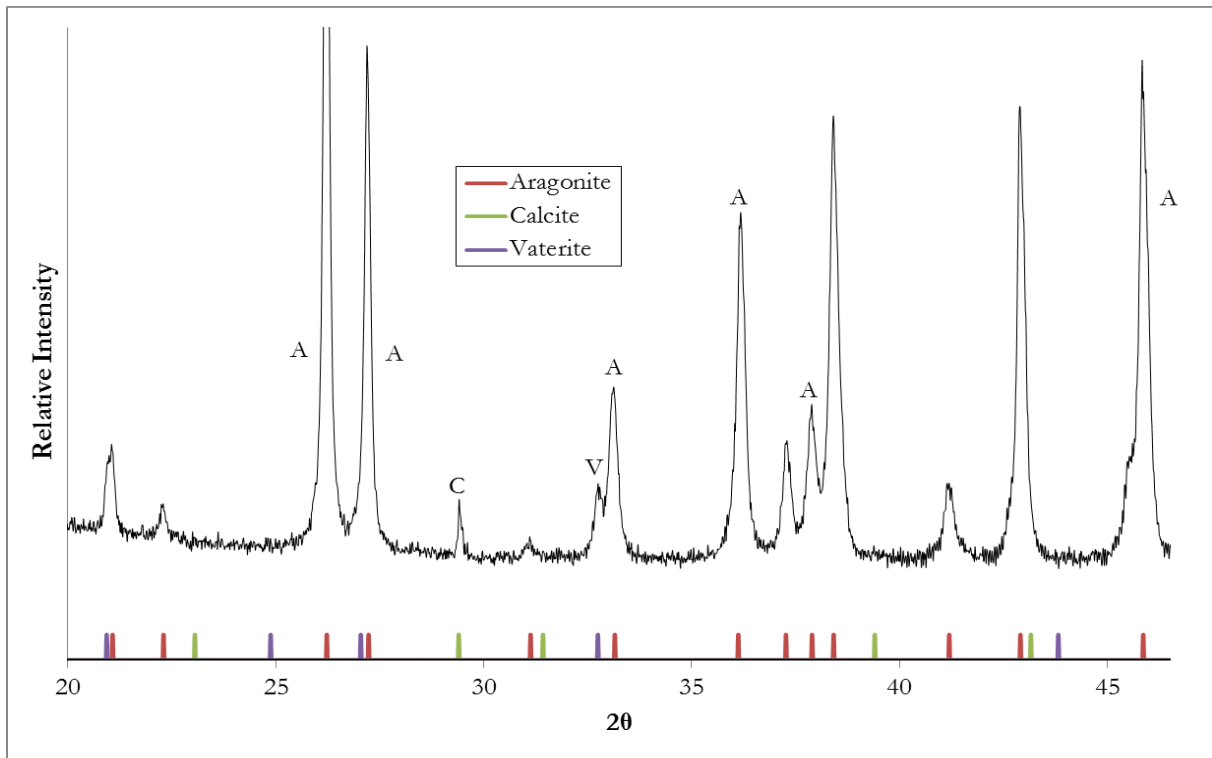
Figure H.7: Schematic of results from XRD analysis of experiment 26.04(2) with S=6.0 and T$_{Tube}$=50°C. First a pre-scale period without MEG for 90 min then 90 min with MEG=70wt%.

I Temperature and pH logging data

Temperature and pH data were logged continuously throughout the experiments. The collected raw data were edited before they were plotted. Temperature and pH fluctuations, due to cleaning of electrode probe, were deleted as these did not reflect the solution conditions.

Stops in the flow from reservoirs mainly occurred due to adjustment of pump speeds or due to the displacement of a silicon tube. The fluctuations caused by this have been omitted in the graphs used in the main report. The start and end points of the graphs were adjusted to reflect the pumping of solution from reservoirs.

Batch reservoirs were changed approximately every 90 minutes in the experiments. The exact time this was done have been marked with a vertical line in the graphical plots when this change of batch had a significant influence on temperature or pH. When no solvent composition has been mentioned, pure de-ionized water has been applied.

This data can be used to observe approximate bulk temperature (impact on actual supersaturation), pH stability (inlet supersaturation stability) and start point of U-tube inlet temperature.

I.1 Graphical plots of inlet/outlet temperature data for U-tube

Figure I.1- Figure I.23 shows a graphical representation of the data collected from measurements of inlet and outlet temperature from the U-tube. The graphs which show temperature data for the U-tube have not been marked with a legend. The graph with the highest temperature represents the inlet of the U-tube in all these plots, while the lowest temperature represents the U-tube outlet.

After the experiment shown in Figure I.4, the procedure was changed to include an initial period with flow of only distilled water through the system to reduce initial fluctuations.
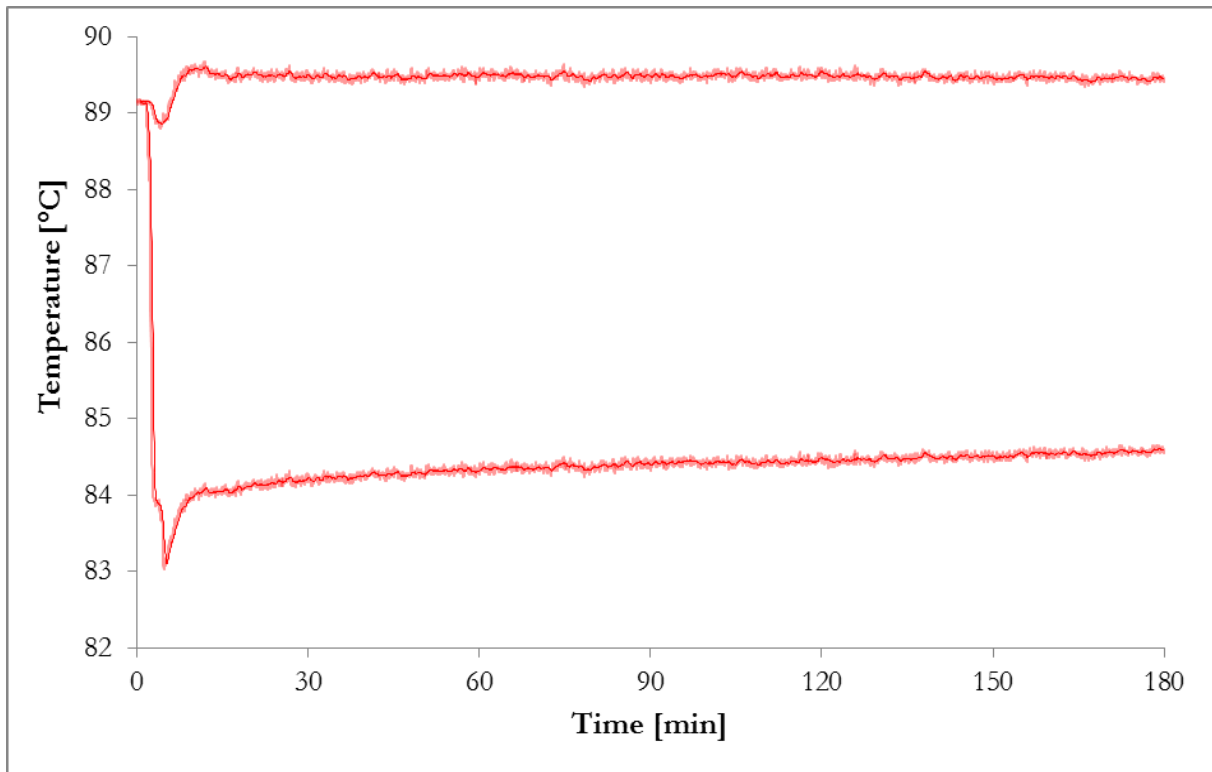
Figure I.1: Temperature inlet/outlet of U-tube, S=4.5, T_{Tube}=90°C, Experiment 08.02
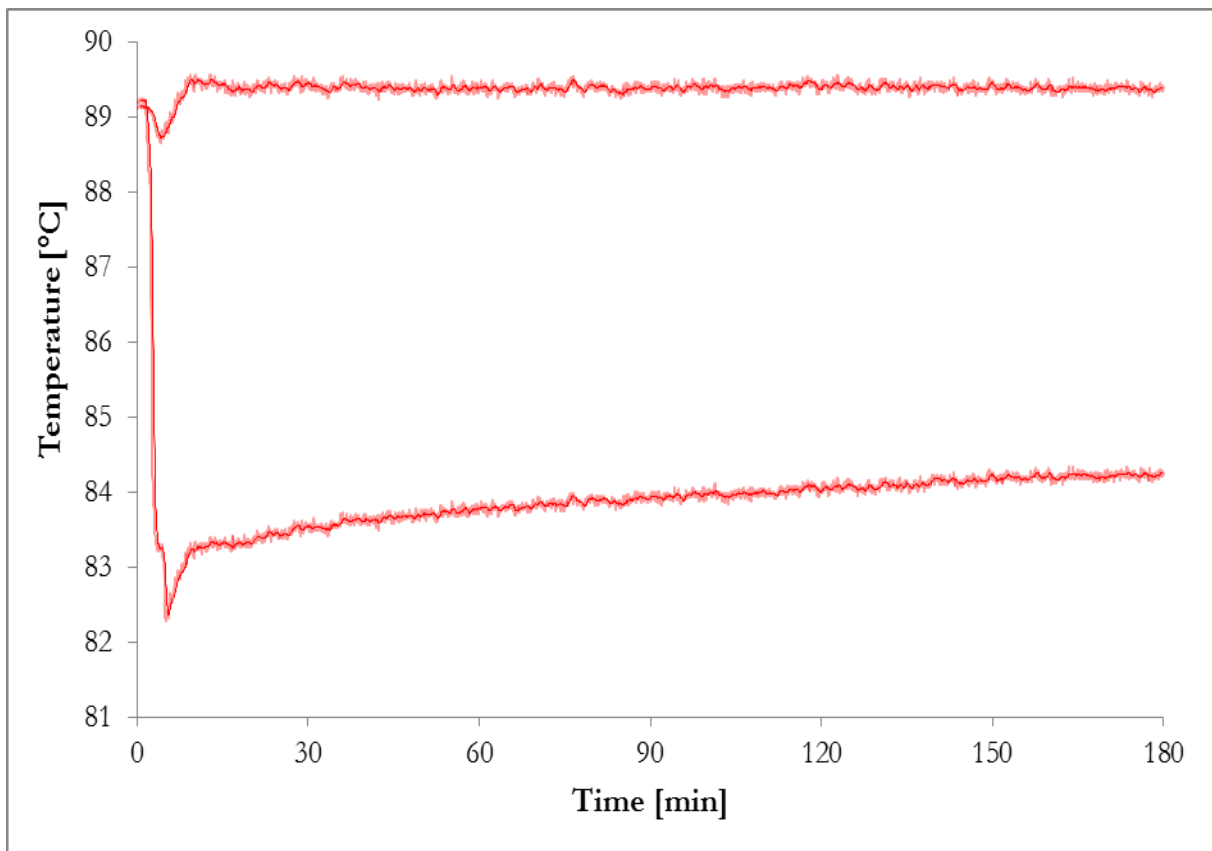
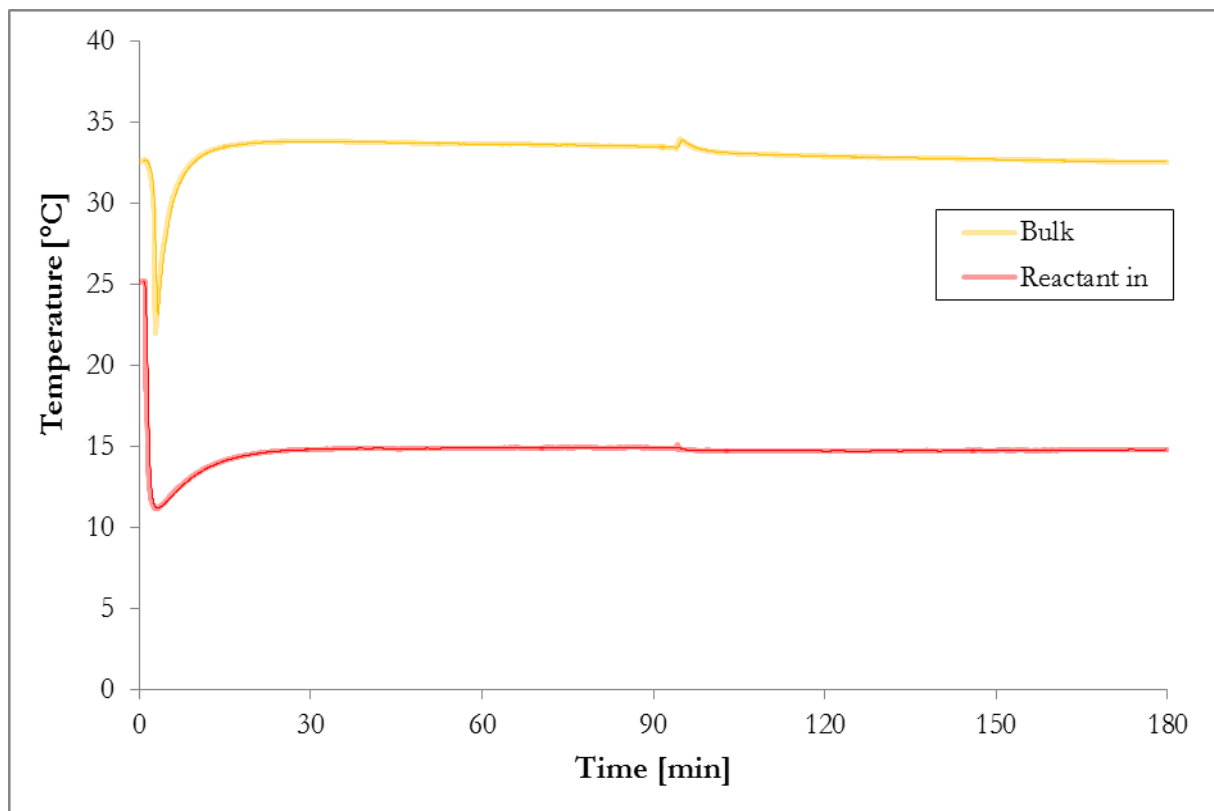**Figure I.2: Temperature inlet/outlet of U-tube, S=4.5, T_{Tube}=90°C, Experiment 15.02**

The peak after approximately ten minutes in Figure I.3 was a result of silicon tube displacement.
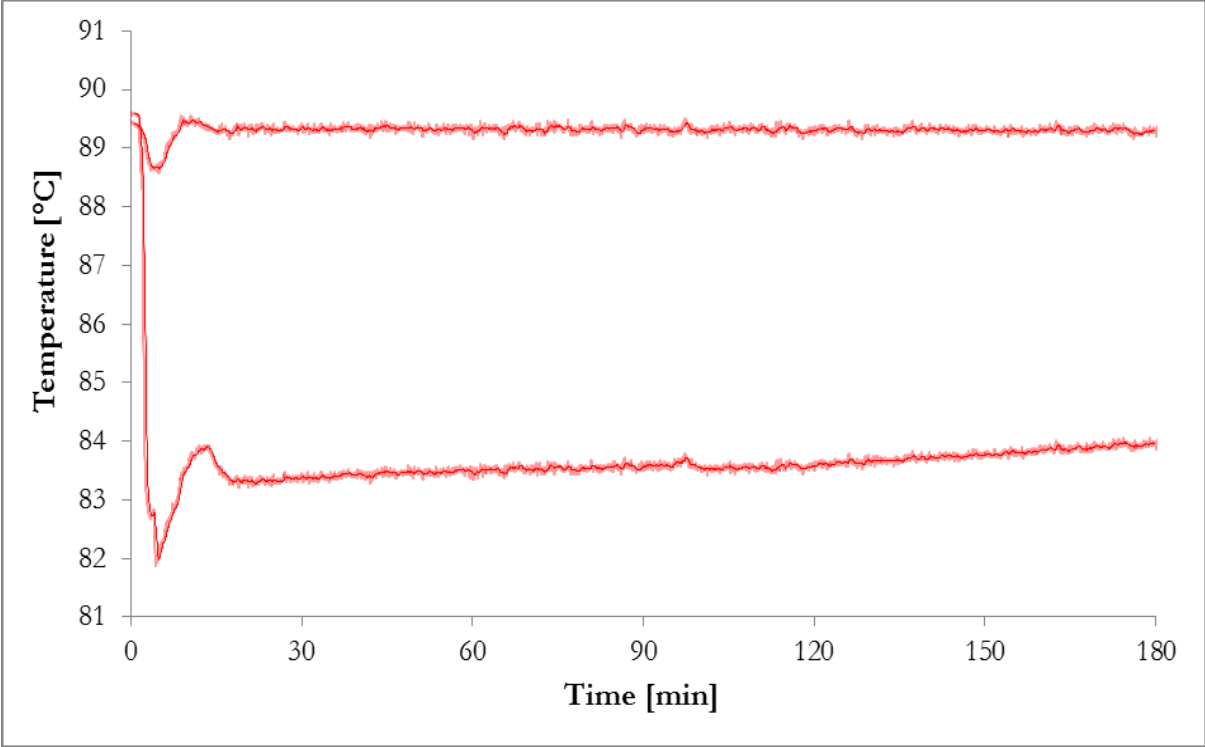
Figure I.3: Temperature inlet/outlet of U-tube, S=4.5, T$_{Tube}$=90°C, Experiment 18.02
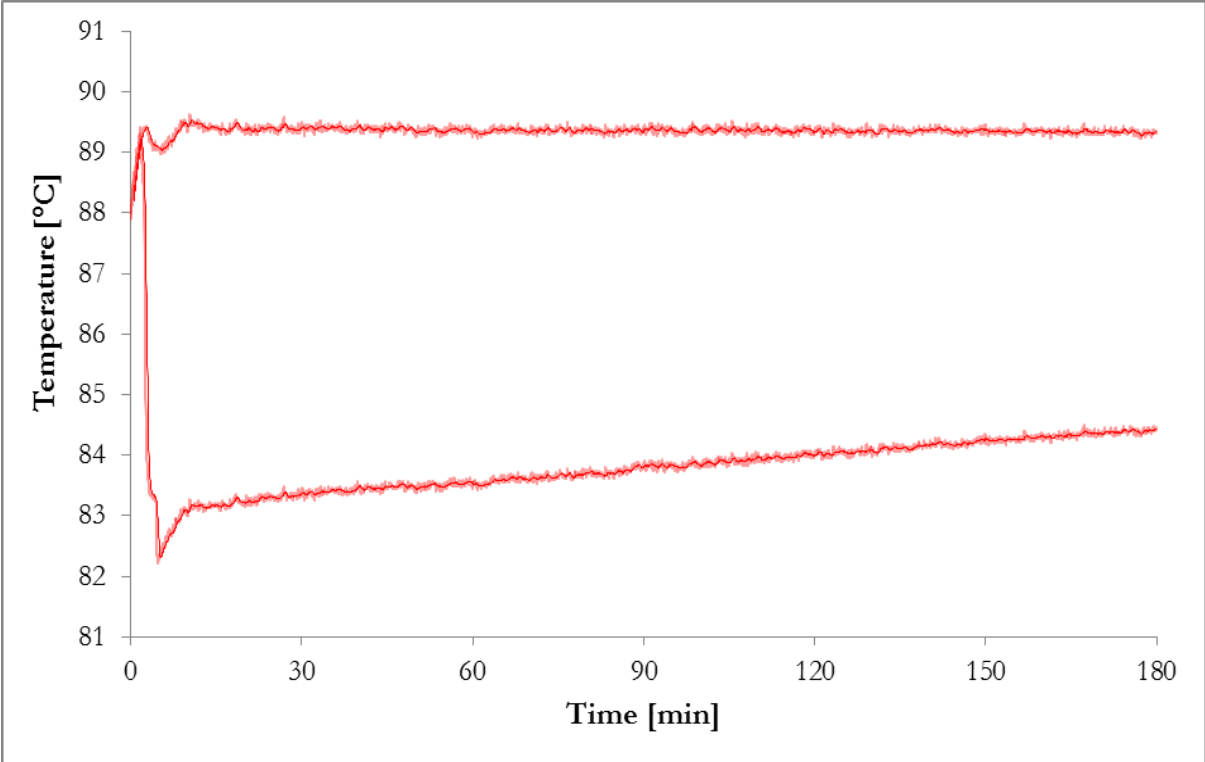
Figure I.4: Temperature inlet/outlet of U-tube, S=4.5, T$_{Tube}$=90°C, Experiment 19.02
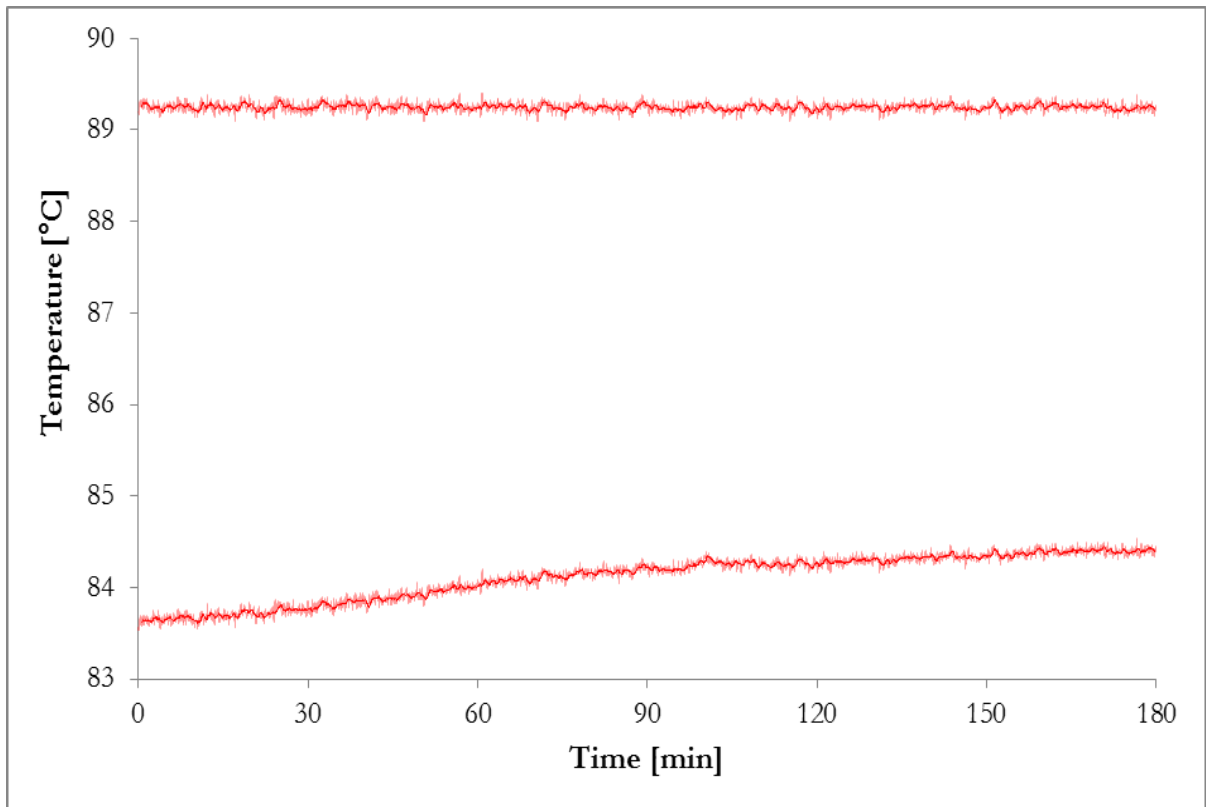
Figure I.5: Temperature inlet/outlet of U-tube, S=4.5, T_{Tube}=90°C, Experiment 22.02
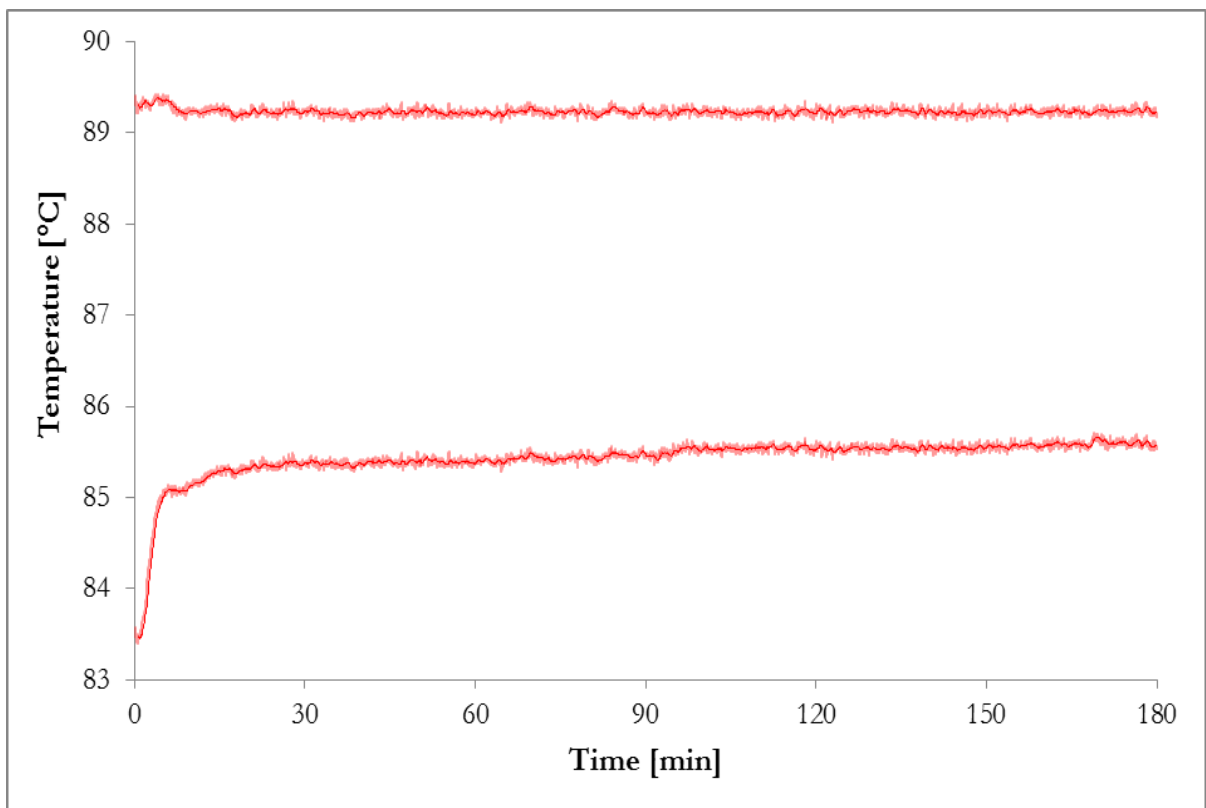
Figure I.6: Temperature inlet/outlet of U-tube, S=6.0, T_{Tube}=90°C, MEG=70wt%, Experiment 26.02

The peak after 164 minutes in Figure I.7 represents a displacement of the reactant-tube which was pumping solution from the Na_2CO_3 reservoir.
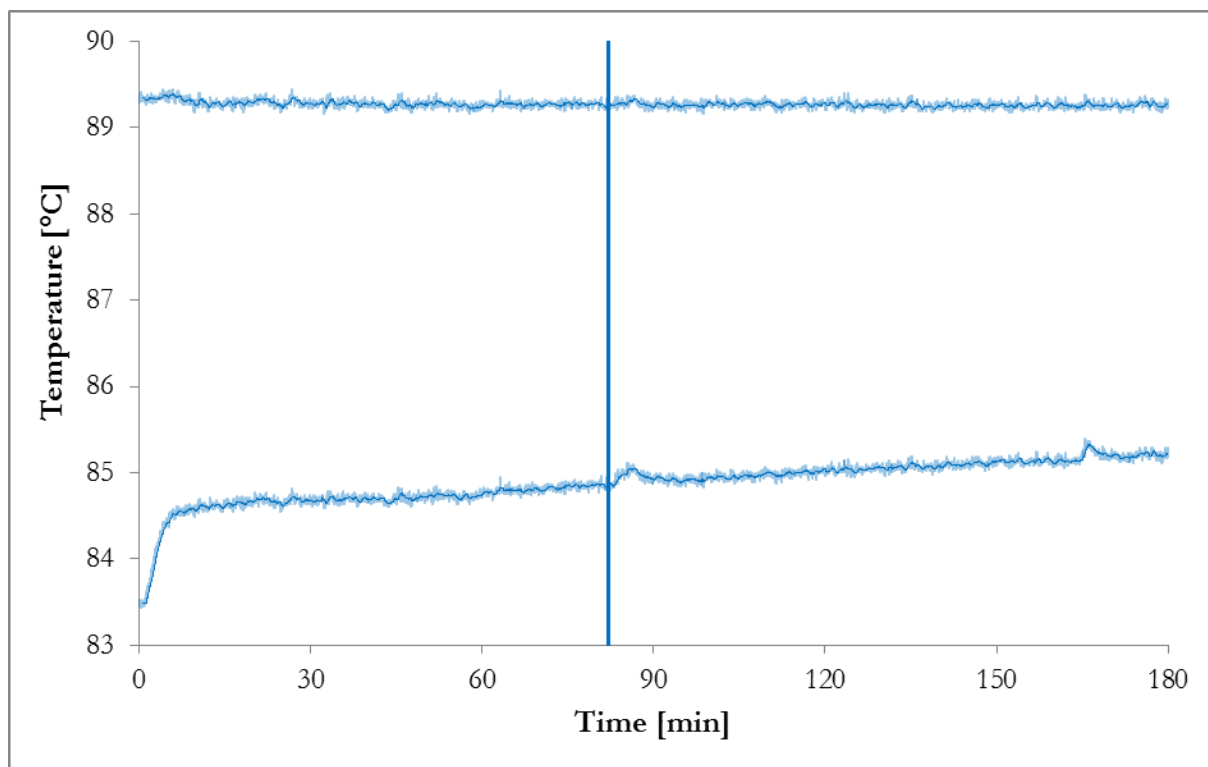
Figure I.7: Temperature inlet/outlet of U-tube, S=6.0, T_{Tube}=90°C, MEG=50wt%, Experiment 05.03
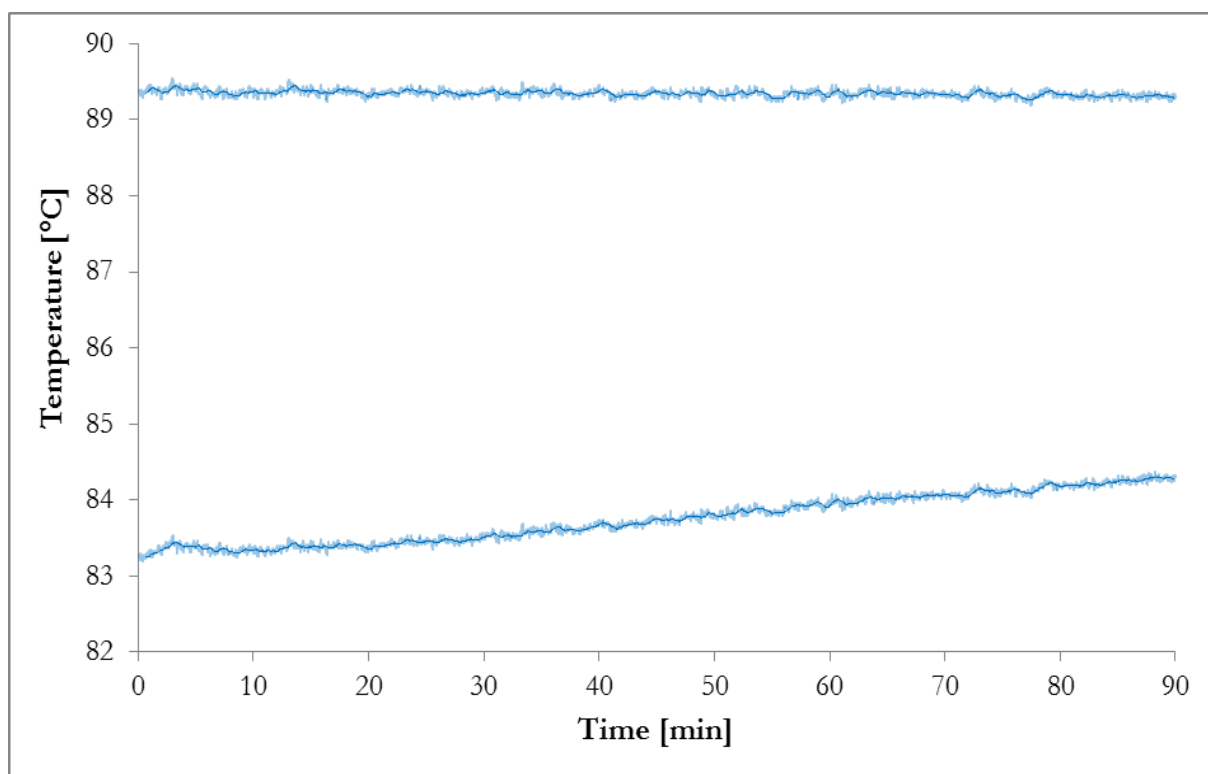
Figure I.8: Temperature inlet/outlet of U-tube, S=6.0, T_{Tube}=90°C, Experiment 12.03
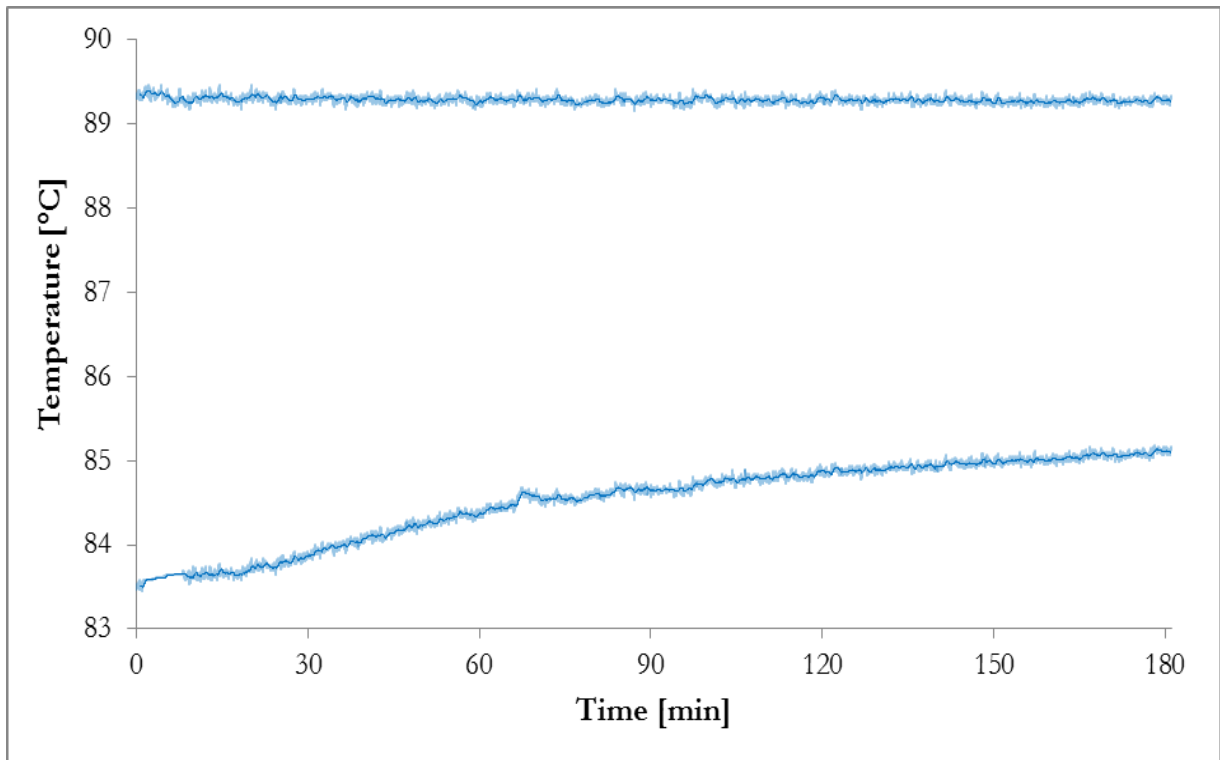
Figure I.9: Temperature inlet/outlet of U-tube, S=6.0, T_{Tube}=90°C, Experiment 13.03
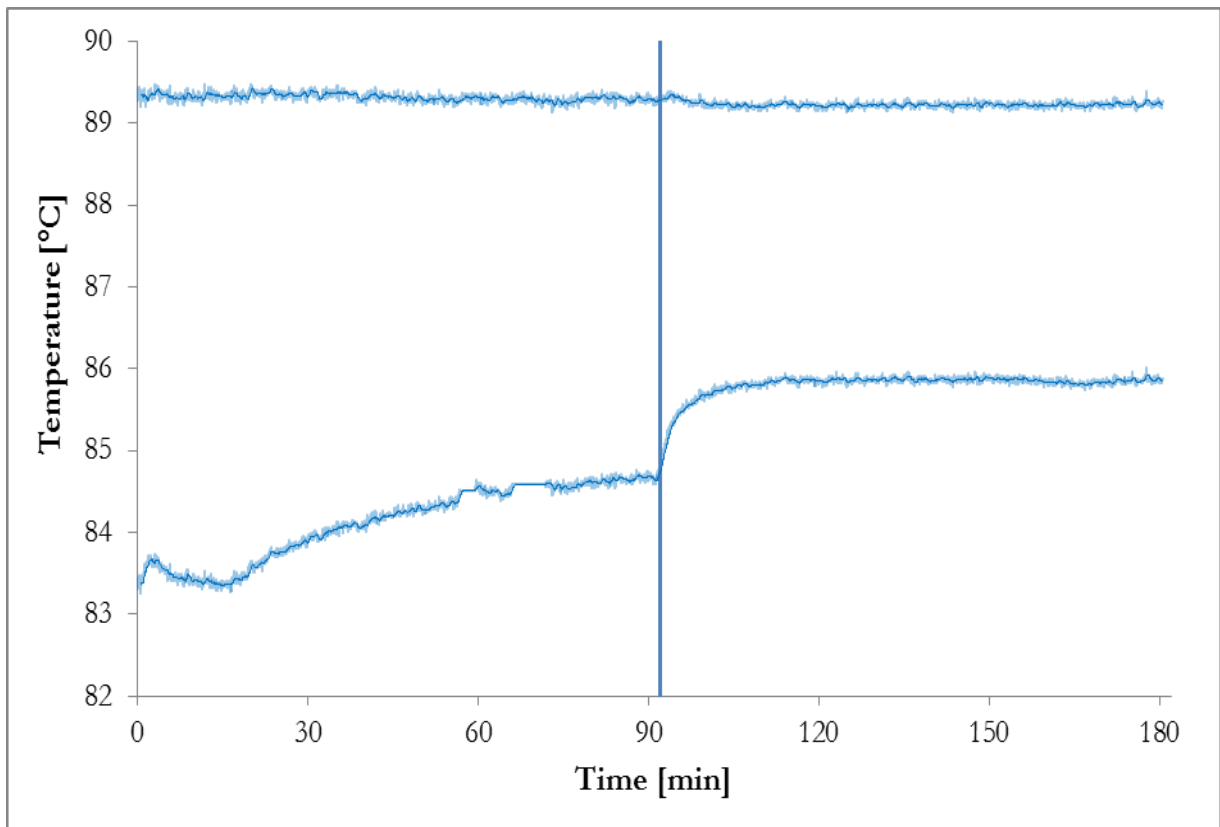
Figure I.10: Temperature inlet/outlet of U-tube, S=6.0, T_{Tube}=90°C, Pre-scale 90 min without MEG then 90 min with MEG=50wt% solution, Experiment 14.03

116
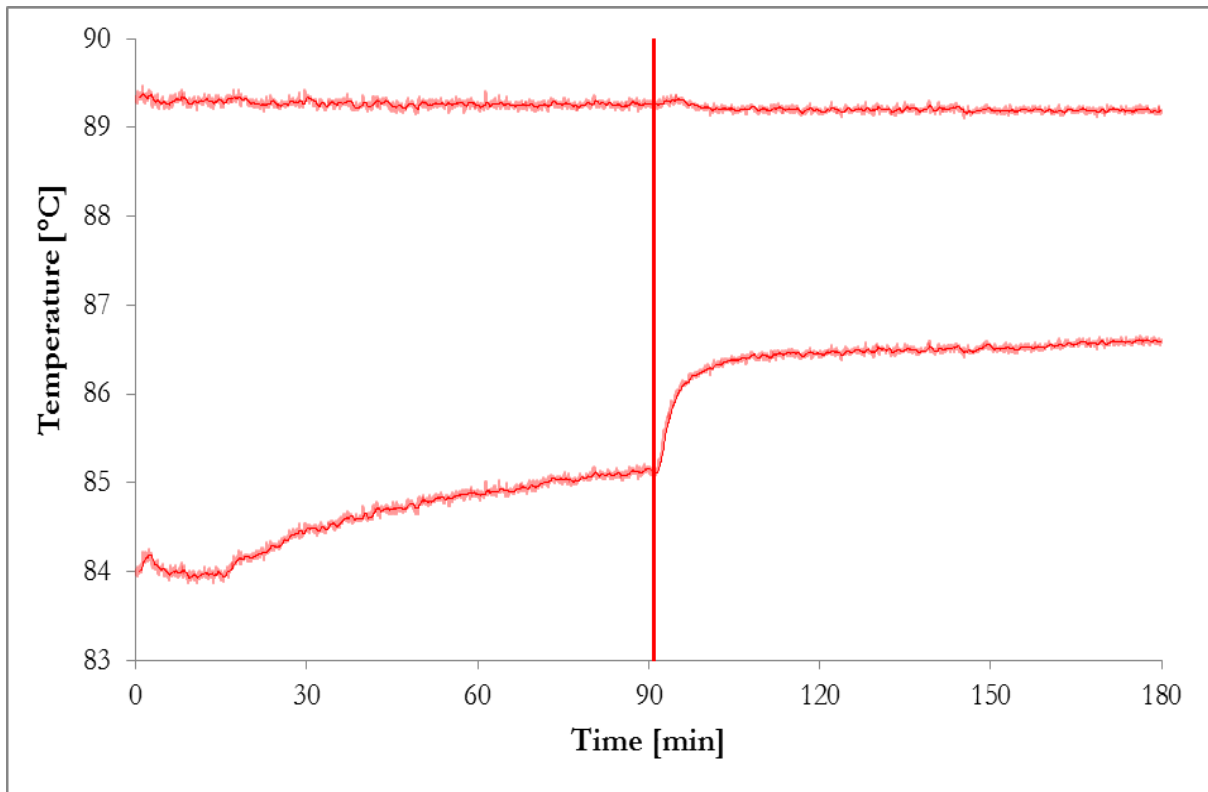
Figure I.11: Temperature inlet/outlet of U-tube, S=6.0, T$_{\text{Tube}}$=90°C, Pre-scale 90 min without MEG then 90 min with MEG=70wt% solution, Experiment 21.03
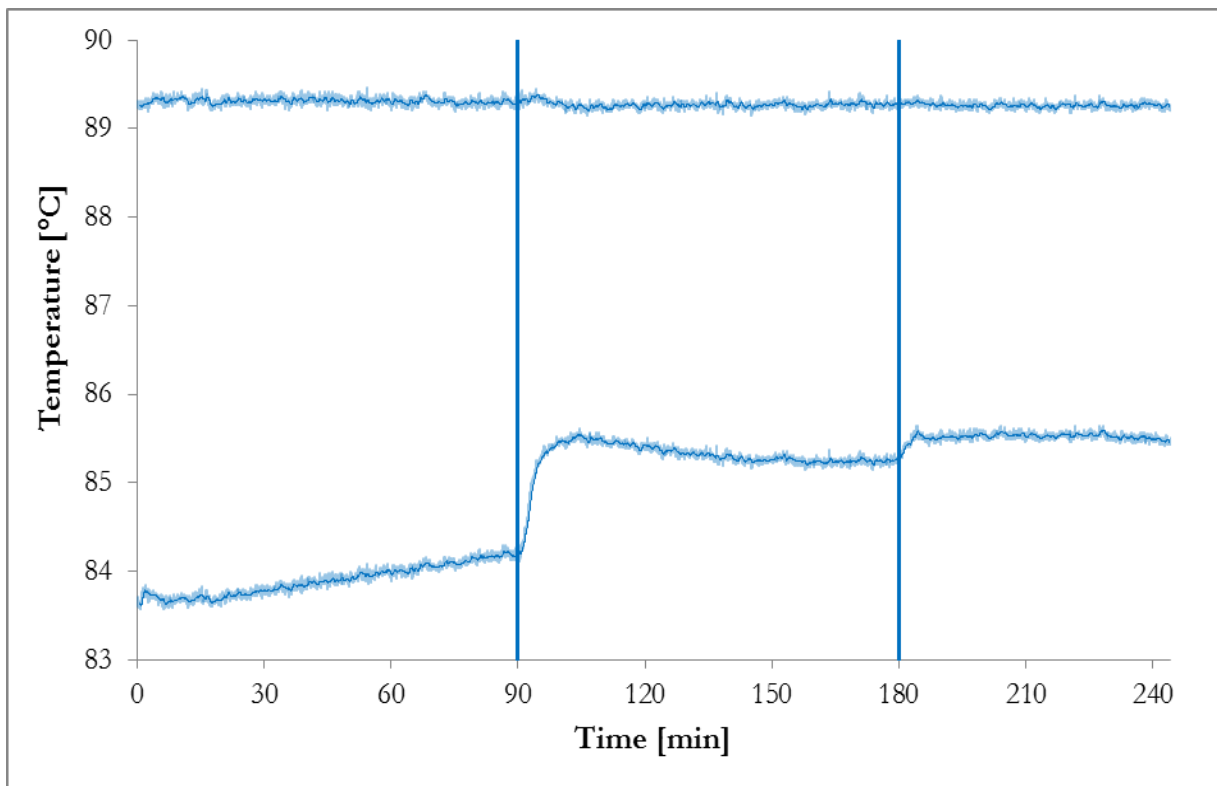
Figure I.12: Temperature inlet/outlet of U-tube, S=6.0, T$_{\text{Tube}}$=90°C, Pre-scale 90 min without MEG then 155 min with MEG=50wt% solution, Experiment 02.04
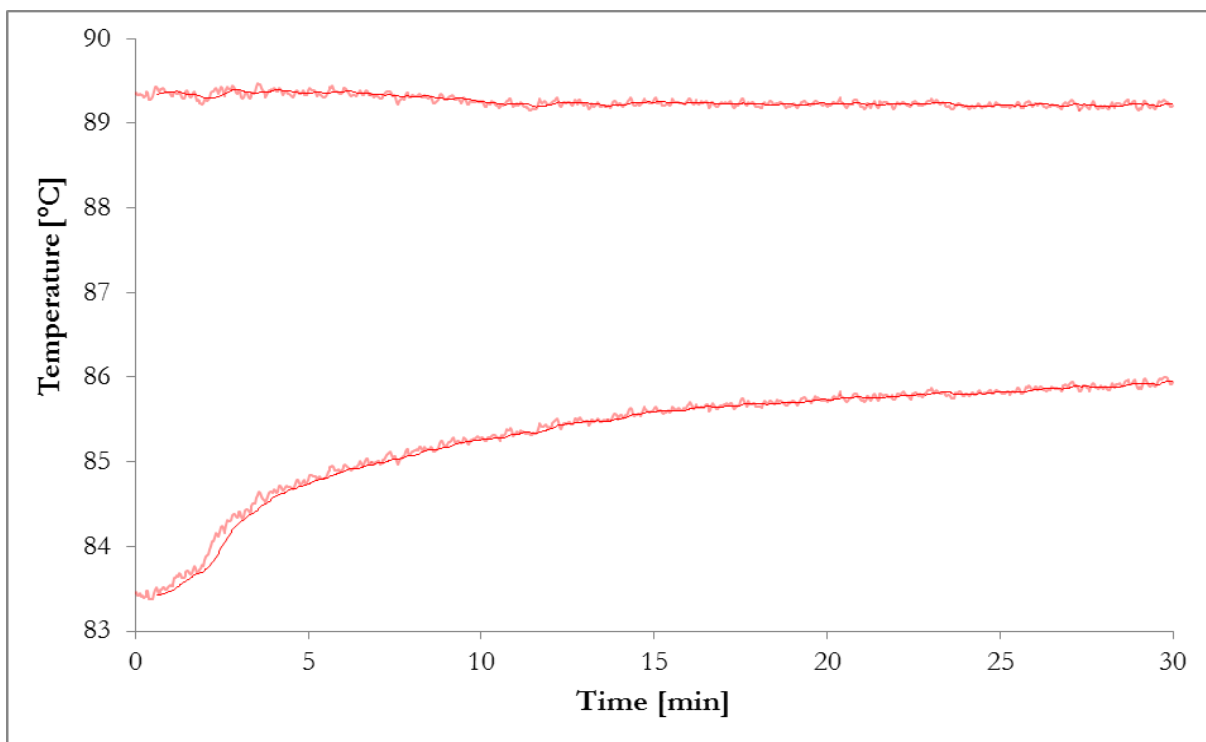
Figure I.13: Temperature inlet/outlet of U-tube, S=12.3, T$_{Tube}$=90°C, MEG=50wt%, Experiment 04.04

The peaks occurring after 65 and 118 minutes in Figure I.14 were due to a temporary tube displacement and a short stop in the pumping of reactant solution.
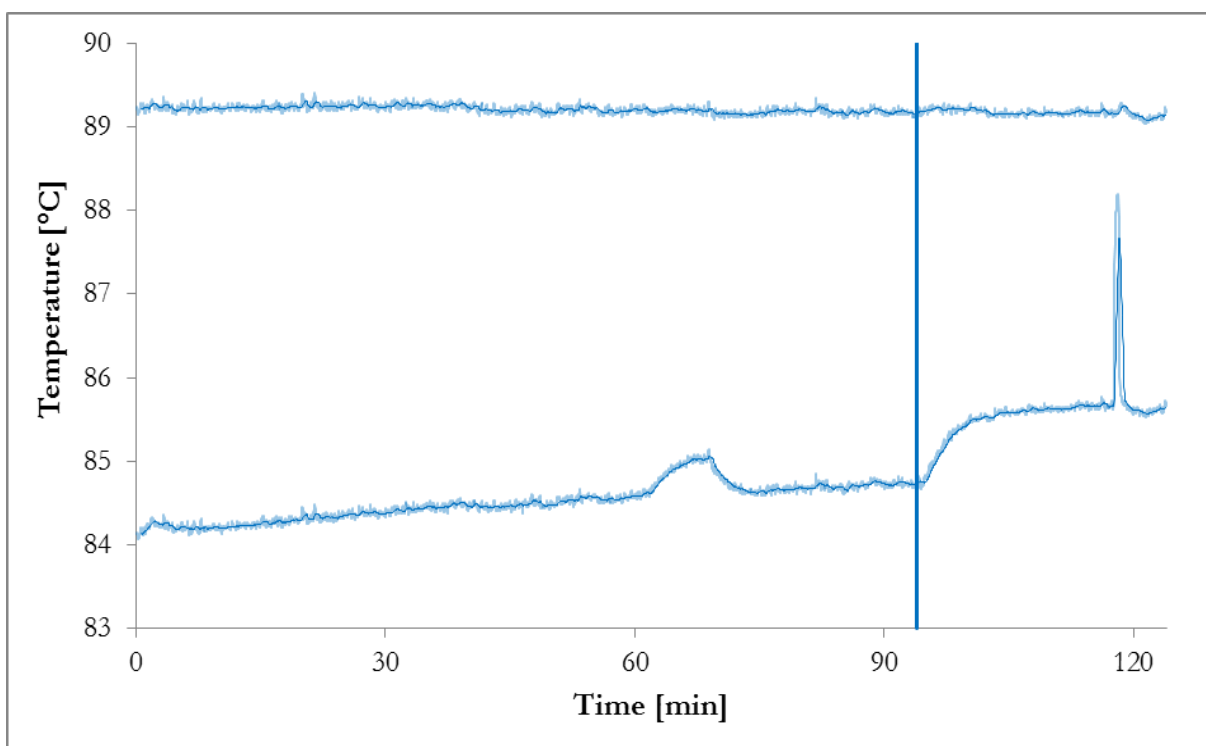
Figure I.14: Temperature inlet/outlet of U-tube, S=6.0, T$_{Tube}$=90°C, Pre-scale 90 min without MEG then 30 min with MEG=50wt% solution, Experiment 06.04
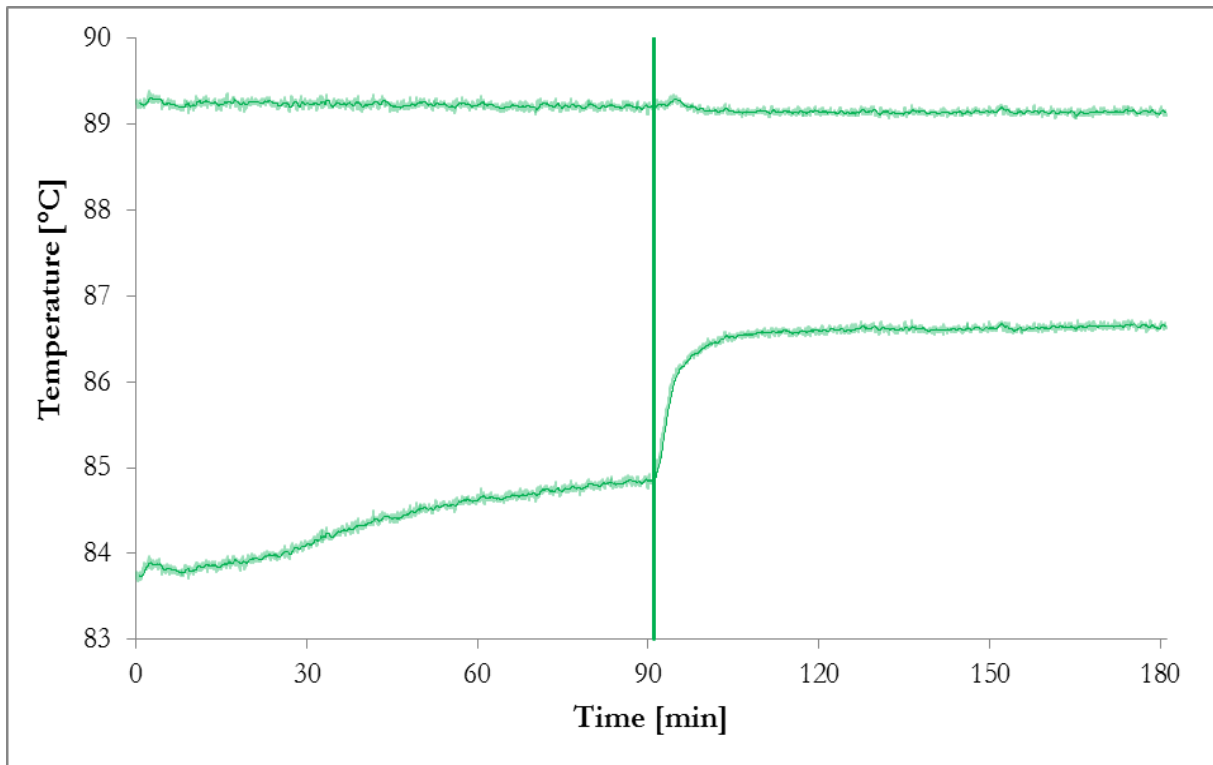
Figure I.15: Temperature inlet/outlet of U-tube, S=6.0, T$_{Tube}$=90°C, Pre-scale 90 min without MEG then 90 min with MEG=90wt% solution, Experiment 09.04
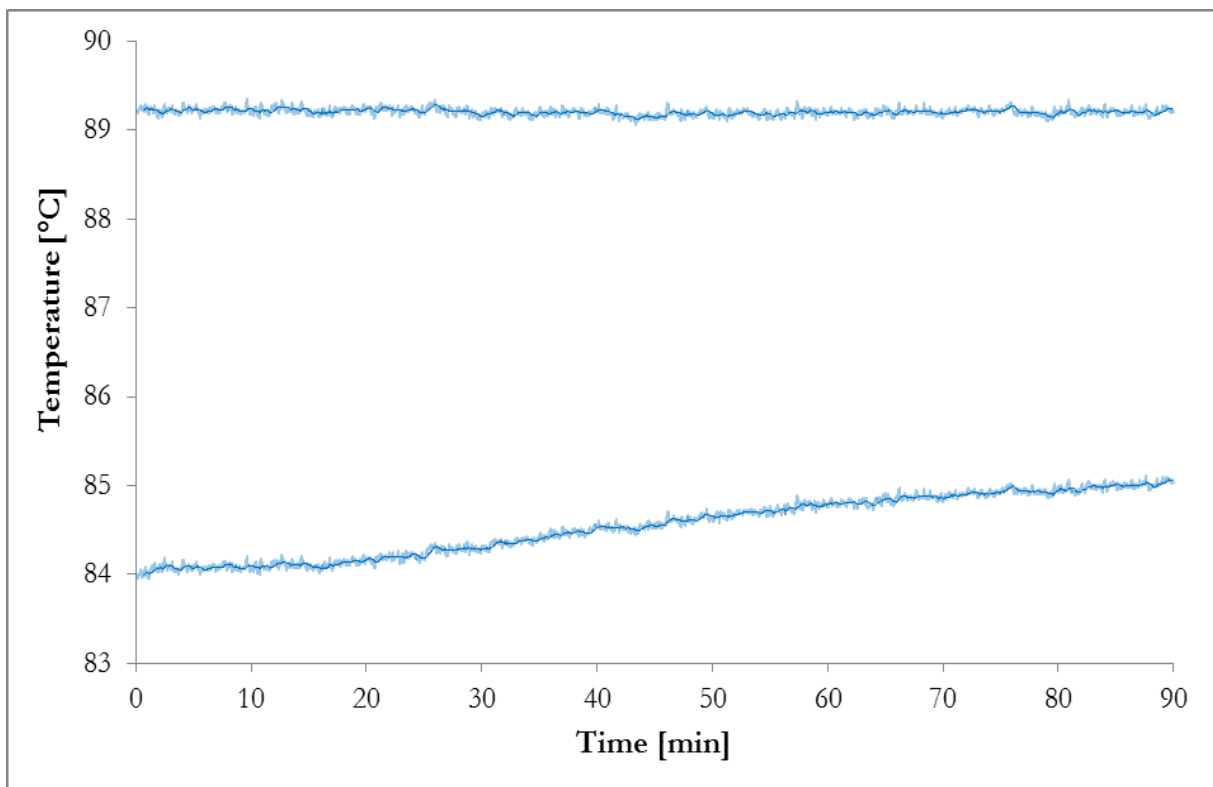
Figure I.16: Temperature inlet/outlet of U-tube, S=6.0, T$_{Tube}$=90°C, Experiment 10.04
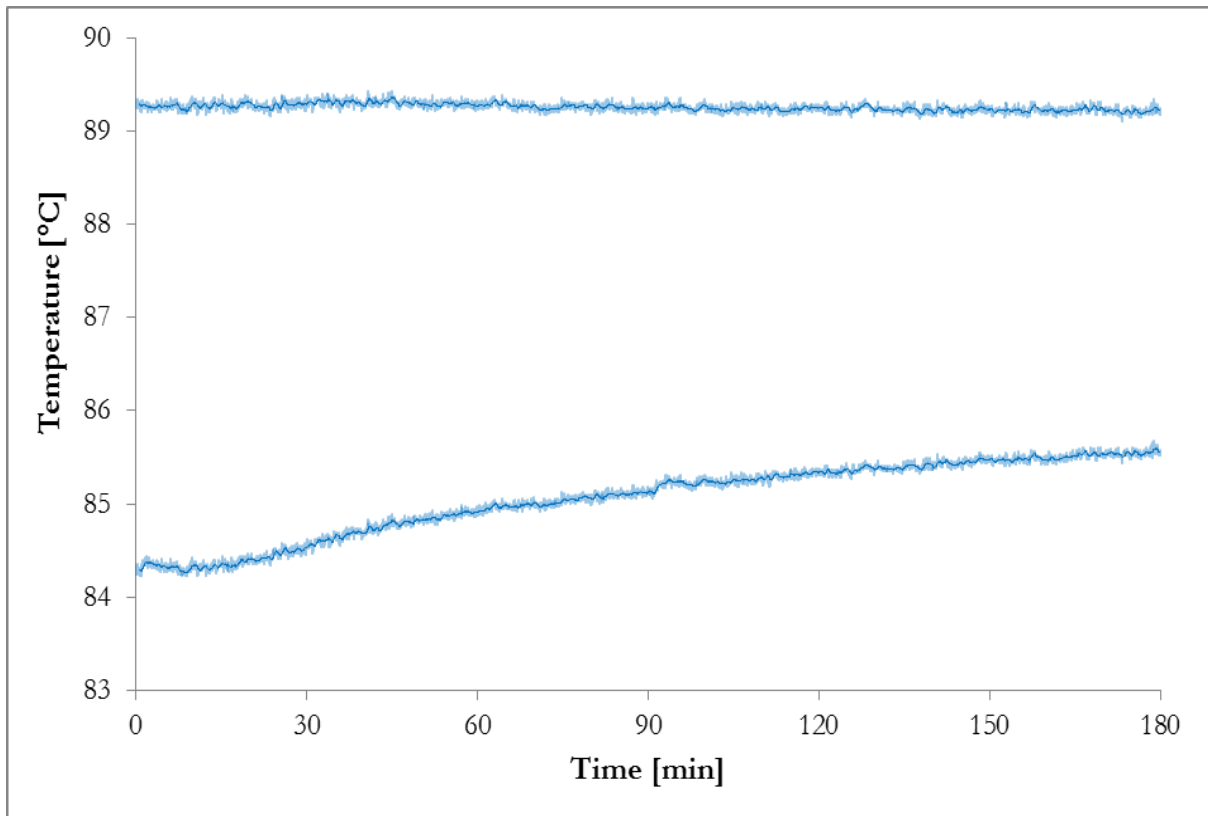
Figure I.17: Temperature inlet/outlet of U-tube, S=6.0, T$_{Tube}$=90°C, Experiment 12.04
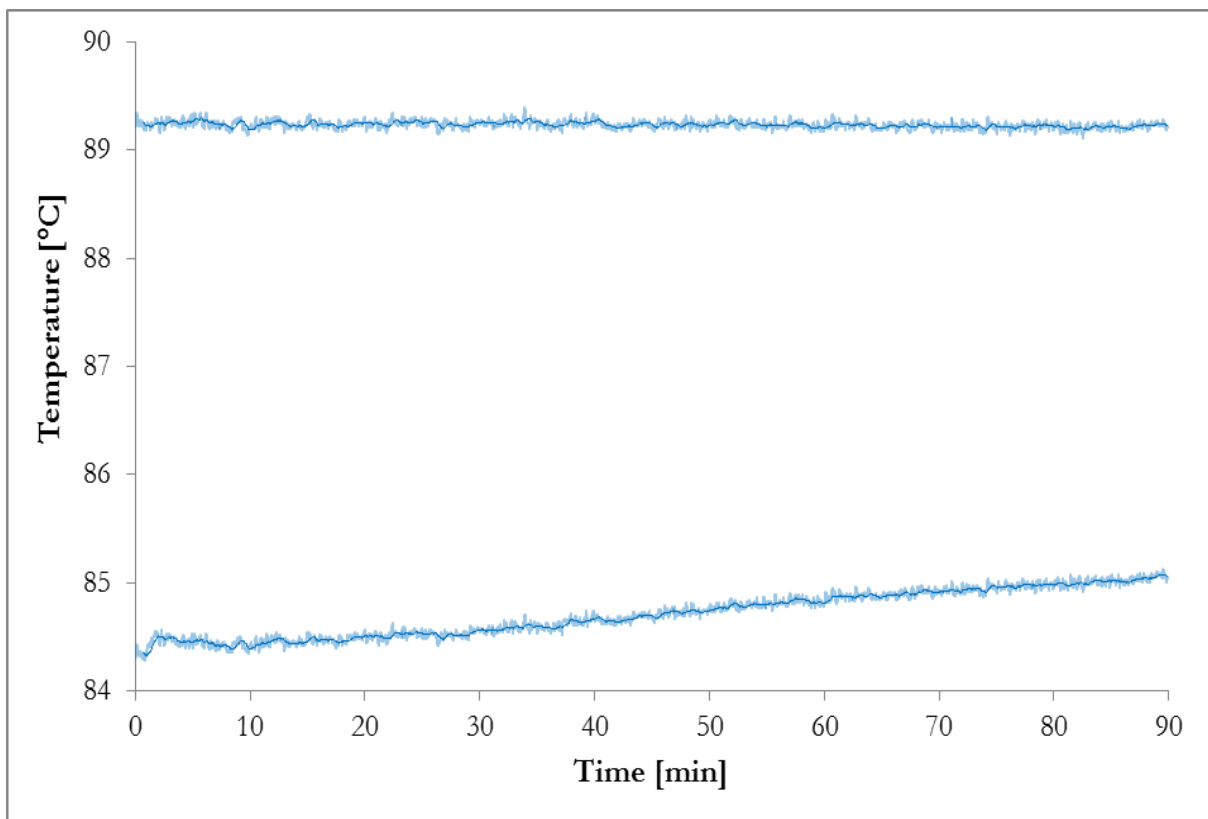
Figure I.18: Temperature inlet/outlet of U-tube, S=6.0, T$_{Tube}$=90°C, Experiment 15.04
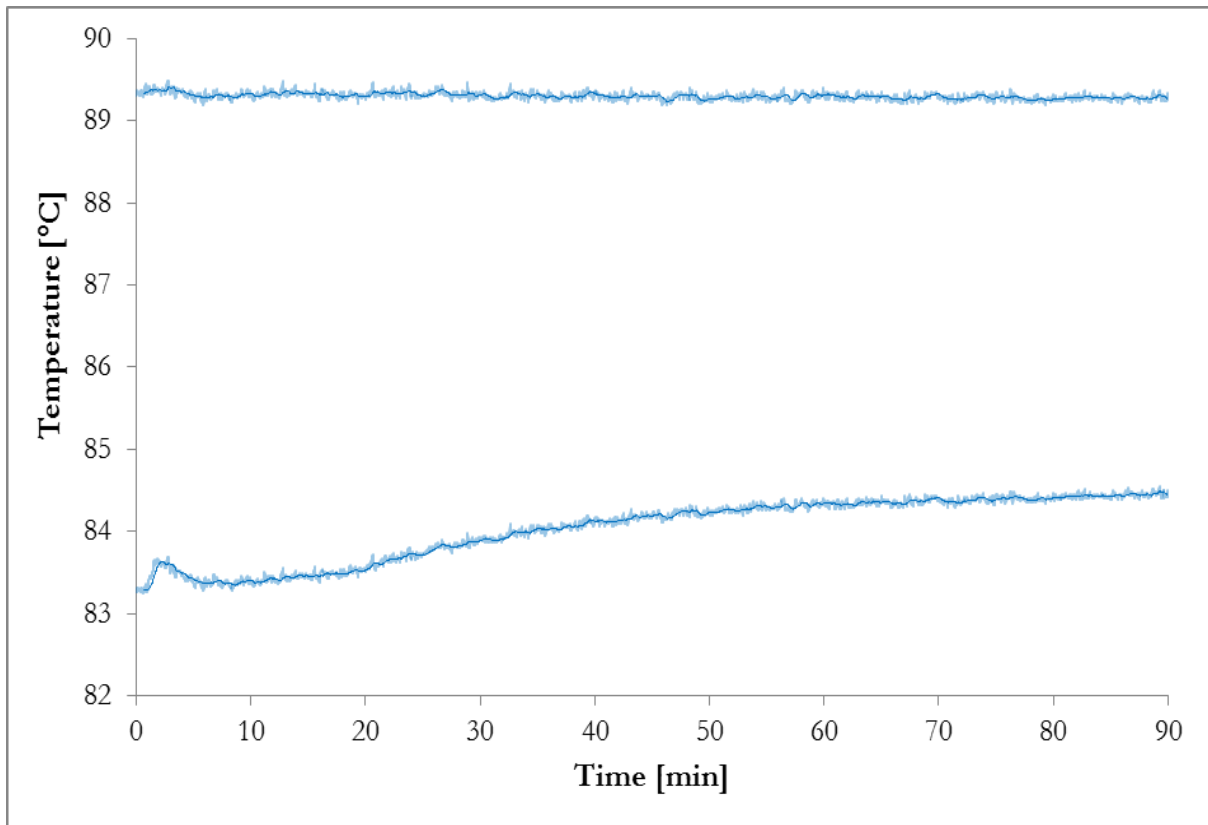
Figure I.19: Temperature inlet/outlet of U-tube, S=6.0, T$_{Tube}$=90°C, Experiment 16.04
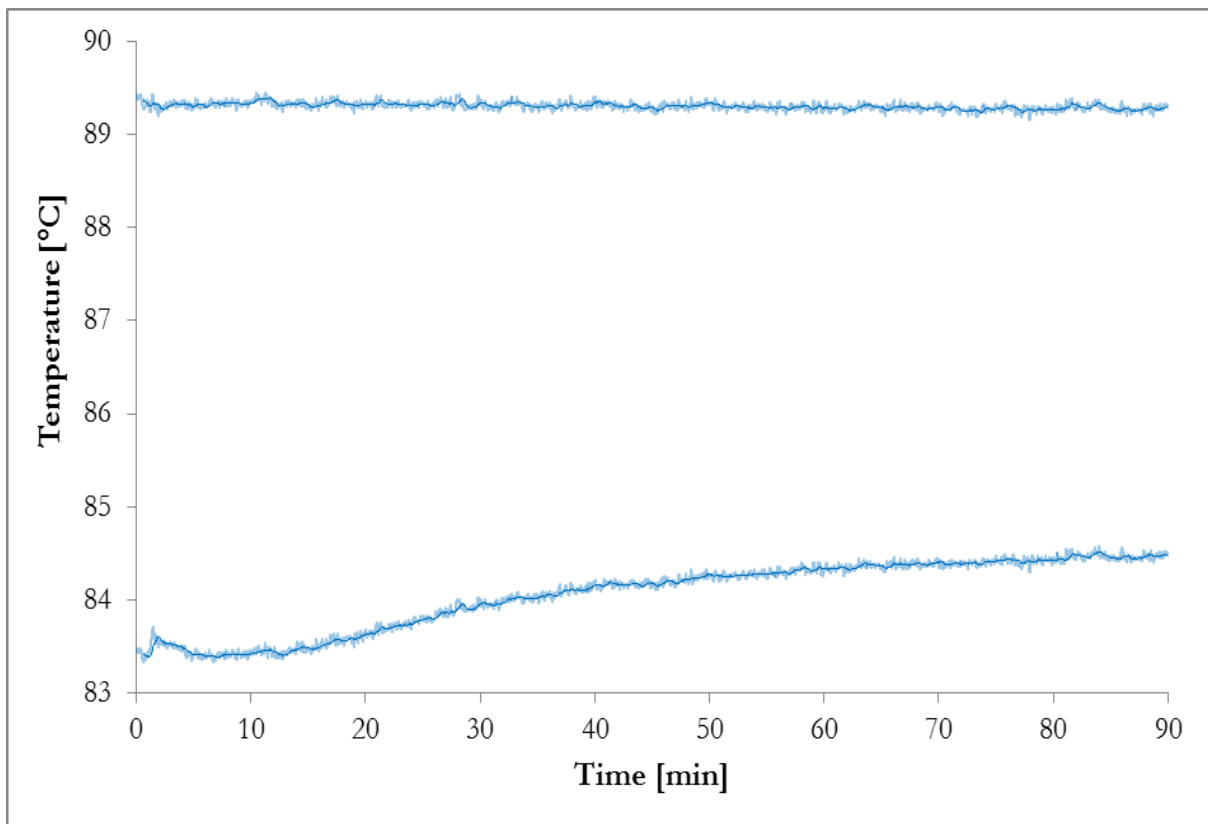
Figure I.20: Temperature inlet/outlet of U-tube, S=6.0, T$_{Tube}$=90°C, Experiment 16.04(2)

The peak after 118 minutes in Figure I.21 was due to a short stop in the pumping of reactant solution to adjust flow rate.
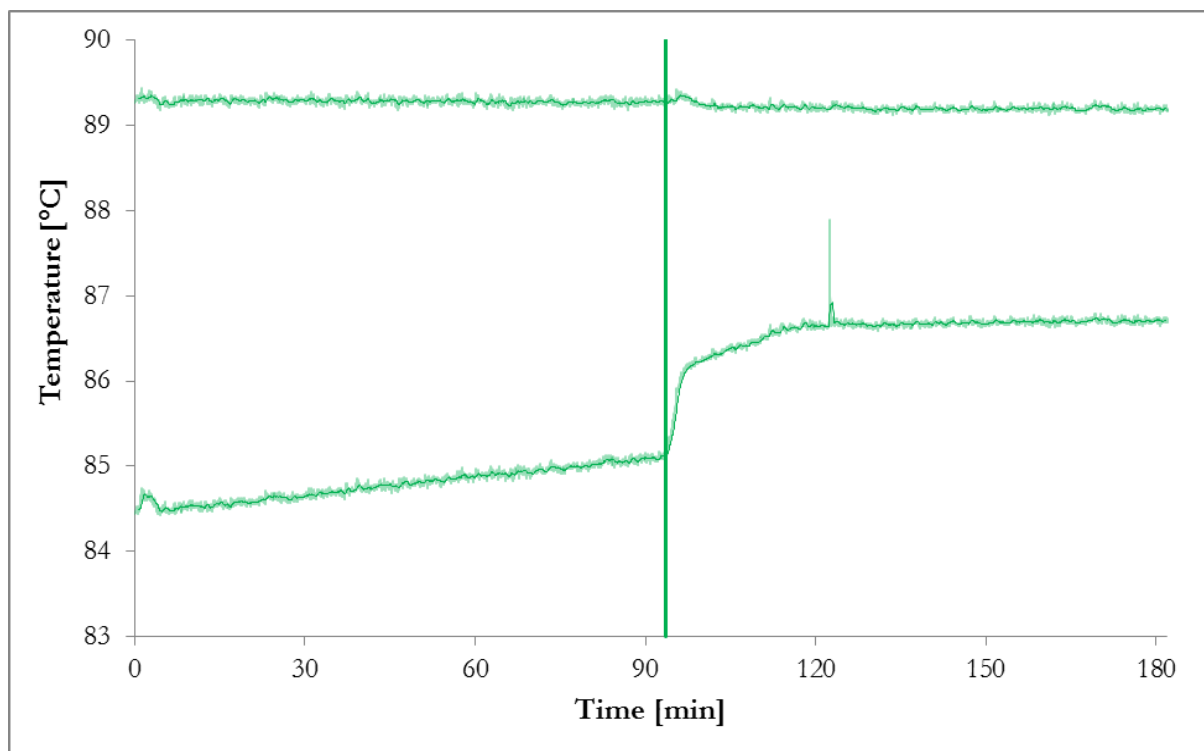

Figure I.21: Temperature inlet/outlet of U-tube, S=6.0, T$_{Tube}$=90°C, Pre-scale 90 min without MEG then 90 min with MEG=90wt% solution, Experiment 22.04
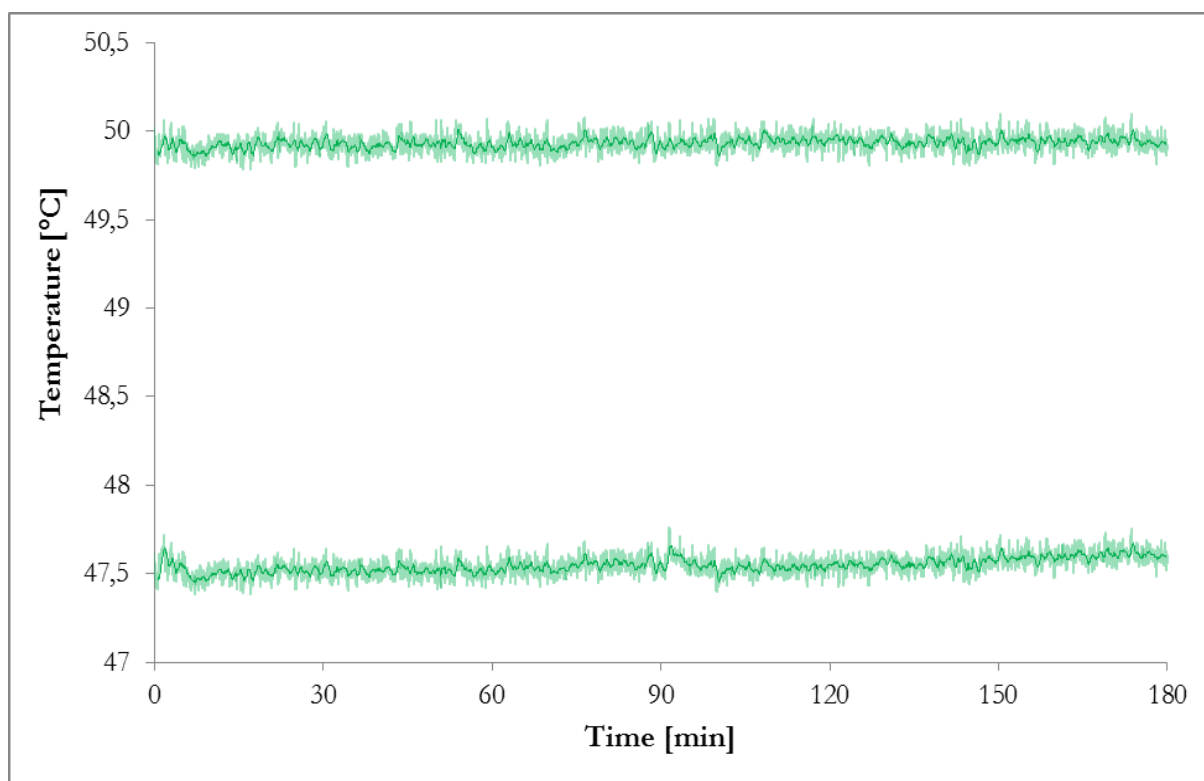
Figure I.22: Temperature inlet/outlet of U-tube, S=6.0, T$_{Tube}$=50°C, Experiment 26.04
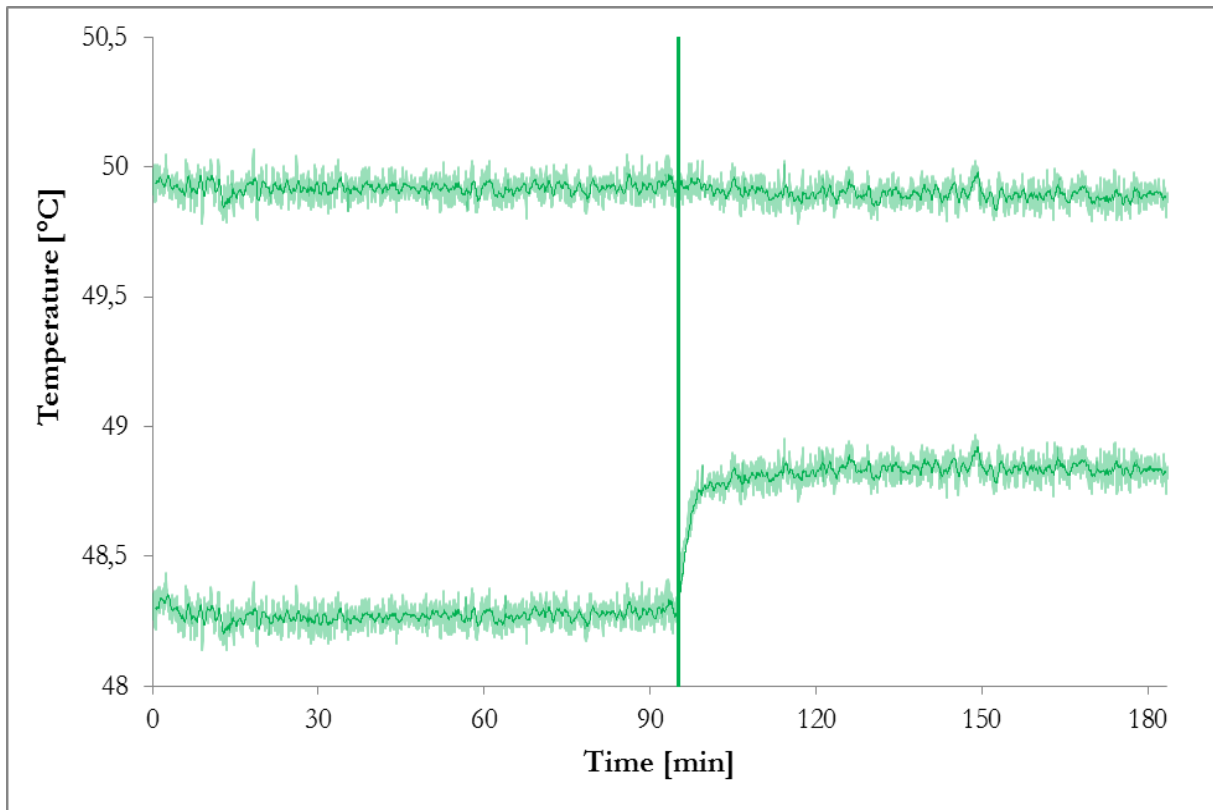
Figure I.23: Temperature inlet/outlet of U-tube, S=6.0, T_{Tube}=50°C, Pre-scale 90 min without MEG then 90 min with MEG=70wt% solution, Experiment 26.04(2)

I.2 Graphical plots of bulk pH and bulk/reactant-inlet temperature data

Figure I.24-Figure I.46 shows a graphical representation of the data collected from measurements of the bulk/reactant-inlet temperatures and pH in the bulk liquid. Measurement of pH was not always done due to errors in the equipment.

After the experiment shown in Figure I.28, the procedure was changed to include an initial period with flow of only distilled water through the system to reduce initial fluctuations.

Figure I.24: Temperature of bulk solution and reactant inlet, S=4.5, T_{Tube}=90°C, Experiment 08.02
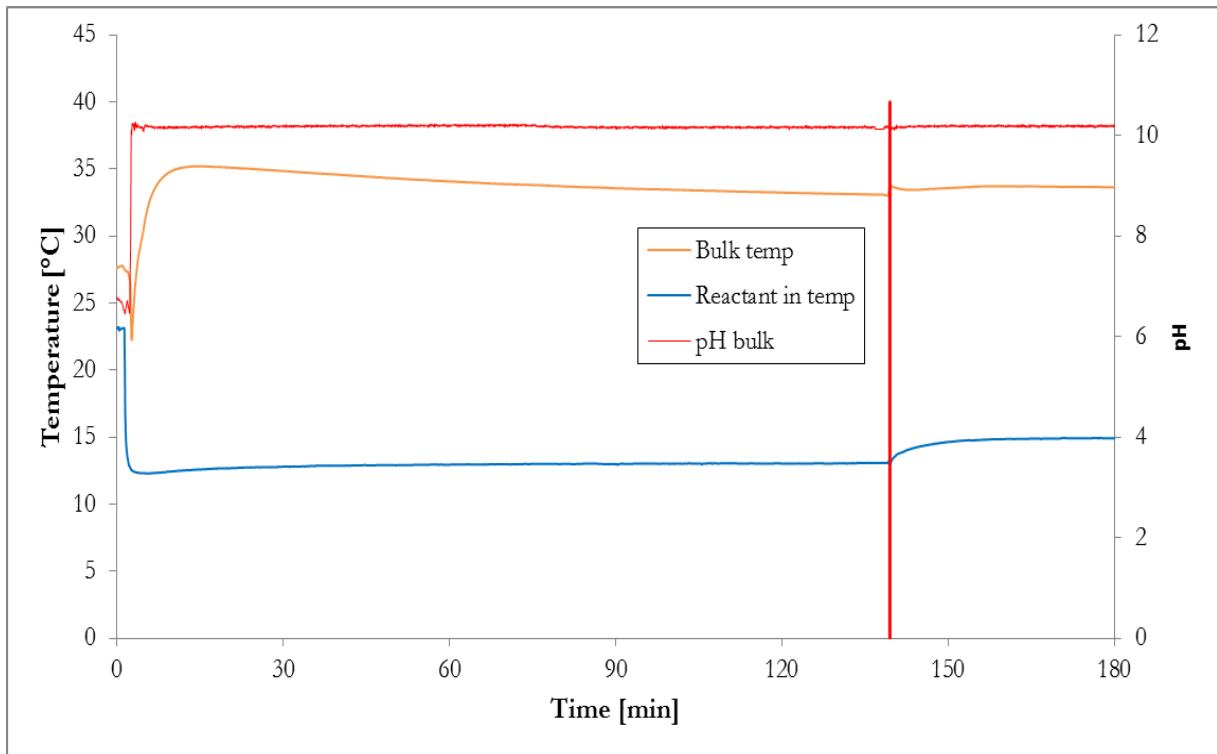
Figure I.25: Temperature of bulk solution and reactant inlet, S=4.5, T$_{Tube}$=90°C, Experiment 15.02

The peak after approximately ten minutes in Figure I.26 was a result of silicon tube displacement.
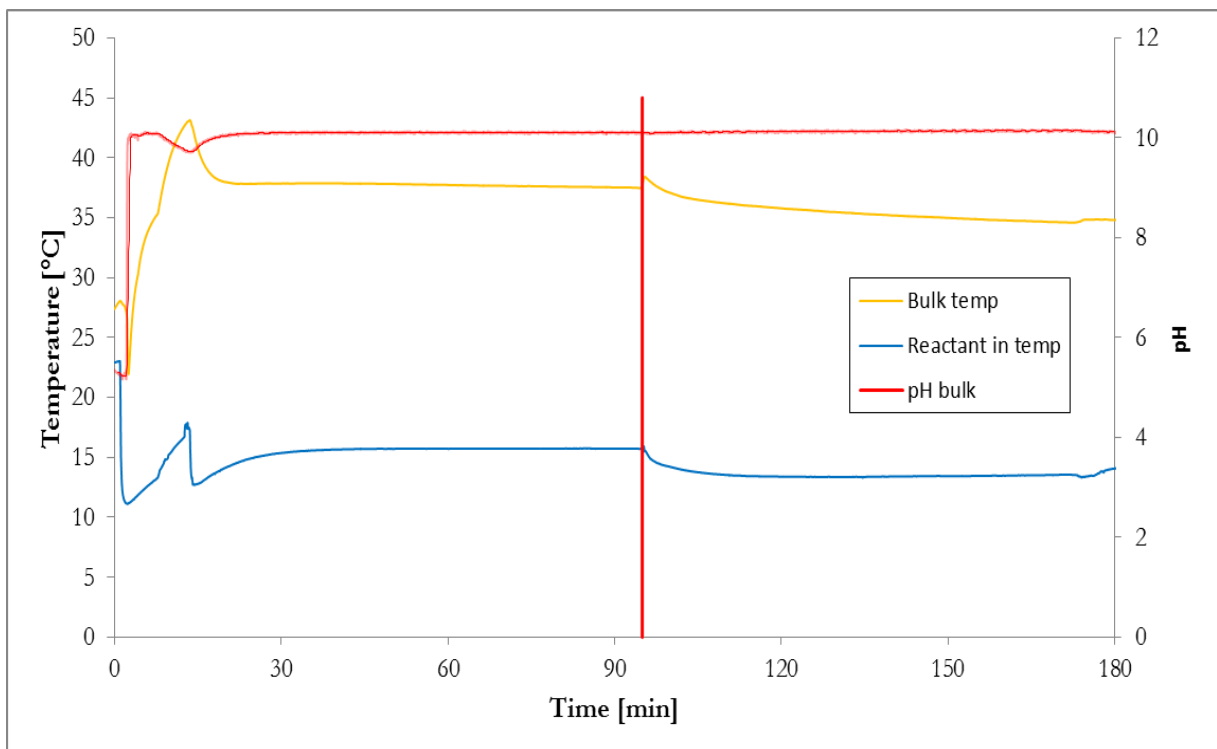
Figure I.26:Temperature of bulk solution and reactant inlet, S=4.5, T$_{Tube}$=90°C, Experiment 18.02

125
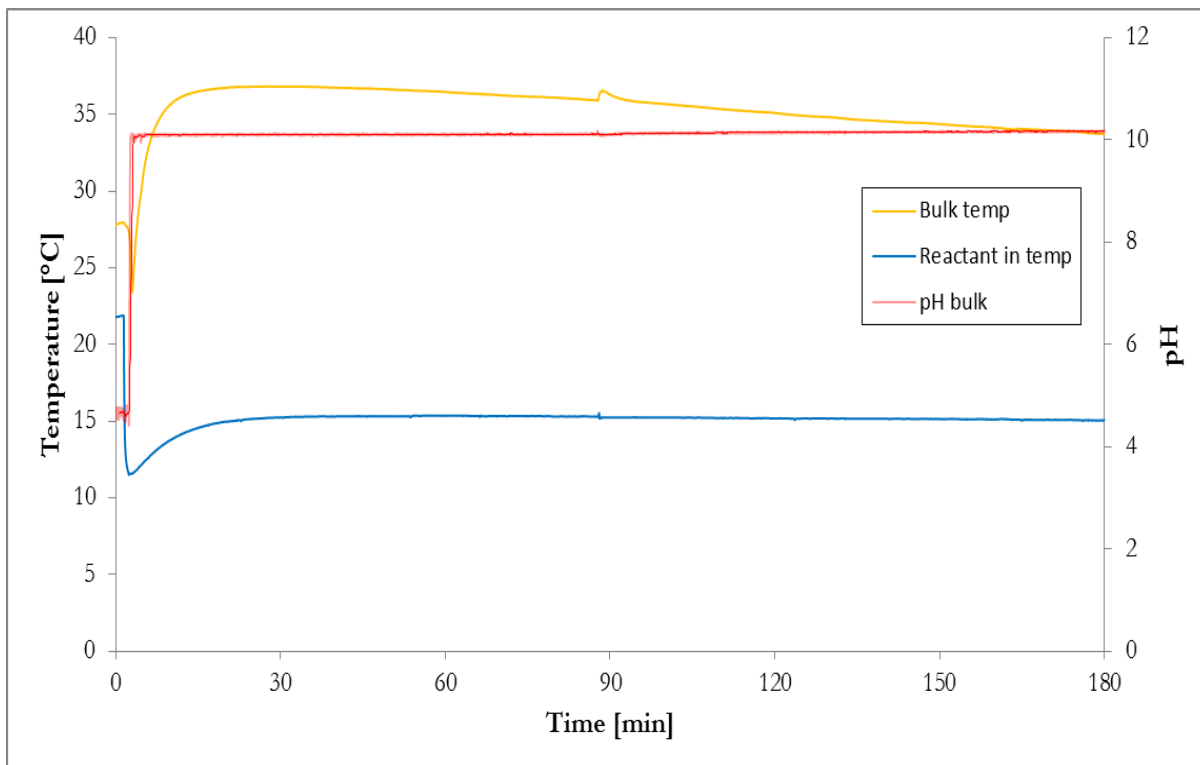
Figure I.27: Temperature of bulk solution and reactant inlet, S=4.5, T_{Tube}=90°C, Experiment 19.02
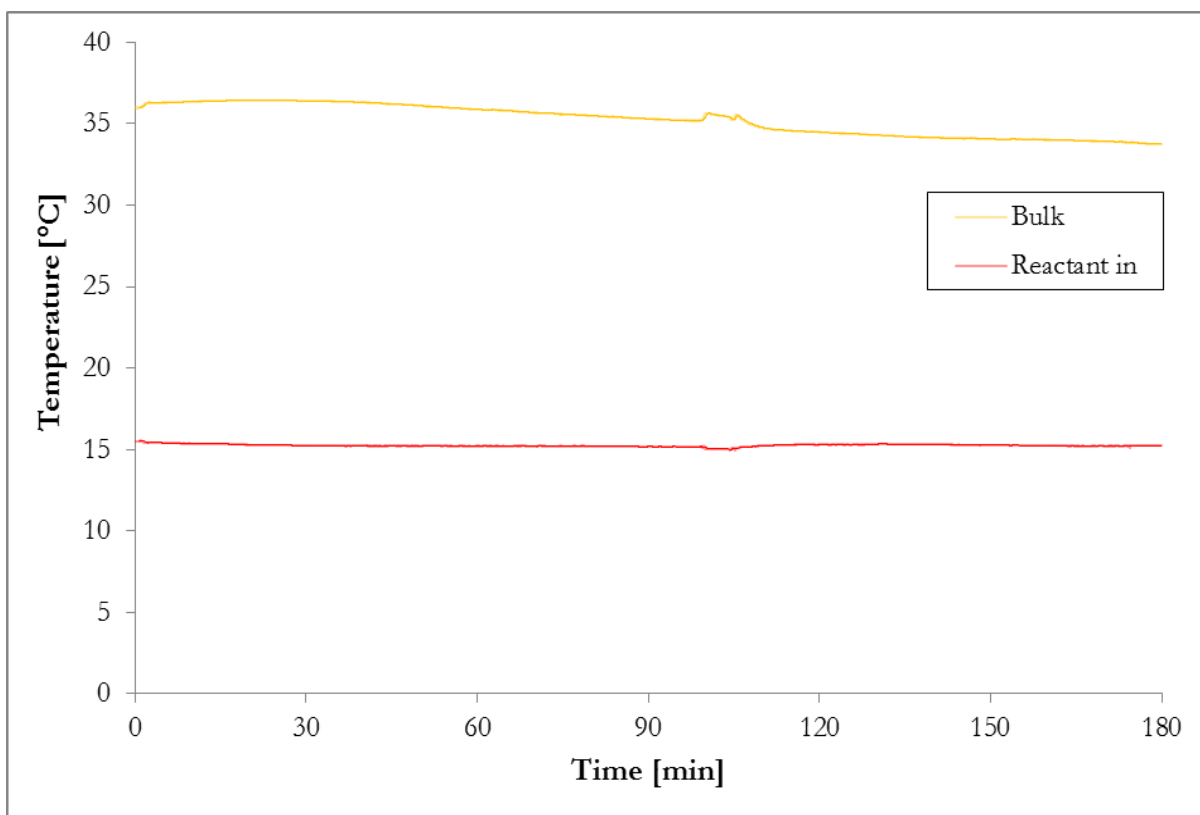
Figure I.28: Temperature of bulk solution and reactant inlet, S=4.5, T_{Tube}=90°C, Experiment 22.02
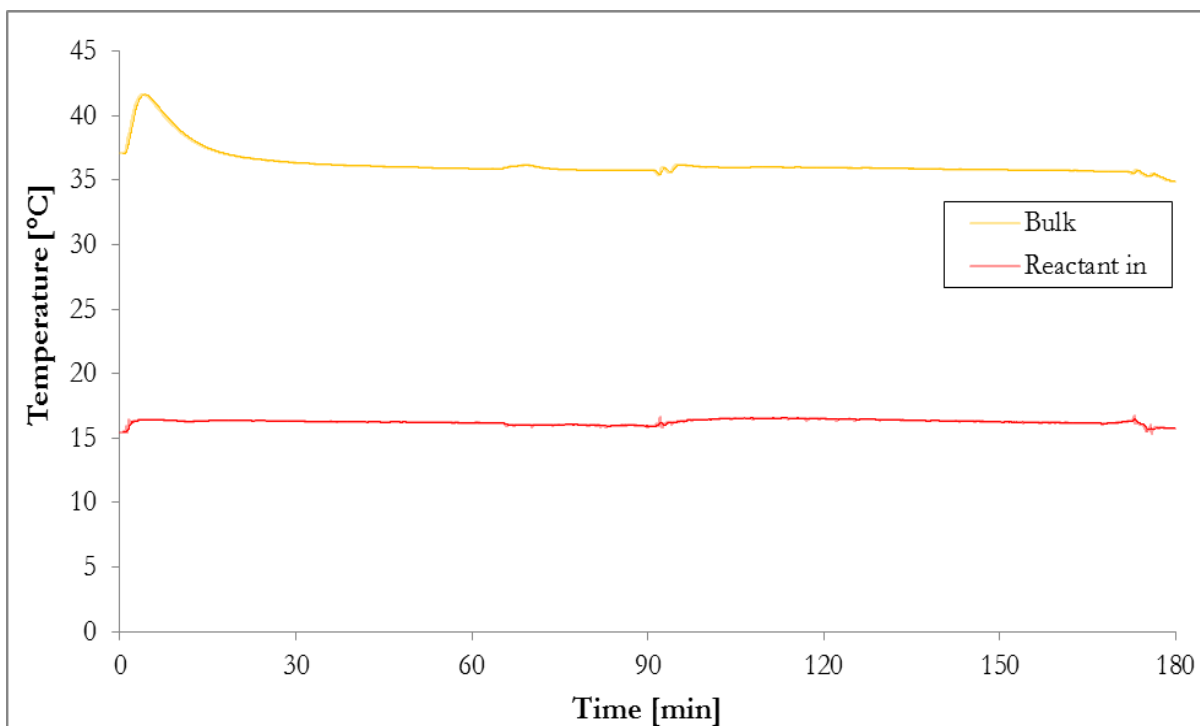
Figure I.29: Temperature of bulk solution and reactant inlet, S=6.0, T_{Tube}=90°C, MEG=70wt%, Experiment 26.02

The peak after 164 minutes in Figure I.30 represents a displacement of the reactant-tube pumping solution from the Na_2CO_3 reservoir.
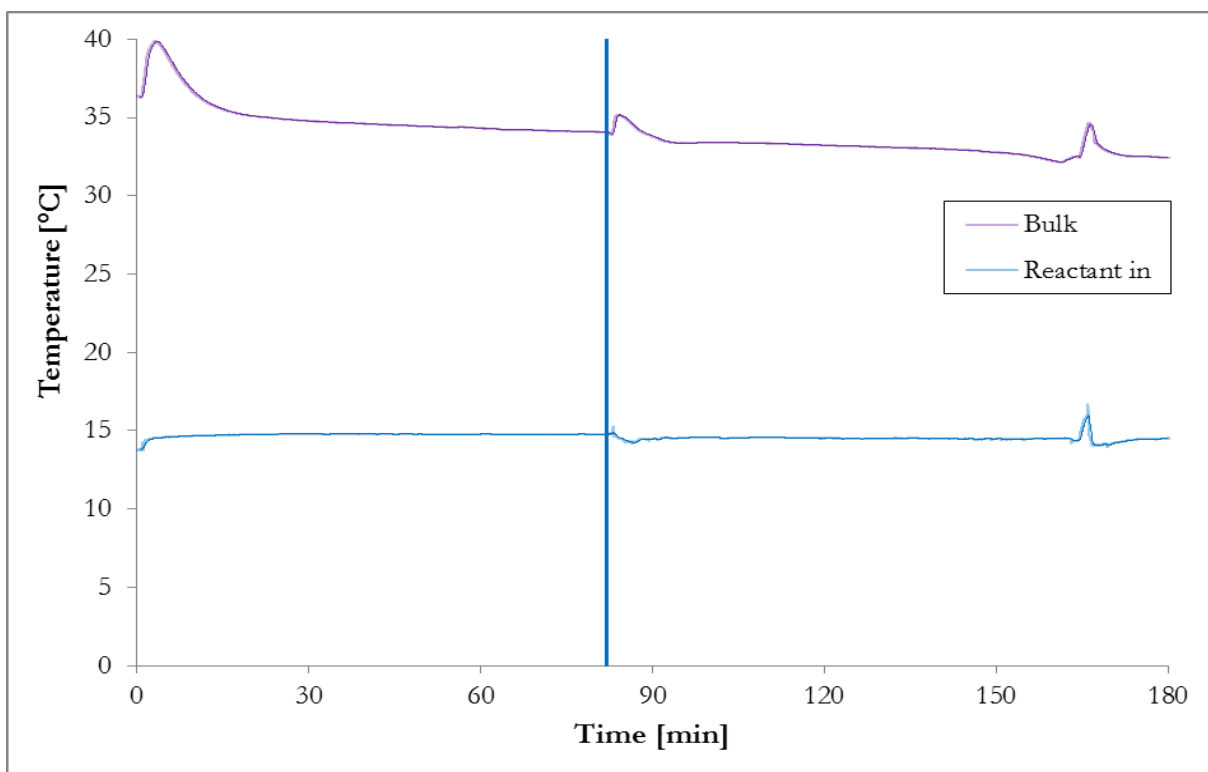
Figure I.30: Temperature of bulk solution and reactant inlet, S=6.0, T_{Tube}=90°C, MEG=50wt%, Experiment 05.03
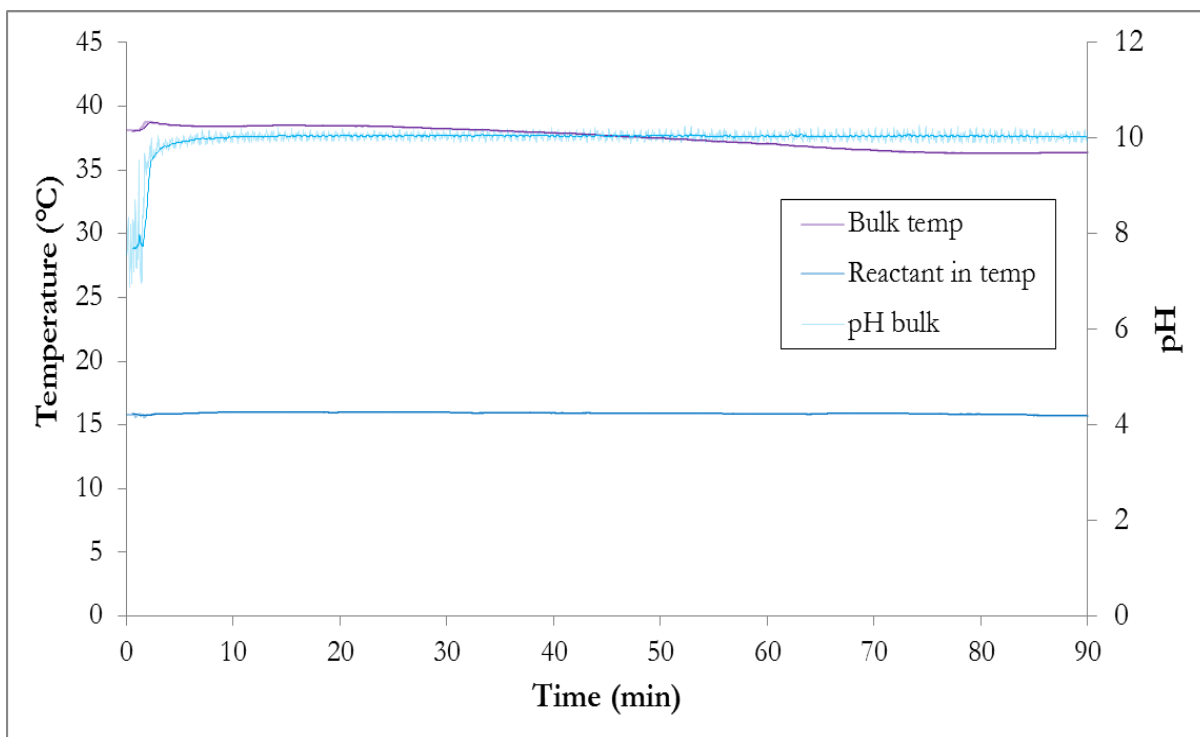
Figure I.31: Temperature of bulk solution and reactant inlet, S=6.0, T$_{Tube}$=90°C, Experiment 12.03

The peak after 67 minutes in Figure I.32 was due to a short stop in the pumping of reactant solution to adjust flow rate.
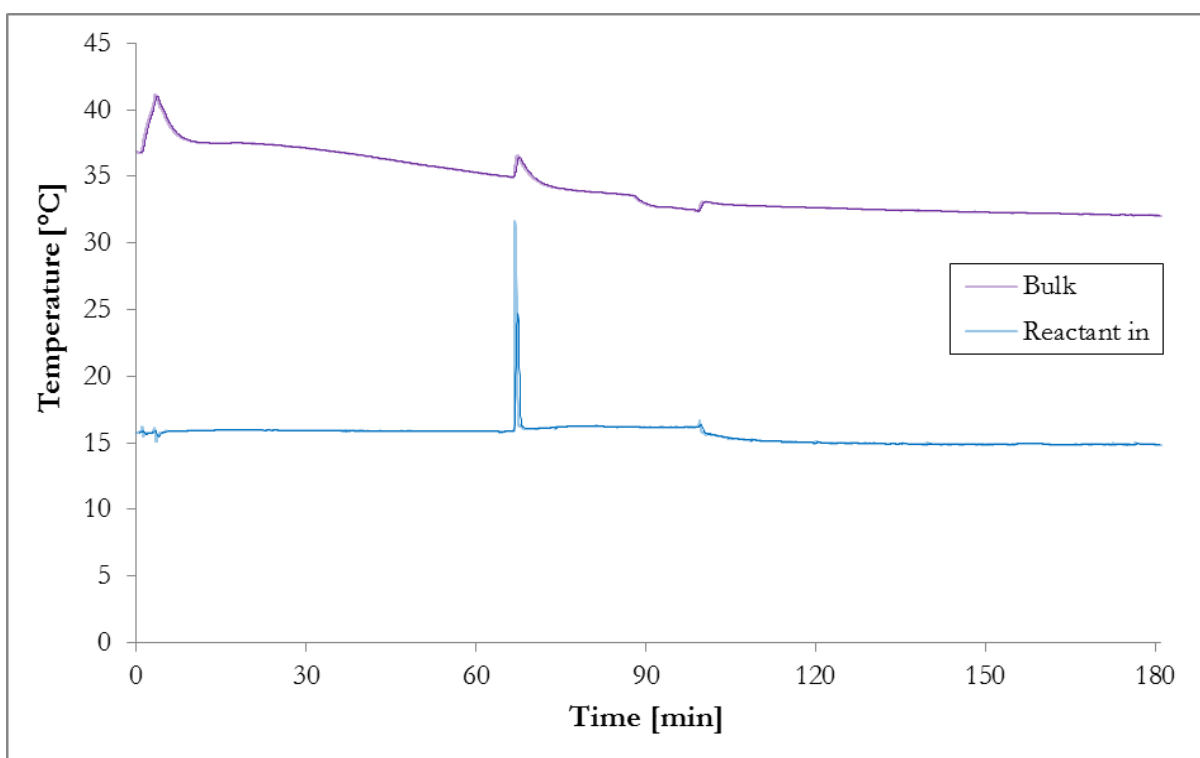
Figure I.32: Temperature of bulk solution and reactant inlet, S=6.0, T$_{Tube}$=90°C, Experiment 13.03

128

The peak after 56 and 69 minutes in Figure I.33 was due to a short stop in the pumping of reactant solution to adjust flow rate and the temporarily displacement of a reservoir tube.
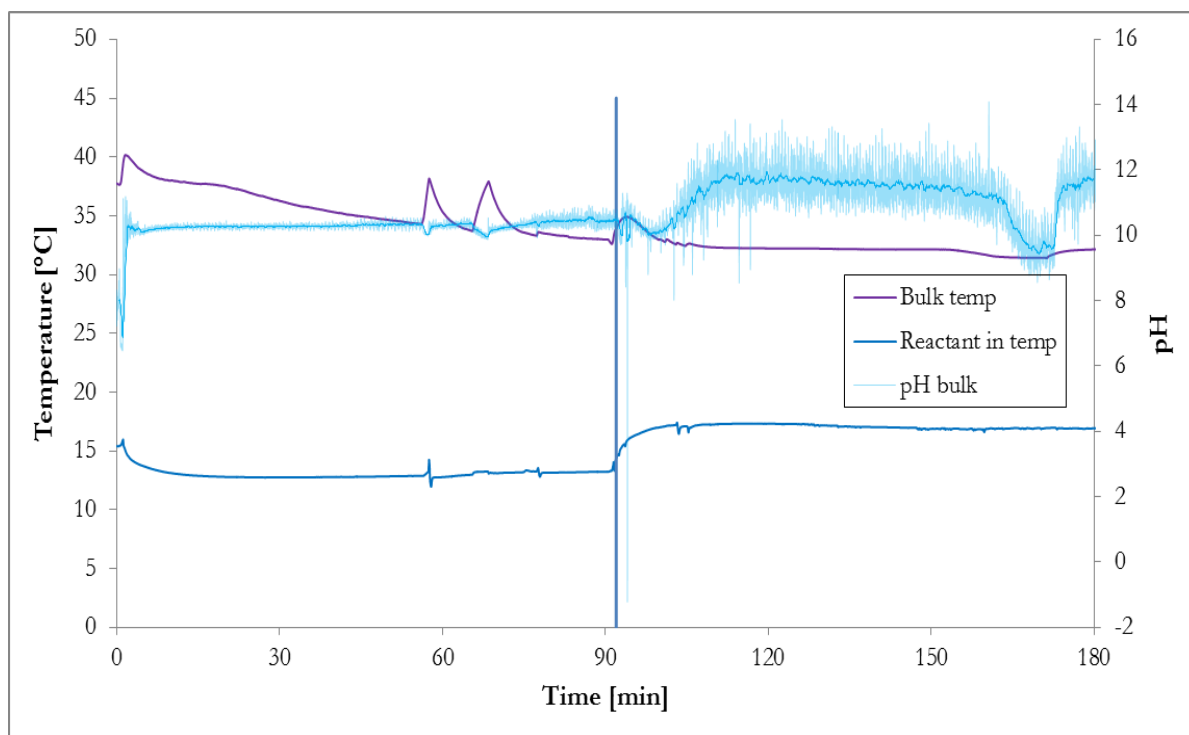
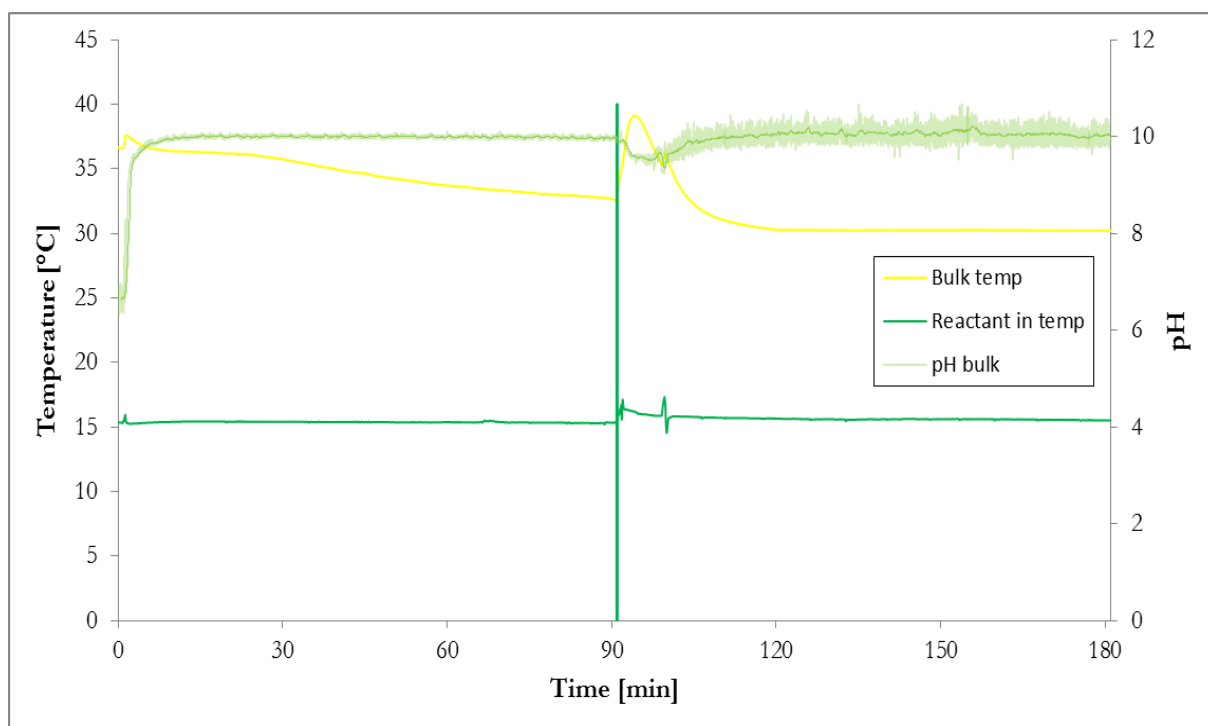**Figure I.33: Temperature of bulk solution and reactant inlet, S=6.0, T$_{Tube}$=90°C, Pre-scale 90 min without MEG then 90 min with MEG=50wt% solution, Experiment 14.03**
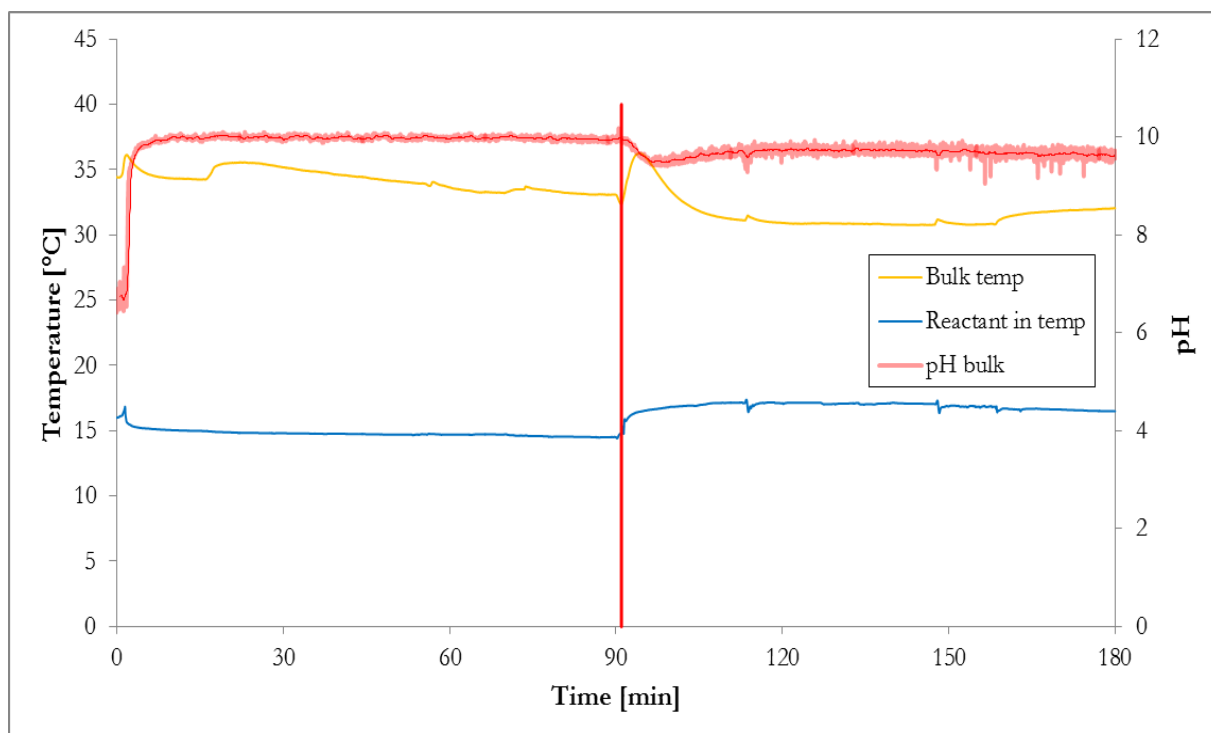
Figure I.34: Temperature of bulk solution and reactant inlet, S=6.0, T$_{Tube}$=90°C, Pre-scale 90 min without MEG then 90 min with MEG=70wt% solution, Experiment 21.03

129
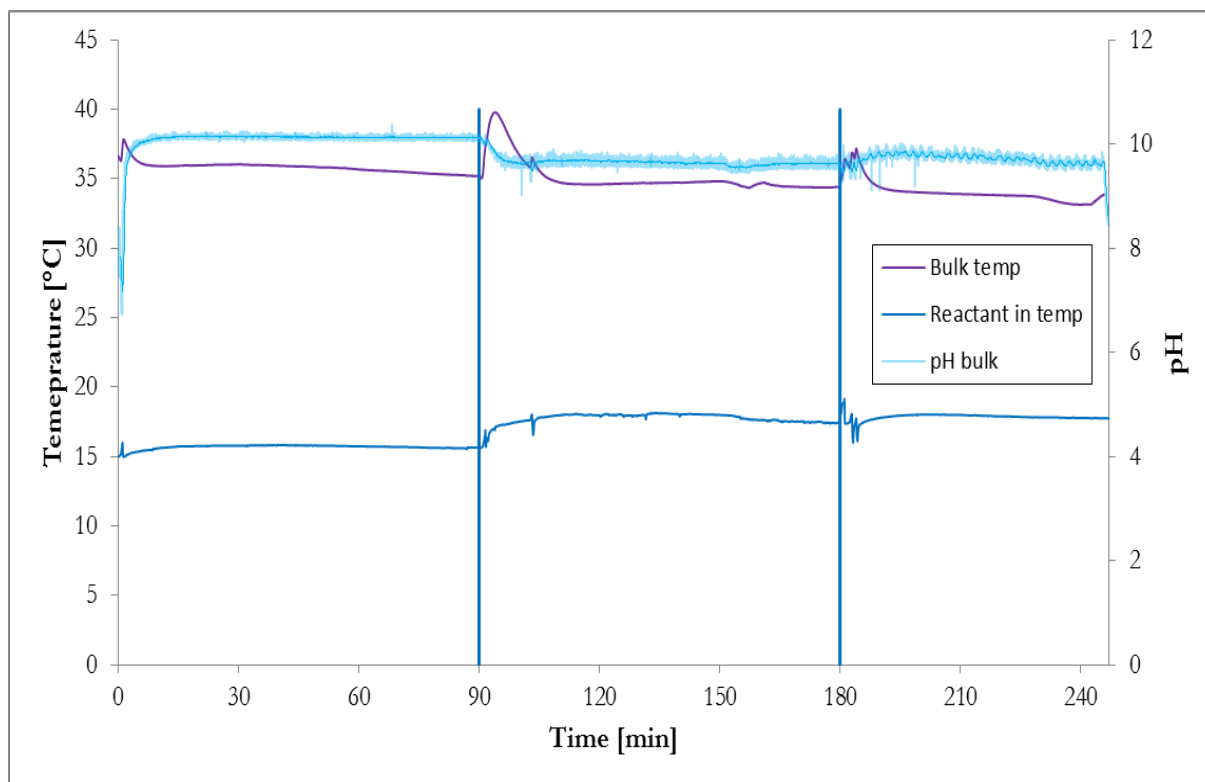
Figure I.35: Temperature of bulk solution and reactant inlet, S=6.0, T$_{Tube}$=90°C, Pre-scale 90 min without MEG then 155 min with MEG=50wt% solution, Experiment 02.04
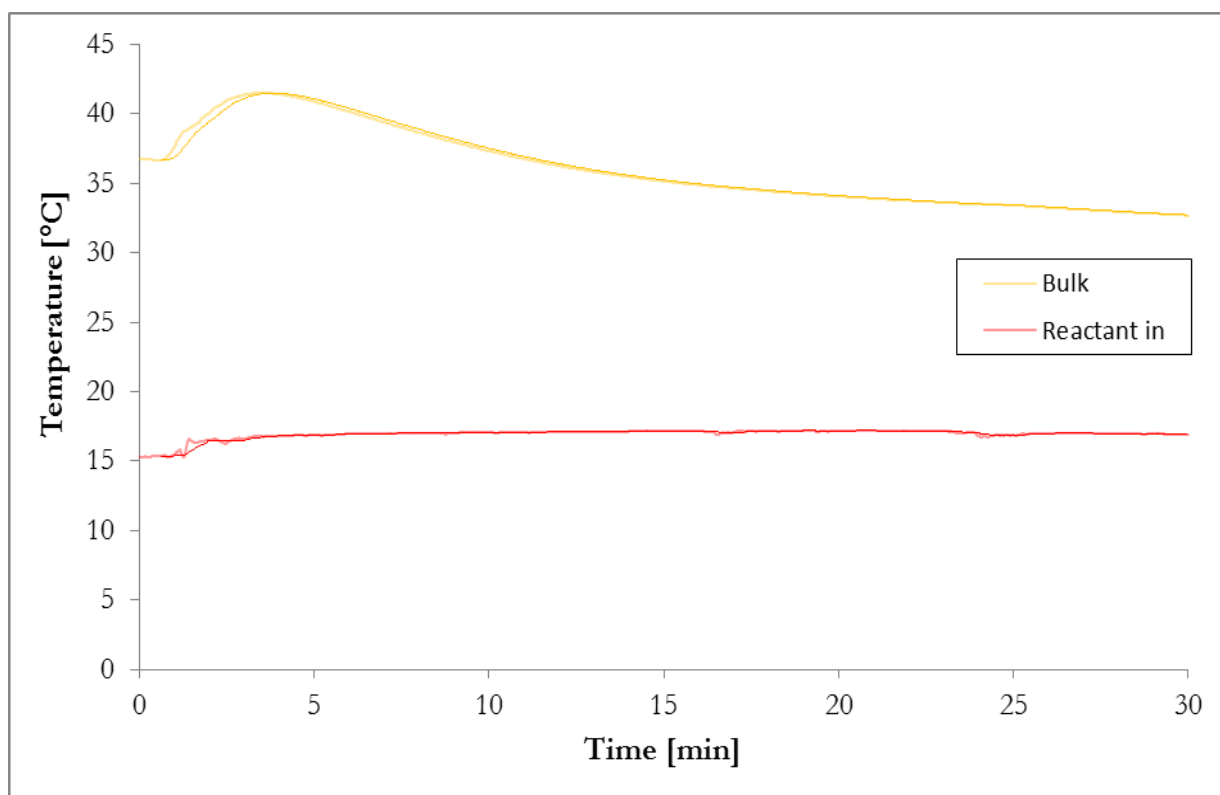
Figure I.36: Temperature of bulk solution and reactant inlet, S=12.3, T$_{Tube}$=90°C, MEG=50wt%, Experiment 04.04

The peaks occurring after 65 and 118 minutes in Figure I.37 were due to a temporary tube displacement and a short stop in the pumping of reactant solution.
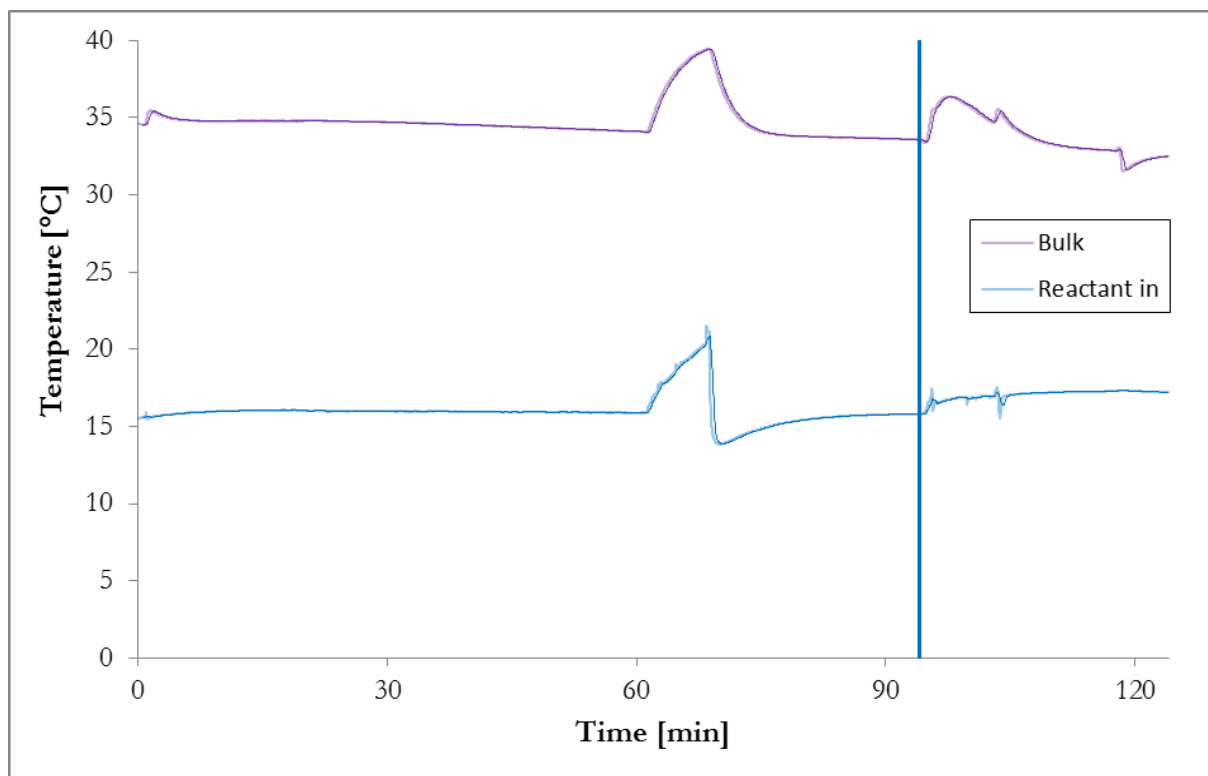
Figure I.37: Temperature of bulk solution and reactant inlet, S=6.0, T$_{Tube}$=90°C, Pre-scale 90 min without MEG then 30 min with MEG=50wt% solution, Experiment 06.04

Figure I.38: Temperature of bulk solution and reactant inlet, S=6.0, T$_{Tube}$=90°C, Pre-scale 90 min without MEG then 90 min with MEG=90wt% solution, Experiment 09.04
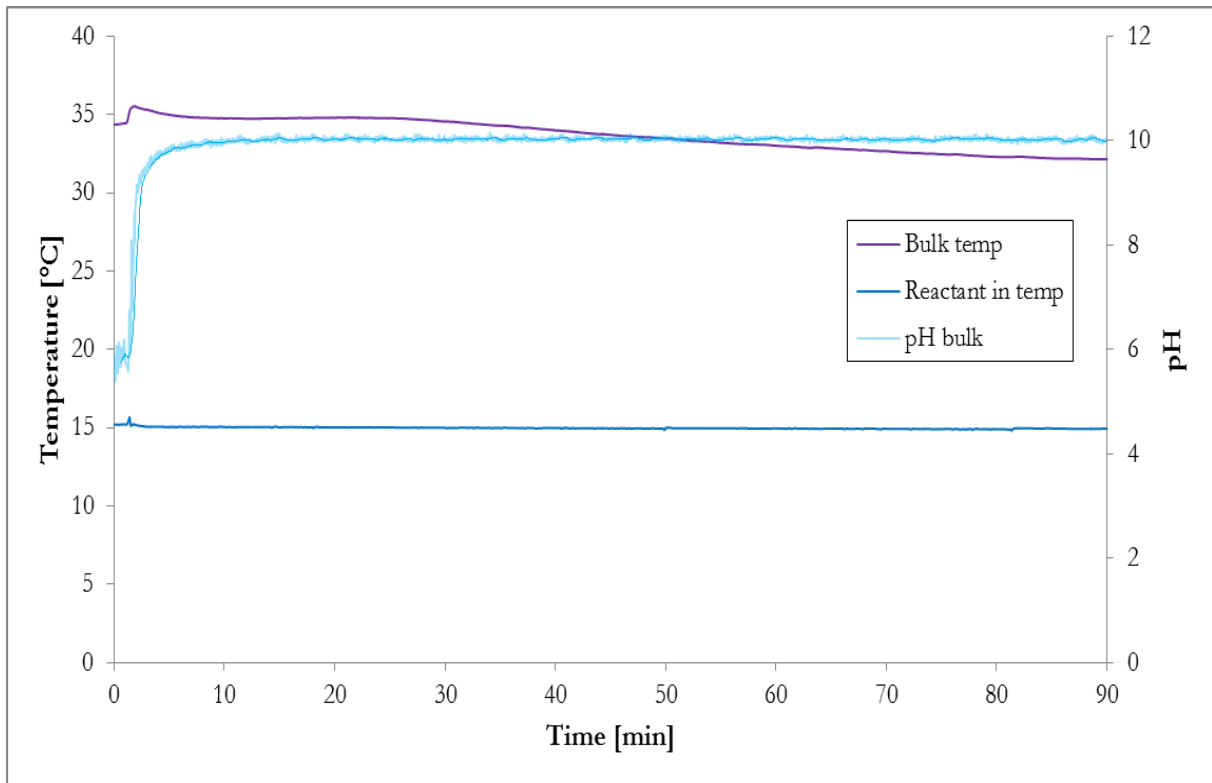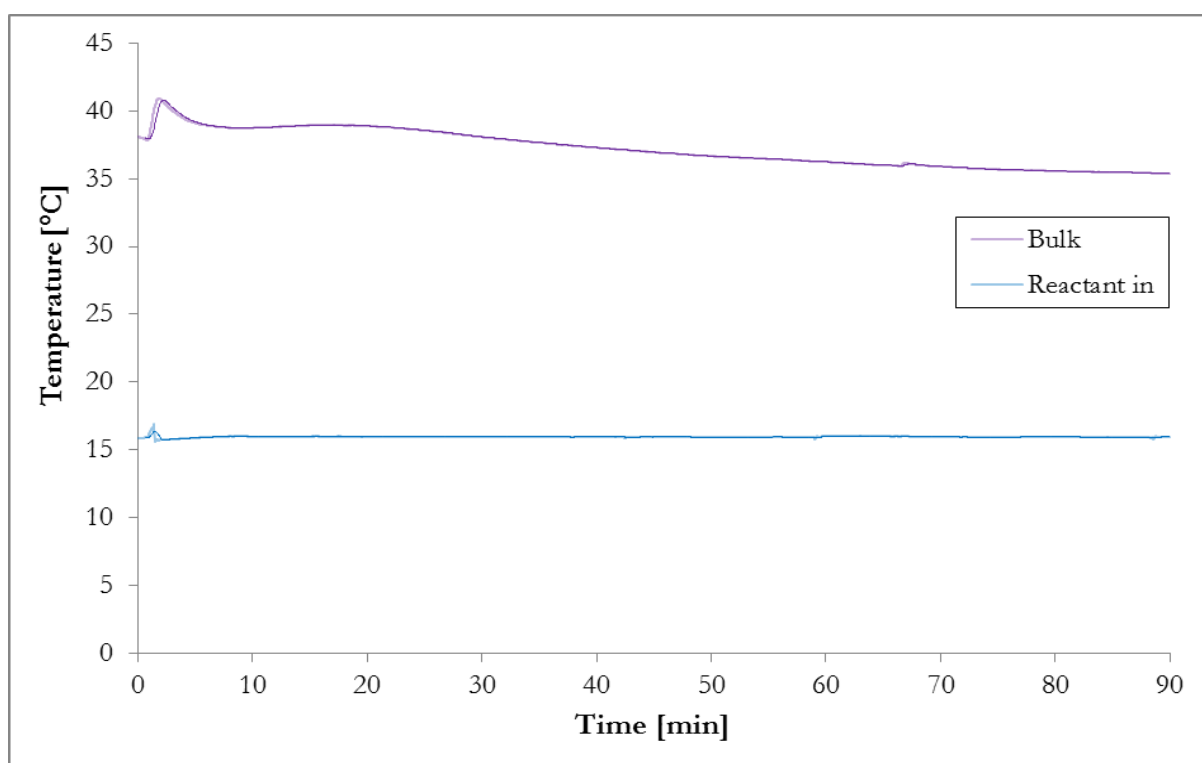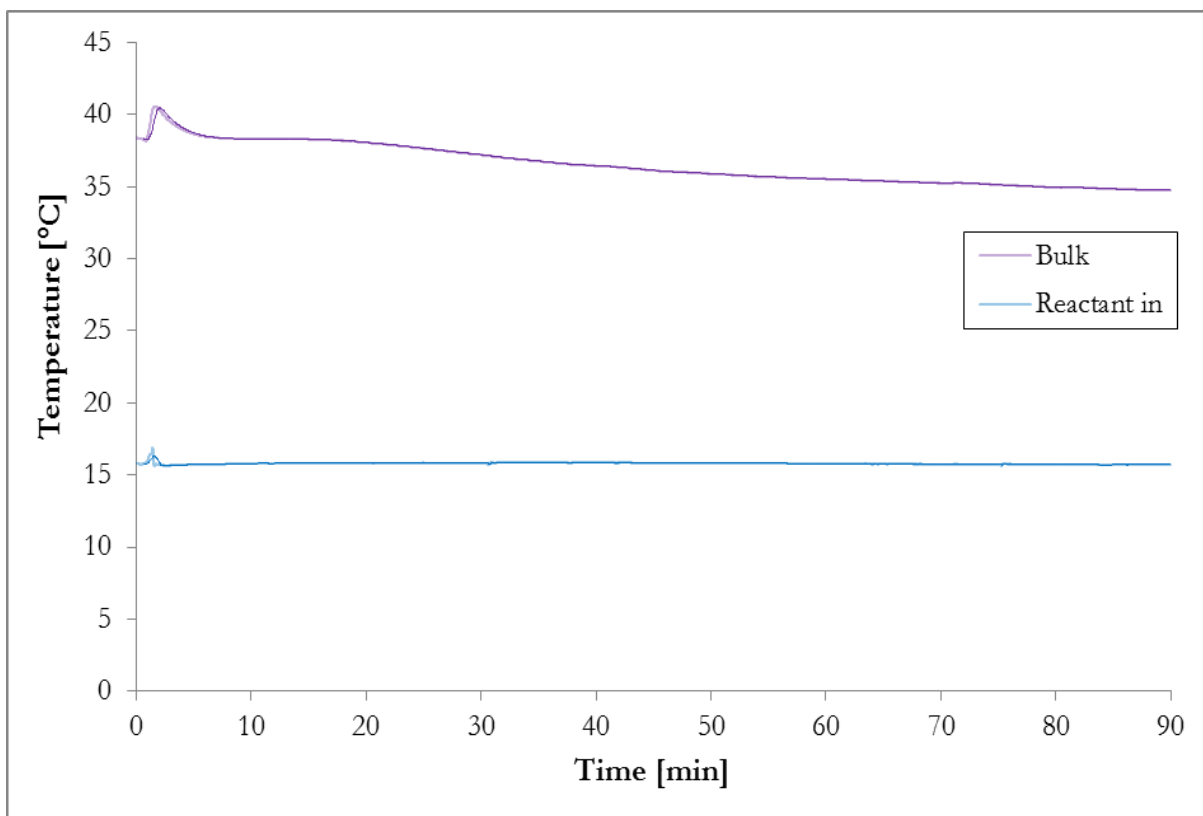
Figure I.39: Temperature of bulk solution and reactant inlet, S=6.0, T_{Tube}=90°C, Experiment 10.04
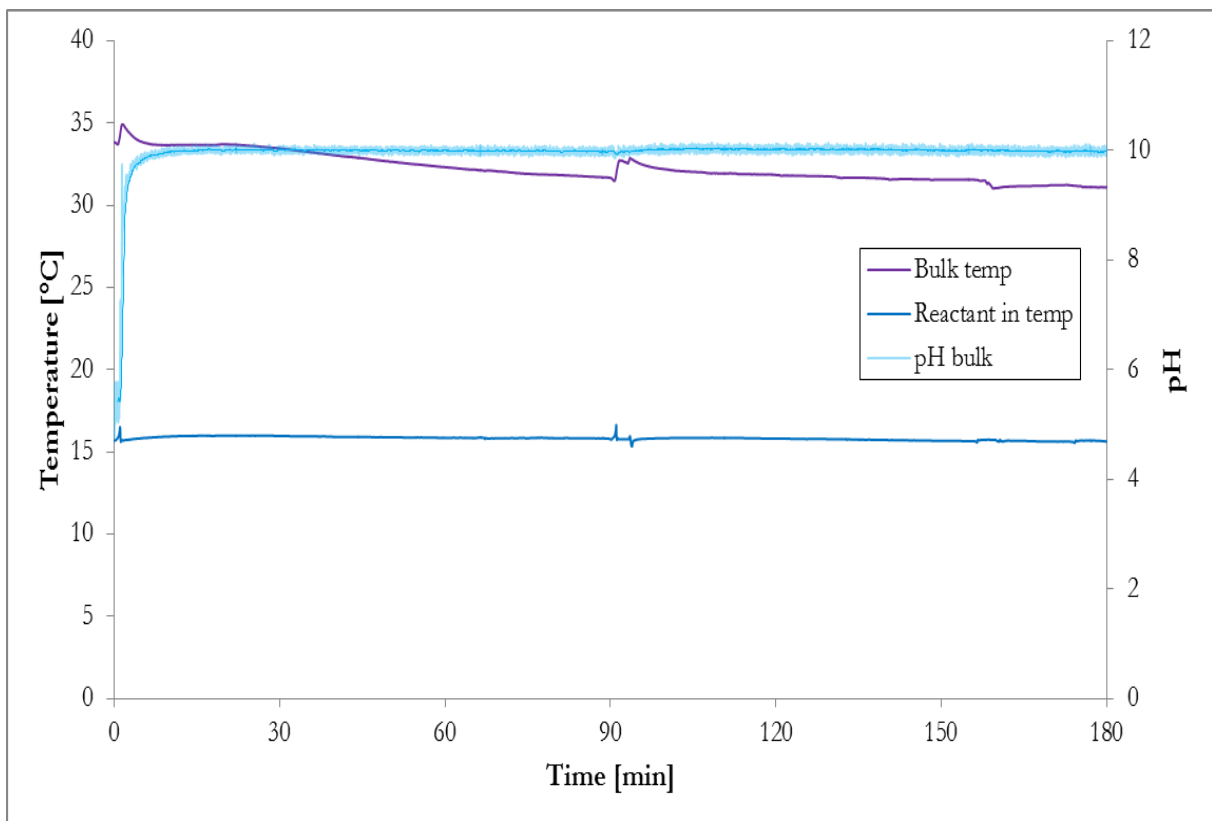
Figure I.40: Temperature of bulk solution and reactant inlet, S=6.0, T_{Tube}=90°C, Experiment 12.04

The level of pH in the experiments represented in Figure I.41- Figure I.43 was completely stabilized around a level of 10.1 which were also shown in Figure I.40. This data was therefore not included for readability.
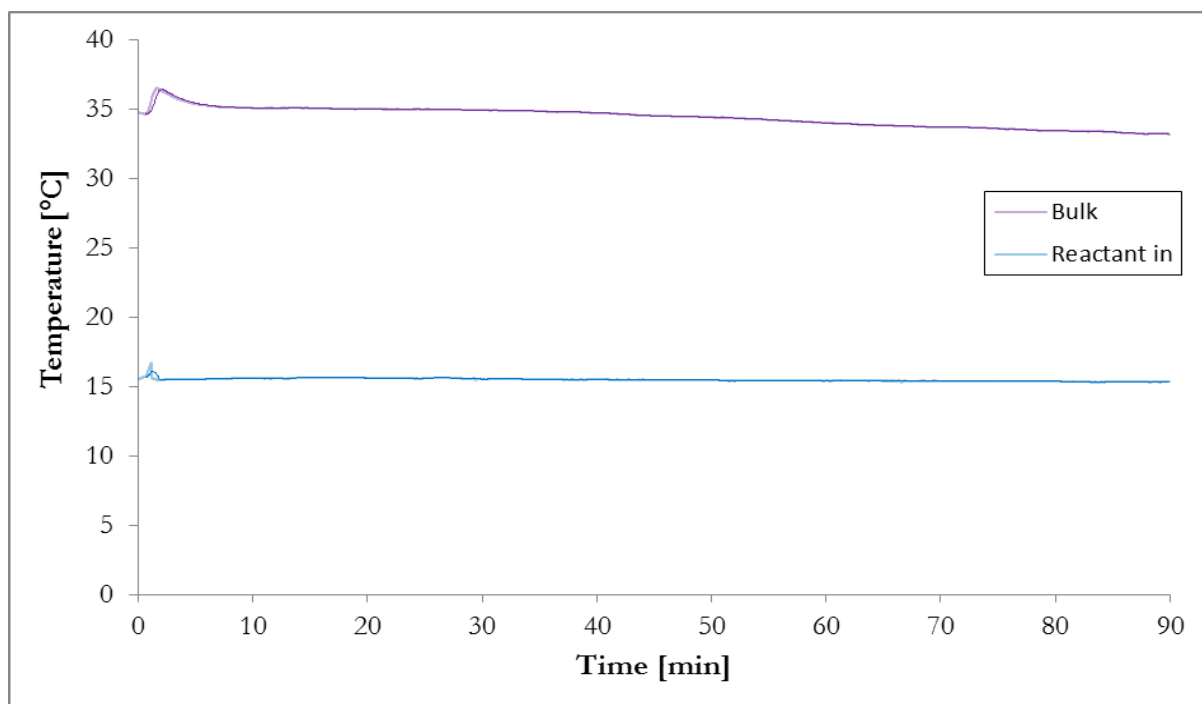
Figure I.41: Temperature of bulk solution and reactant inlet, S=6.0, T$_{Tube}$=90°C, Experiment 15.04

Figure I.42: Temperature of bulk solution and reactant inlet, S=6.0, T$_{Tube}$=90°C, Experiment 16.04

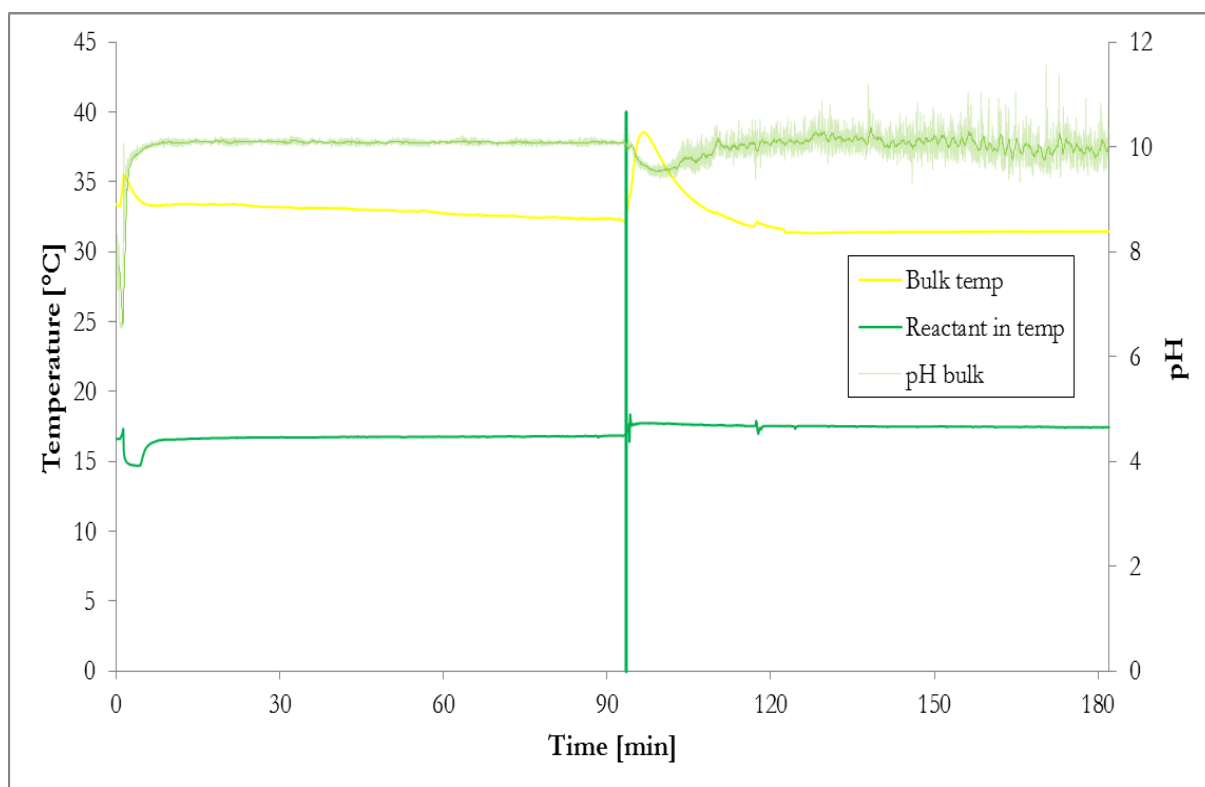**Figure I.43: Temperature of bulk solution and reactant inlet, S=6.0, T$_{Tube}$=90°C, Experiment 16.04(2)**

Figure I.44: Temperature of bulk solution and reactant inlet, S=6.0, T$_{Tube}$=90°C, Pre-scale 90 min without MEG then 90 min with MEG=90wt% solution, Experiment 22.04

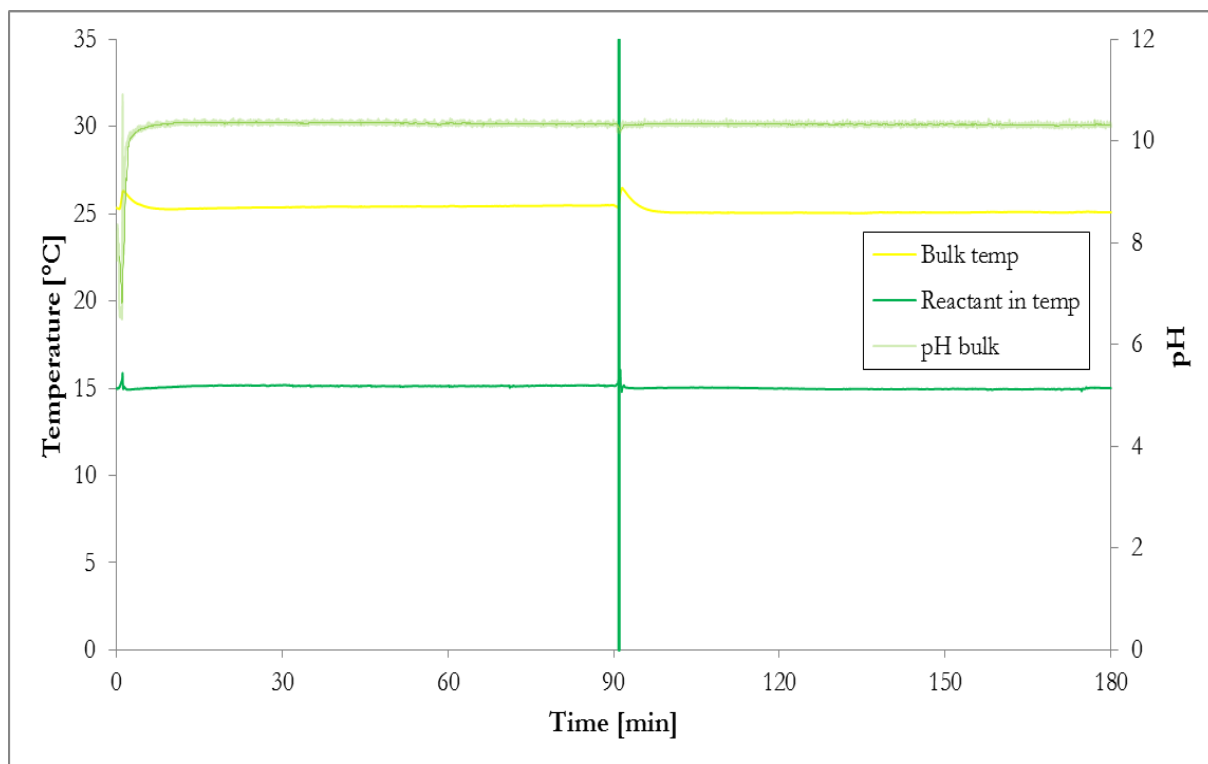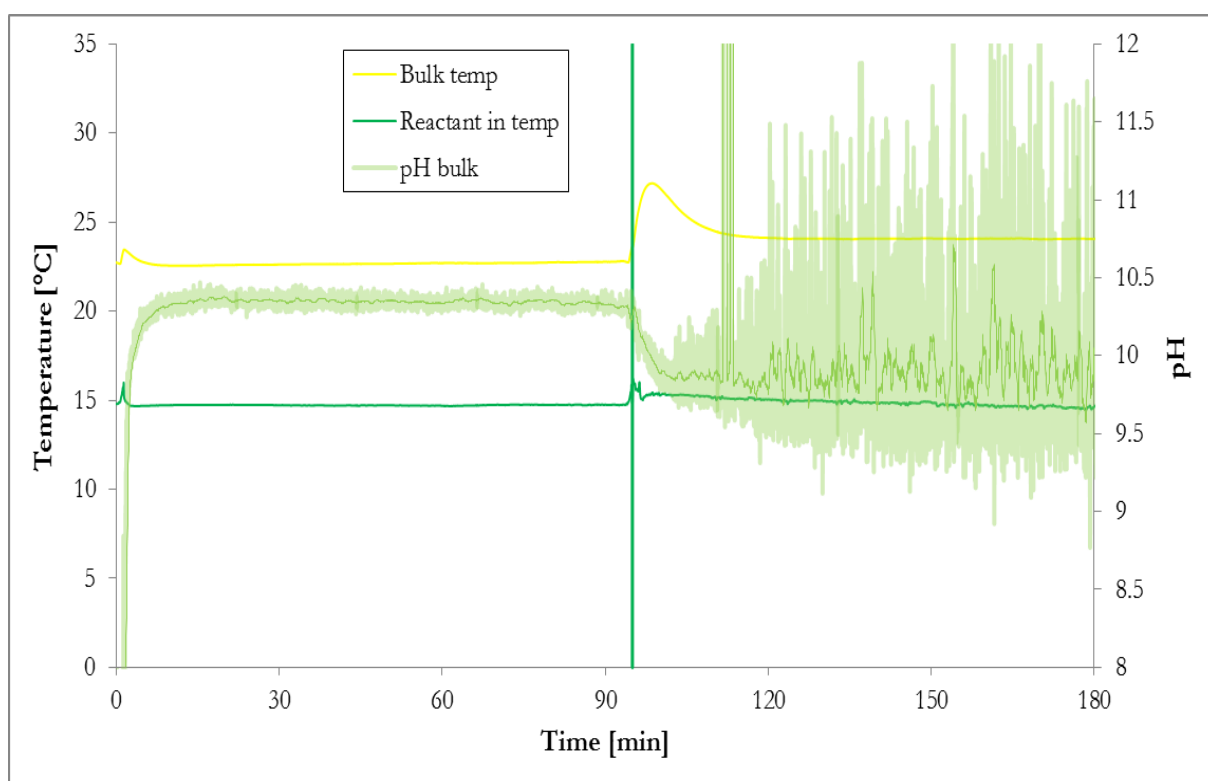**Figure I.45: Temperature of bulk solution and reactant inlet, S=6.0, T$_{Tube}$=50°C, Experiment 26.04**

Figure I.46: Temperature of bulk solution and reactant inlet, S=6.0, T$_{Tube}$=70°C, Pre-scale 90 min without MEG then 90 min with MEG=70wt% solution, Experiment 26.04(2)